Deltares

Study on the impacts of floating seaweed on wind waves

Yi Mou

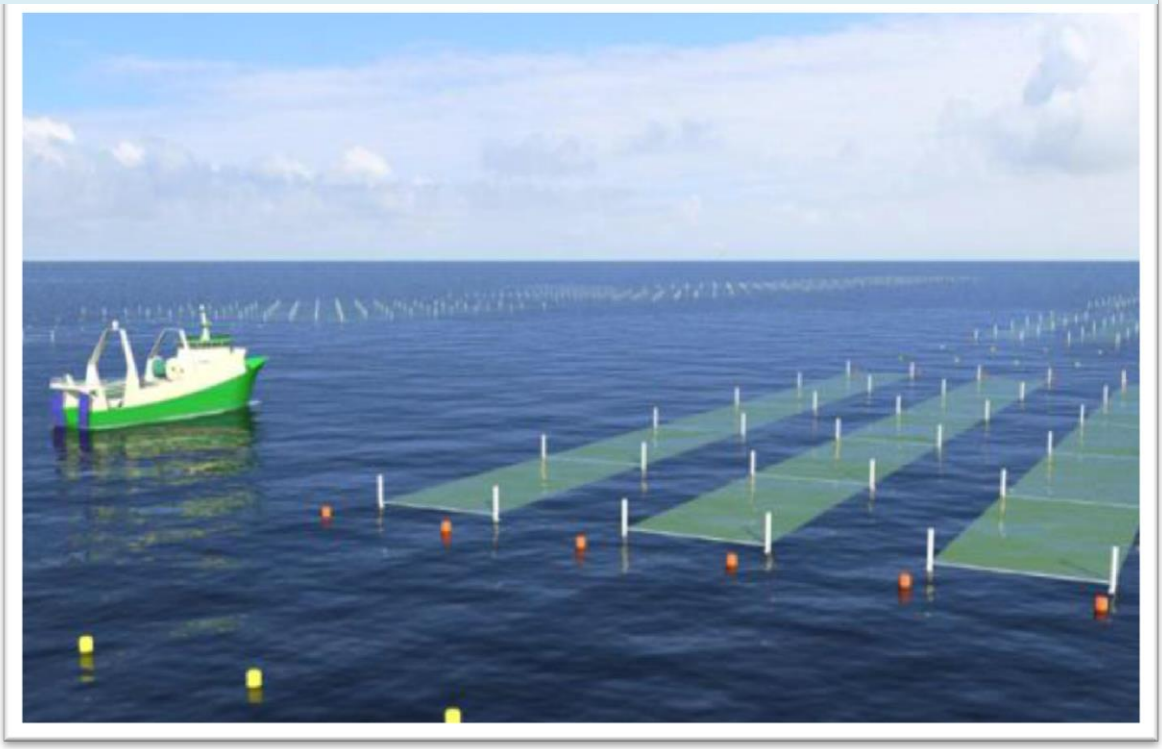

TU Delft Delft University of Technology

Deltares Enabling Delta Life

Deltares

Study on the impacts of floating seaweed on wind waves

Master thesis – Final report

By Yi Mou

October 2015

In collaboration with:

Graduation committee

Prof.dr.ir. Ad J.H.M Reniers (Delft University of Technology)

Ir. Jan-Joost Schouten (Deltares)

Dr. ir. Marcel Zijlema (Delft University of Technology)

Ir. Vincent Vuik (Delft University of Technology)

Haijin Cao (Delft University of Technology)

Summary

As human beings are becoming more and more aware of importance of the environment, resorts to clean energy have provoked great interest for the past decades. As a sort of clean power, wind has been widely considered as an ideal energy source to generate electricity. That is why the offshore wind farm plans have been drawn up, specifically in North Sea in Europe. Besides, in order to comply with marine spatial planning which aims to make use of marine resources sustainably, seaweed aquaculture will also be operated among wind farm zone under wind turbines, which provides the food necessity for mankind. The introduction of seaweed aquaculture may have influences on local hydrodynamics as seaweed attenuates waves, which may further affect the environment. This effect has not been understood. Therefore this study is conducted to investigate the impact of seaweed aquaculture on wind waves.

As a relatively young sector, few studies have been found on the effect of floating vegetation on waves. Since there is no ready-to-use hydrodynamic model which can deal with floating seaweed, it is required to set up a numerical model and calibrate this model with experimental data.

In this research the wave modelling program SWAN is used owing to the fact that there exists a vegetation model in SWAN. In this model the vegetation is schematised as stiff cylinders mounted at the bottom. The energy dissipation by vegetation is calculated as work carried out by the drag force induced by cylinders. However, the function of this vegetation model in SWAN is somewhat different from what is required for this study.

- Firstly, the SWAN deals with bottom-mounted vegetation while in this research floating vegetation is addressed.
- Secondly, in SWAN model stiff objects are considered while in current research the vegetation possesses flexibility. With flexibility the drag force will become smaller as the relative velocity between water particle and vegetation gets smaller. On the other hand, the inertial force may have an impact on the wave energy dissipation.

Considering these two differences, corresponding measures need to be taken to meet the requirement of this study. To model the floating vegetation, the original vegetation model has been modified. In the beginning, the floating vegetation model is achieved by dividing the vegetation into two vertical layers and making the lower layer virtual. There is drawback in this model: only flatbed can be applied. For sensitivity analysis and calibration this model works well, but it is not applicable in the case study as non-flat seabed is implemented in the

model setup. It leads to a second modification in the SWAN model. The method is to alter the interval of integration of dissipation term by vegetation, which results in further change in the source code. To account for the flexibility, the bulk drag coefficient is adjusted. This parameter accommodates the influence of flexibility of vegetation and uncertainty of other parameters related to the model.

To test this floating vegetation model a sensitivity analysis is performed. Relevant parameters in this model are varied to see its individual influence on the wave dissipation. It has been observed that a larger wave height results in a higher dissipation rate. The opposite has been seen for wave period. Wave with a larger peak period gives a smaller wave height behind the vegetation field. It has been also demonstrated that larger vegetation length, larger vegetation diameter and larger vegetation density give rise to greater dissipation rates. In addition, spectrum analysis shows that the energy dissipation rate varies along the frequency domain with the greatest magnitude of energy dissipation observed at around the peak frequency.

To calibrate this model the experimental data is used, obtained from flume test in Technology University of Braunschweig. The calibration is conducted by adjusting the bulk drag coefficient until that the floating vegetation model describes the experiment data. By this method a fitted drag coefficient is obtained for each wave condition. It has been verified that drag coefficient depends on both the wave condition and vegetation parameters. The relation between wave condition and vegetation characteristic is indicated by KC-number or Reynolds number. Through this calibration a relation between drag coefficient and Reynolds number or KC-number is obtained.

With the calibrated model, a case study is conducted in the North Sea. The dominant wave data for the period 1991-2010 is used, as well as corresponding wind information. The vegetation parameters (vegetation density, vegetation width and vegetation length) are set according to local cultivation. With this information and the drag coefficient function obtained from the calibration stage, the drag coefficient for the field condition is obtained. Implementing all relevant input parameters in the model, the result shows that the dissipation is species specific. Also from the results it is shown that wave attenuation occurs mainly in the local scale. Behind the vegetation field waves develop due to the directional spreading. At the South boundary 85% of the wave height remains.

Reflecting on the uncertainty associated with this study, such as measurement data, calibration of drag coefficient and parameterising the vegetation diameter in the field condition, it is still questionable whether seaweed aquaculture has a significant impact on the wind waves or not.

Preface

Finally, it comes to the end of my master thesis. Through this year of master study, I have gained knowledge and skills more than I would expect, such as better understanding of fluid mechanics, learning to use SWAN and Mat lab, doing source code change in SWAN, etc. I believe I have made quite a big step in my life. I would not have known how much potential one can possess without experiencing this year. It is a good opportunity to do my master thesis in Deltares. I was amazed by its academic atmosphere. During my master thesis, I have gained a lot of help from many nice persons. Without those kindnesses I would not have accomplished the thesis. Thanks to all of them from the bottom of my heart.

Firstly, I would like to thank my professor Ad Reniers. You are very warm-hearted and very helpful when I turned to you if I had question or faced some problems in the progress. You spare your precious time to have quite some discussions with me during the progress, helping me with a Mat lab script, for which you even skipped your lunch. No words can express my appreciation for your kindness to me.

Secondly, big thanks to my supervisor Jan-Joost Schouten, for you held meetings with me regularly and provided suggestions to the progress. You revised my report meticulously and provided a lot of critical reviews. You taught me how to write a report scientifically. This is of great importance for my future career.

Then, I am very grateful for the guidance from Marcel Zijlema when I struggled with the compiling of SWAN. You explained me the procedures patiently and solved the questions I bombarded on you. Without your help I would not figure out the compiling, or at least it would take much longer.

Also, I appreciate a lot the help from Vincent Vuik. Each time when I asked question you explained the answer in a very detailed way and it was very comprehendible. Besides, you provided many good comments on my report, which improved the quality of my work a lot.

In addition, special thanks to my committee and friend CAO Haijin. You inspired me some good ideas and helped me a lot with SWAN.

I would also like to give my thanks to Menno Genseberger from Deltares, who kindly helped me with the compiling SWAN in the h5 cluster. Thanks to Ivo Wenneker who provided me the Mat lab script to process the irregular wave. Much appreciation to Elly Diamantidou who suggested me to turn to Ivo Wenneker for the processing of irregular wave data and who also helped me with the Mat lab script. Also I am much grateful for Frank Habets who corrected my Mat lab script and gave me a good company. In addition, thank Nefeli Palaiogianni for revising my report.

Last but not least, thanks to all those Deltares mates without their names being mentioned, with whom I had joyful lunch and nice coffee breaks. I enjoyed a lot with your company.

Yi Mou

Delft, October 2015

Contents

1 Introduction **1**

1.1 Background 1

1.2 Research objectives and research questions 2

1.3 Methodology 3

1.4 Outline 4

2 Floating seaweed model **5**

2.1 Vegetation module in SWAN 5

2.2 Floating seaweed model 5

3 Sensitivity analysis **9**

3.1 Theory 9

3.2 Literature study on wave damping studies 11

3.3 Model setup 12

3.4 Varying wave characteristics 13

3.4.1 Significant wave height 13

3.4.2 Peak wave period 16

3.5 Varying vegetation characteristics 18

3.5.1 Vegetation height 18

3.5.2 Vegetation diameter 19

3.5.3 Vegetation density 20

3.6 Wave spectrum 21

3.7 Other aspects of sensitivity 22

3.8 Discussion 25

3.9 Conclusion 25

4 Calibration **27**

4.1 Approach 27

4.2 Experiments setup 30

4.3 Vegetation description 32

4.4 Numerical model setup 33

4.4.1 Model setup for regular waves 33

4.4.2 Model setup for irregular waves 33

4.5 Determination damping effect caused by only vegetation 33

4.6 Data processing and acquisition 34

4.6.1 Regular waves 34
4.6.2 Irregular waves 35
4.7 Results of data analysis 36
4.7.1 Regular waves 36
4.7.2 Irregular waves 37
4.8 Calibration for regular waves 37
4.8.1 Calibration of Laminaria digitata 37
4.8.2 Calibration of Saccharina latissima 41
4.8.3 Calibration of Ulva lactura 42
4.9 Calibration for irregular waves 44
4.9.1 Calibration of Laminaria digitata 44
4.9.2 Calibration of Saccharina latissima 45
4.9.3 Calibration of Ulva lactura 46
4.10 Horizontal particle velocity 47
4.11 Discussion 48
4.12 Conclusion 49

5 Case study 51
5.1 Background 51
5.2 Scenario definition 52
5.3 Boundary condition determination 52
5.3.1 Boundary wave condition 52
5.3.2 Boundary wind condition 55
5.4 Model setup 57
5.4.1 Bathymetry 57
5.4.2 Vegetation parameters determination 58
5.4.3 Drag coefficient determination 58
5.4.4 Vegetation field 59
5.5 Case study results 61
5.5.1 Laminaria digitata 61
5.5.2 Saccharina latissima 65
5.5.3 Ulva lactuca 67
5.5.4 Quantification of wave dissipation 68
5.6 Discussion 71
5.7 Conclusion 71

6 Conclusions and recommendations 73

6.1 Conclusion 73
6.2 Reflection on the results 74
6.3 Recommendations 75
6.3.1 Recommendations for the modified SWAN-model 75
6.3.2 Recommendations for the experiments 76
6.3.3 Recommendations for case study 77

Appendix A – Background of wave physics and SWAN 79

Appendix B – Exploration on the width of simulation domain and grid cell 83

Appendix C – Wave spectrum analysis in sensitivity analysis 85

Appendix D – Exploration the reason behind unexpected data 87

Appendix E – Horizontal particle velocity analysis 89

Appendix F – Formulation of new expression of dissipation term by vegetation 91

Appendix G – Source code change 95

Appendix H – Boundary condition and drag coefficient for all direction sectors 101

Appendix I – Varied square vegetation field 103

Appendix J – Diagrams for Laminaria digitata for other direction sectors 105

References 109

1 Introduction

This opening chapter is intended to provide the background information on this research: the study of influence of seaweed aquaculture on wind waves. Also, what is expected to be obtained from this research is formulated before commencing the exploration. Hereafter the methodology is presented in which it is explained how to approach the research questions. Finally the structure of this report is described.

1.1 Background

In recent years, significant investments have been made in offshore electricity generation by making use of natural power of wind. This results from the advantage that wind is clean energy source and it conforms to sustainable development. It makes great sense from the standpoint of environmental conservation. Consequently offshore wind farms emerged in an increasing trend. In addition, consumption of sea food increased with dramatic population increase in coastal area (Newkirk, 1996). The majority of sea food comes from fishing, but it appears to be insufficient to satisfy the consumption of human beings. As a result, a trend of massive development for marine aquaculture has been noticed in order to accommodate the increasing demand for sea food such as mussel and seaweed (Folke & Kautsky, 1992).

What's especially notable in North Sea, the ocean will be subject to massive development of marine infrastructure for energy exploitation, such as gas, oil and wind energy. Among those infrastructure developments, a most important thing will be offshore wind farms as it is a manner to reduce fossil-based energy, which is one aspect of EU strategies. As human beings are becoming increasingly aware of sustainable development, the resort to clean energy sources has sparked rising interest. The pressure is expected to increase due to additional offshore wind plans. Furthermore, in order to make full use of the ocean space and satisfy food necessity, marine aquaculture will also be operated in the wind farm region. This is also aimed to become a major player in sustainable aquaculture, which is also a consideration under EU strategies. As a result, large scale of marine structures for offshore wind farms and aquaculture will be installed at various sites. Multi-use of the ocean is manifested through the combination of wind-powered electricity generation and aquaculture. This conforms to marine spatial planning which aims at using marine resources sustainably. However, the economic costs and environmental impact have to be identified and reduced so as to increase the feasibility of the use of ocean. All these aspects are considered under EU-funded project called "MERMAID" which focuses on the study on the innovative multi-purpose offshore wind farms: planning, design and operation.

Being a relatively young sector, still little is known about the environmental impact of such large scale of wind farms and aquaculture. Such infrastructure may have a significant influence on the environment, such as local hydrodynamics, waves, currents, turbulence energy etc. This generates possible adverse effects 1) on the local morphology around the multi-use wind farm and 2) on a large scale influencing the transformation of adjacent coastlines due to changes of local wave climate. As one sort of aquaculture, the seaweed aquaculture has an influence on the local waves as the large scale of floating seaweed attenuates waves. Therefore, the individual impact of seaweed aquaculture on waves should be understood. The impact of floating seaweed will be addressed within this master thesis project. The approach is to apply advanced hydrodynamic models to simulate the interaction between seaweed and waves, as well as experimental measurements in laboratory serving as auxiliary tool to make the research feasible.

1.2 Research objectives and research questions

Many studies have been conducted on wave dissipation due to sea bed mounted vegetation. For example, the influence of vertical surface area on wave dissipation has been investigated by Bela et al (2005). It has been confirmed that, the larger the vertical surface area of single plant is, the more dissipation is achieved (Buck & Buchholz, 2005). Also, Lauren Nicole Augustin (2007) conducted a laboratory test to testify the influence of vegetation length on the wave attenuation. It has been concluded that larger plant length contributes to higher dissipation. In addition, the stiffness of the seaweed has been also identified as an influencing factor to the wave energy dissipation effect (M. Paul, 2004). It was shown that larger flexibility gives less capability of dissipation. Besides these studies, many other researches have been conducted in various aspects. Among those studies the most classical research is attributed to Dalrymple et al (1984). Their result is the most common applied reference. In this study, the mounted vegetation is schematized as cylinder and the energy dissipation is calculated by work carried out by drag force induced by plant which is expressed in a Morison-type equation (Dalrymple et al, 1984). This principle is also implemented in SWAN, which is a wave modeling program developed in Delft University of Technology and is used in this research. In SWAN model, the energy dissipation by vegetation is quantified using the formula from Mendez & Losada (2004), who made a minor modification based on the result of Dalrymple et al (1984). However, all the studies performed previously only focused on the sea bed mounted vegetation. Limited research has been conducted regarding the impact of floating seaweed. Its influence remains to be investigated. Therefore, this research focused on impact of the floating seaweed on waves. Through this study it is aimed to achieve the following objective:

- Assessing the impact of seaweed aquaculture on local wave climate

As a result the research questions are formulated:

1. How to model floating vegetation with the available vegetation module in SWAN?
2. How to make the floating seaweed model applicable to real situation?
3. What is the impact of the large-scale seaweed aquaculture in the offshore wind farm on wave climate in the North Sea?

1.3 Methodology

Based on the research questions the applied study methodology is discussed in this section. At first a numerical model is set up, taking into consideration the special aspect of "floating seaweed" in this study. Then it is followed by a sensitivity analysis in which the wave characteristics and vegetation properties are varied to give some insights into the response of the model. Also this stage is carried out to check whether the model results comply with the theory of wave dissipation. Afterwards the model is calibrated with experimental data from laboratory. The flume test was conducted in Technology University of Braunschweig in Germany. This experiment is also addressed under MERMAID project. Through calibration it aims to make the model capable of describing the real situation through fitting model simulation and flume test results. Finally, a case study is performed with the calibrated model to study the impact of floating seaweed in Borssele wind farm in the North Sea. The scope of this study is presented as below.

- Different from a stiff cylinder, vegetation is able to move and reconfigure when it is exerted by wave forces. This characteristic is called flexibility. Flexibility is an important feature when wave energy dissipation caused by vegetation is concerned. With flexibility the vegetation shows less ability of attenuating wave since the relative horizontal velocity would become smaller. However, describing flexibility in a mathematical way is too complicated to be directly interpreted in the SWAN model. Instead, it is indicated via a "bulk parameter" named bulk drag coefficient. Flexible vegetation is inferior to stiff vegetation in the respect of capability of energy dissipation, indicated by a smaller drag coefficient.
- Source code change is performed during the case study. At the beginning, a modified model based on original SWAN is presented to do sensitivity analysis and is also utilized in the calibration stage. Later on it was realized that this model is not able to be applied in case study due to its inability in non-flat-bottom circumstance, leading to necessity to change the dissipation term by vegetation in SWAN and subsequently the source code. These two models are essentially the same in terms of representing the energy dissipation by floating vegetation.

- In aquaculture the seaweed is attached to some supporting structures or mooring lines. These structures or mooring lines can have an influence on the wave propagation. Nonetheless, supporting structure itself is not considered in the model as SWAN does not have the capability of handling it.
- Since few studies have been carried out regarding this topic of floating seaweed, a flume test is required to provide the data basis for the calibration of this model. Experiment was carried out in Technology University of Braunschweig in Germany to cooperate with the numerical model.

1.4 Outline

This study presents the research on influence of seaweed aquaculture on the wind waves. The process to address this study is elaborated in the following chapters of this report. The report is structured as following: In chapter 2 the background information of SWAN and relevant wave knowledge is presented, as well as the description of the floating seaweed model. Chapter 3 sees the sensitivity analysis regarding varying both wave and vegetation parameters. In chapter 4 the calibration is described with the purpose to make the floating seaweed model capable of representing real situation. After that a specific case in North Sea is carried out in chapter 5. As concluding of this study, some conclusions are drawn from this research and recommendations are given for future study in chapter 6.

2 Floating seaweed model

This chapter describes the floating seaweed model which is going to be employed in subsequent study. The modeling program used in this study is SWAN. There exists also a few other wave modeling programs like AQUA, WAMIT and Multisurf. SWAN is opted rather than the others due to the inherent vegetation module in SWAN. It can be adapted when it is necessary. Preceding the presentation of my model, a brief introduction regarding energy dissipation of bottom-mounted seaweed which is implemented in SWAN is given, on which my floating vegetation model is based. More details regarding wave attenuation, as well as wave physics and background of SWAN are given in Appendix A.

2.1 Vegetation module in SWAN

The principle of wave attenuation by vegetation in SWAN results from the research of Mendez & Losada (2004). Their finding is achieved based on the work of Dalrymple et al (1984). With schematizing the vegetation as cylindrical objects and employing a Morison-type equation, Dalrymple et al (1984) came up with an energy dissipation term by vegetation. This formula reads as:

$$\varepsilon_v = \frac{2}{3\pi}\rho C_D b_v N \left(\frac{kg}{2\sigma}\right)^3 \frac{(\sinh k\alpha h)^3 + 3\sinh k\alpha h}{3k(\cosh kh)^3} H^3$$

Equation 2-1

ε_v is time-averaged rate of energy dissipation per unit horizontal area induced by vegetation. Based on this, Mendez & Losada (2004) rewrote this term by applying Rayleigh distribution for wave height and came to a modified dissipation term:

$$\varepsilon_v = \frac{1}{2\sqrt{\pi}}\rho C_D b_v N \left(\frac{kg}{2\sigma}\right)^3 \frac{(\sinh k\alpha h)^3 + 3\sinh k\alpha h}{3k(\cosh kh)^3} {H_{rms}}^3$$

Equation 2-2

This formula is implemented in SWAN and forms the essence of the vegetation module. The related vegetation parameters are C_D (drag coefficient), b_v (vegetation width or diameter), N (number of stems per square meter) and αh (vegetation height). The concerned wave parameters are σ (wave angular frequency), k (wave number) and H_{rms} (root mean square wave height). In SWAN the significant wave height (H_s) is used instead of H_{rms}. The relation between them is: $H_s = \sqrt{2}H_{rms}$.

2.2 Floating seaweed model

The vegetation model for this study is based on the vegetation module available in SWAN. First a schematic model is developed to meet the requirement of this study in the beginning. In this model a virtual layer is present between floating vegetation and bottom. This model

works well in the sensitivity analysis and calibration. However, there is one disadvantage about this model: it can only be used for flat bed. This disadvantage is not noticed until the case study commences. The previous model cannot be applied anymore due to the non-flat bathymetry implemented in case study setup. Then a new approach is come up with to meet the requirement of model input for non-flat sea bed. There comes the second model, which eliminate the limitation of the first model.

The first model is formed as two vegetation layers with the lower layer as virtual layer plus a vegetation layer at the upper water column, as shown in Figure 2-1. It is formed in such way to make the "floating seaweed" realistically presented in SWAN. Since SWAN reads the vegetation information starting from the bottom, it is required to make the lower layer virtual as only water is present in this layer in case of floating vegetation. This model is feasible since in SWAN the vegetation can be divided over a number of vertical segments, so the possibility to vary the vegetation vertically is included. The virtual layer can be achieved through applying drag coefficient as zero, namely no damping caused by vegetation is applied on the waves. This model is originally come up with to simulate the floating seaweed. In this model, it is required to give vegetation commands to SWAN twice. The first command is to cover the virtual layer and the second one is to include the floating seaweed information.

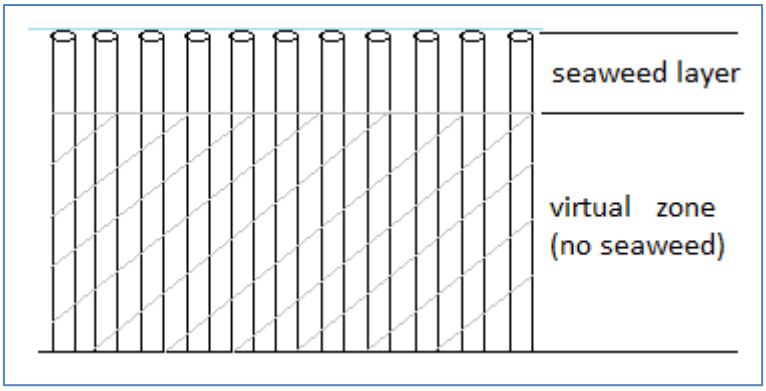

Figure 2-1: Vertical schematisation of vegetation

The second model is obtained through re-expressing the dissipation term. The original dissipation formula lets SWAN read the vegetation input starting from the bottom upwards. By means of changing the interval of the integration, it can be achieved that the SWAN can read the vegetation information starting from the water surface downwards. In this model only one vegetation command is needed since the information of floating seaweed on the water surface is read by SWAN first.

These two models possess exactly the same functions in terms of simulating energy dissipation caused by vegetation. The advantage of the second model is that it is more

general than the first model. The first model can only be used for flat-bottom simulation and it is used in the sensitivity analysis and calibration. The second model is used in the case study as it accommodates the non-flat seabed. The deduction of the new expression of dissipation term is illustrated in Appendix F.

3 Sensitivity analysis

This chapter discusses the sensitivity analysis which has been carried out to investigate how wave damping effect varies with respect to various parameters related to the model. By varying the value of each parameter, different results which represent various amount of dissipated wave energy are obtained. Based on these results it can be checked whether they are in accordance with theories. This chapter consists of a few sections as followed: the first section presents theory of wave dissipation by vegetation. The second section lists a few literature studies on wave attenuation due to vegetation and floating structures. Its relevance to this research is also discussed. Then the model setup is described in the next section. Hereafter the two sections 'varying wave conditions' and 'varying vegetation characteristics' are presented with respect to sensitivity response of the model. 'Varying wave conditions' are divided into 'significant wave height' and 'peak wave period', while 'varying vegetation characteristics' consists of 'vegetation height', 'vegetation diameter' and 'vegetation density'. Afterwards, the energy spectra for various peak wave periods are presented to show the variance of energy damping along the frequency domain. Finally, other aspects related to this model are discussed.

3.1 Theory

The theory regarding wave dissipation by vegetation can be deduced from the vegetation dissipation term. Relevant parameters are discussed concerning their impact on energy dissipation.

- According to vegetation dissipation term Equation 2-2, wave energy dissipation by vegetation per unit horizontal length is proportional to third power of wave height. From this it can be deducted that a higher wave leads to a higher rate of wave dissipation than a lower wave.
- Wave period also makes a difference from the perspective of energy dissipation. For simplification deep water is assumed here to present the influence of wave period on the wave dissipation.

  For deep water wave length is expressed as $L = \frac{gT^2}{2\pi}$. Wave number is $k = \frac{2\pi}{L}$. Wave angular frequency is $\sigma = \frac{2\pi}{T}$. Substituting in the Equation 2-2, the dissipation term reads:

$$\varepsilon_v = \frac{\sqrt{\pi}}{24}\rho C_D b_v N \frac{\left(\sinh\frac{4\pi^2}{gT^2}\alpha h\right)^3 + 3\sinh\frac{4\pi^2}{gT^2}\alpha h}{T\left(\cosh\frac{4\pi^2}{gT^2}h\right)^3} {H_{rms}}^3$$

Equation 3-1

Since only the wave period is interested here, influences of all other parameters are disregarded. Setting those parameters which are not dependent on period as 1, the following relation is obtained:

$$\varepsilon_v \sim \frac{\left(\sinh\frac{4\pi^2}{gT^2}\right)^3 + 3\sinh\frac{4\pi^2}{gT^2}}{T\left(\cosh\frac{4\pi^2}{gT^2}\right)^3}$$

Equation 3-2

The right part is denoted as Dv and it decreases as wave period increases, as shown in Figure 3-1.

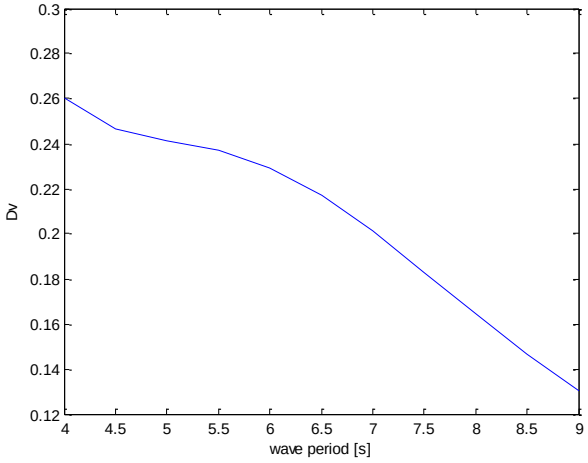

Figure 3-1: Relation between Dv and wave period

Correspondingly, the amount of dissipation decreases with an increasing wave period.

- As can be easily seen in the dissipation term, dissipation is proportional to vegetation density and diameter. It indicates that larger vegetation density and vegetation diameter will result in more dissipation.
- Similar with the approach used in determining the influence of wave period, the relation between dissipation term and vegetation length is obtained as:

$$\varepsilon_v \sim \sinh \alpha h^3 + 3 \sinh \alpha h$$

Equation 3-3

The right hand of this relation is an increment function with respect to vegetation length αh, as shown in Figure 3-2. It indicates dissipation increases when vegetation length increases. The right part of Equation 3-3 is denoted as Ev.

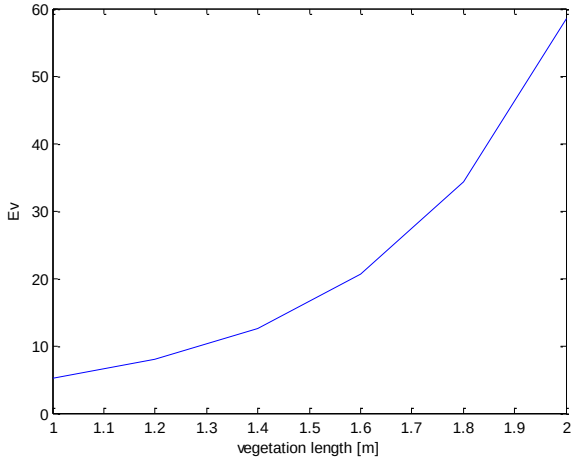

Figure 3-2: Relation between Ev and vegetation height

3.2 Literature study on wave damping studies

Many studies have been carried out on wave damping due to the vegetation mounted on the sea bed. Also some researches have been performed on the floating structure.

- (Dijkstra & Uittenbogaard, 2010) developed a numerical model that describes the dynamic interaction between very flexible vegetation and flow. In this study this aspect is not considered as SWAN is not able to cope with interaction between flexible vegetation and wave. The impact of flexibility is indicated in the bulk drag coefficient.
- Suzuki et al (2011) developed SWAN-VEG model which is used in this research. In his model layer schematization is included, making the first model used in this study feasible.
- (Anderson & Smith, 2014) conducted a flume test on the wave attenuation by flexible, idealized salt marsh vegetation. It has been concluded from the test that wave attenuation are most dependent on stem density and the ratio of stem length to water depth. Besides, wave dissipation increases slightly with wave height. It also revealed a preferential dissipation of higher-frequency wave. This test is similar to the

experiment which was conducted in Technology University of Braunschweig except that bottom mounted vegetation was used. It may provide some insight into the result of the flume test associated with this research.

- Spectral energy dissipation of random waves due to salt marsh vegetation has been conducted by (Jadhav, Chen, & Smith, 2013). It concluded that the energy dissipation varies across the frequency domain with the largest magnitude observed near the peak frequency. This conclusion can be checked in the sensitivity analysis regarding wave spectrum.
- Zhan Hu et al (2014) performed a laboratory study on wave dissipation by vegetation in combined current-wave flow. It has been found that currents can either increase or decrease wave dissipation depending on the ratio of imposed current velocity to amplitude of horizontal wave orbital velocity. In this study current is not considered due to the fact that current will complicate the wave dissipation mechanism by floating vegetation on the one hand, one the other hand current is not addressed in the flume test, rendering its influence cannot be represented accurately in the numerical model through calibration.
- A large-scale physical modeling of wave damping by floating mussel structures has been conducted by (Van Steeg & Van Wesenbeeck, 2011). A prediction tool for wave transmission, reflection and dissipation is developed by them. Also, floating brushwood mattresses has been tested by them in terms of wave damping. As the material used by them shows different property from floating seaweed, consequently the application of their result to this research remains quite limited.

3.3 Model setup

A model is set up for the sensitivity analysis, in which the computational area, bathymetry, wave boundary conditions and vegetation conditions are defined. A simple square shape of computational domain is chosen, with side width of 125 m × 125 m. The width of computational area is required to reach certain value in order to eliminate the boundary effect. The grid cell of this model is set as 5 m × 5 m, as a proper resolution is required to increase the accuracy of output. An exploration about width of computational domain and the grid size is shown in Appendix B.

Water depth is set as 20 m which is a representative value of the water depth for offshore conditions. Shape of JONSWAP spectrum is used for boundary wave. Waves (blue arrows in Figure 3-3) approach perpendicularly to the left side of the domain and is present along the whole left boundary. The vegetation field is set identical to computational area. Also, the output locations are chosen approximately along the center line of computational area (the

black line in the figure), and three output locations (asteroids in Figure 3-3) for spectrum analysis are at 0 m, 60 m and 125 m in horizontal axis and all at 65 m in vertical axis. They are represented in the Figure 3-3.

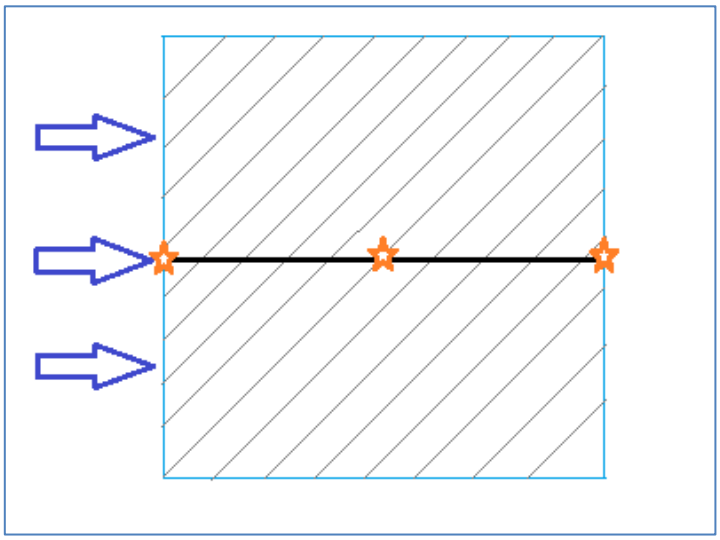

Figure 3-3: Presentation of computational area

All the physical processes which exist in the real situation are disregarded in the sensitivity analysis due to specific reasons. Wind is not considered as an input because the objective of this sensitivity analysis is to investigate the influence of seaweed only. For the same reason bottom friction is omitted in the simulation. Besides, as the bottom is flat, no influence of depth-induced breaking will be involved. Also, the process of white capping is turned off in order to eliminate possible influences on wave damping caused by wave breaking due to large steepness.

All varied parameters are listed in Table 3-1. When one parameter is varied to determine its effect on wave attenuation, all other parameters are kept constant in their default value. All default values are set as shown in Table 3-1:

Table 3-1: Default values for parameters

Parameter	Default value
Peak wave period	5 s
Significant wave height	1 m
Drag coefficient	0.2
Vegetation diameter	0.01 m
Vegetation density	200/m^2
Vegetation height from the surface	3 m

3.4 Varying wave characteristics

3.4.1 Significant wave height

In this analysis the wave height is varied for five values. The peak period remains constant for the five conditions with a value of 5 s. Attention is paid to the choice of wave height in terms of wave steepness. Wave steepness (s) is defined as the ratio of wave height (H) to the wavelength (L).

$$s = \frac{H}{L}$$

Equation 3-4

In deep water wave length is expresses as:

$$L = \frac{gT^2}{2\pi}$$

Equation 3-5

g is gravitational acceleration, T is wave period.

Due to the limit of wave steepness the wave height cannot be chosen too large. The limit of wave steepness for regular waves in deep water is 0.14 (Miche, 1944), for irregular waves the limit is normally set as 0.05. In this case the limit wave height is calculated as 1.95m. The value of significant wave height is varied as followed:

Table 3-2: Significant wave height

Significant wave height [m]
0.6
0.8
1.0
1.2
1.4

The results are interpreted by the ratio between the significant wave height at the end of vegetation (remaining wave height) and the initial significant wave height at the front edge of vegetation. It is named as ratio of remaining wave height. “End of vegetation” is interpreted from the point of view of wave approaching direction. The wave height along the vegetation field is presented in Figure 3-4. The ratios of remaining wave height for different wave heights are presented in Figure 3-5.

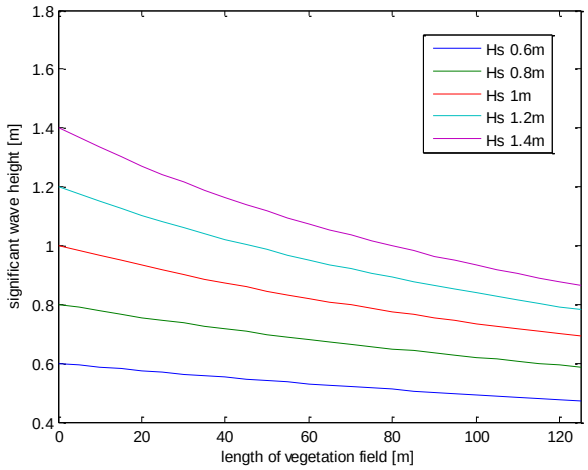

Figure 3-4: Effect of wave height on dissipation

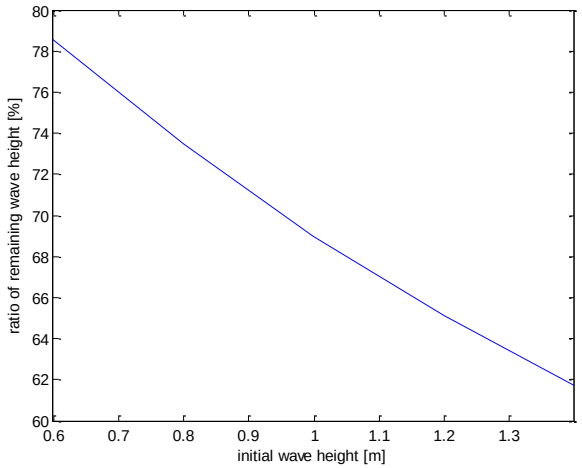

Figure 3-5: Ratio of remaining wave height

Figure 3-4 shows that wave attenuation is more significant for larger significant wave heights. This is indicated by the largest steepness of the curves at the beginning of vegetation field where the wave height has not been reduced. The steepness decreases gradually along the vegetation field. In order to present it more mathematically, the ratio of remaining wave height is plotted versus initial wave height in Figure 3-5. It is found that larger initial wave height results in a smaller ratio of remaining wave height, which means higher rate of energy damping. From the result it can be concluded that wave damping does not change in a linear relation with respect to wave height, i.e., the reduced wave height is not proportional to initial wave height.

This conclusion can also de deduced manually from equation *(A- 2)* and *(A- 6)*. With transformation the following relation is obtained:

$$\frac{\partial {H_{rms}}^2}{\partial x} \sim -{H_{rms}}^3$$

Equation 3-6

H_{rms} is root mean squared wave height which represents the wave energy most closely. Further the following relation is reached:

$$\frac{\partial H_{rms}}{\partial x} \sim -{H_{rms}}^2$$

Equation 3-7

Obviously this relation does not show linear relation between reduced wave height and significant wave height.

3.4.2 Peak wave period

In this section variance of energy damping for various peak wave periods is shown. Five periods are used in this analysis. The period is supposed to fall in certain range to meet the requirements of wave steepness. With the steepness relation the minimum peak wave period is found as 3.6 s. The significant wave height is kept constant for the five simulations to determine merely the influences of wave period. The five simulations use the period values specified in Table 3-3 and the result is shown in Figure 3-6.

Table 3-3: Peak wave period

Peak wave period [s]
5
6
7
8
9

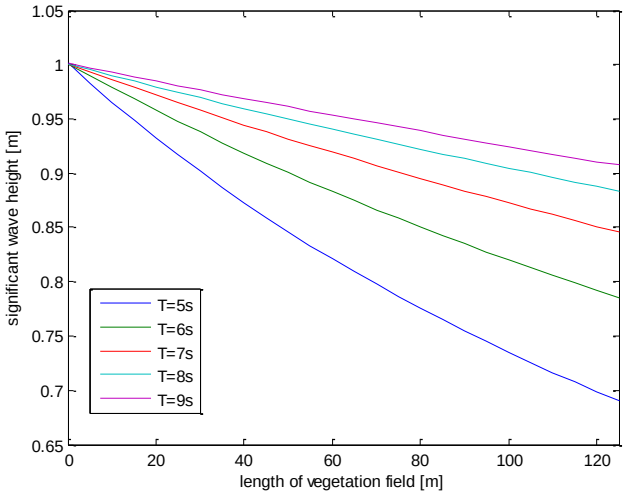

Figure 3-6: Effect of Tp on wave attenuation

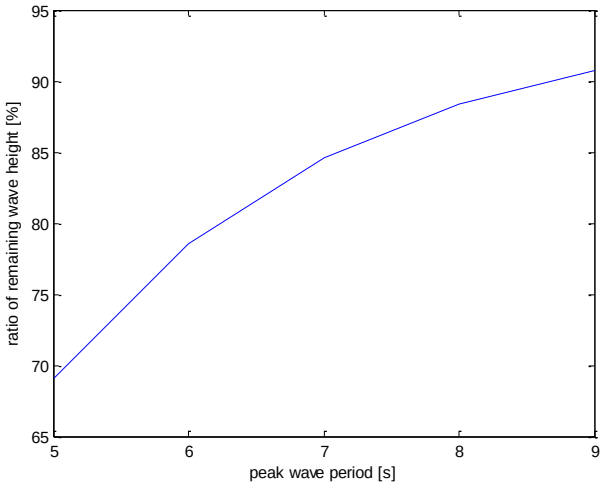

Figure 3-7: Ratio of remaining wave height versus period

It can be clearly observed that the wave period makes a significant difference on wave damping. Waves with the same wave heights but different periods lead to various degree of energy damping. It appears from this figure that the larger wave period results in less wave damping. Ratio of remaining wave height (the same as in Figure 3-5) is plotted along wave period as in Figure 3-7. A larger ratio of remaining wave height refers to less damping. It shows an opposite trend compared with the influence of wave height.

In order to see the combined effect of wave height and wave period on the wave energy damping, a matrix is made with various combinations between wave height and wave period. The ratios of remaining significant wave height are presented.

Table 3-4: Ratio of remaining wave height for H/T combinations

H/T	5s	6s	7s	8s	9s
0.6m	0.786	0.857	0.901	0.927	0.943
0.8m	0.735	0.819	0.873	0.905	0.925
1m	0.691	0.786	0.846	0.884	0.907
1.2m	0.652	0.754	0.821	0.863	0.891
1.4m	0.618	0.726	0.799	0.845	0.875

From Table 3-4 it can be observed that with the wave period remaining constant, increasing wave height leads to decreasing ratio of remaining wave height, which means greater extent of energy dissipation. With the same wave height, when wave period goes larger, less energy dissipation is seen. This is conclusion from the previous two sections. Also it is seen that larger wave period does not necessarily leads to larger ratio of remaining wave height as the wave height can also have an influence on it, vice versa. As a result the effect of wave attenuation is determined by the combination of wave height and wave period. It is not accurate to say larger wave height must lead to more dissipation or larger wave period results in less attenuation.

3.5 Varying vegetation characteristics

3.5.1 Vegetation height

Six values of vegetation height are employed to show the contrast of wave attenuation effect between them. The vegetation height is measured from the water level downward as seaweed is floating in the upper water column. The wave height and wave period use default values.

Table 3-5: Vegetation height

Vegetation height [m]
1
2
3
4
5
6

The result is plotted as below:

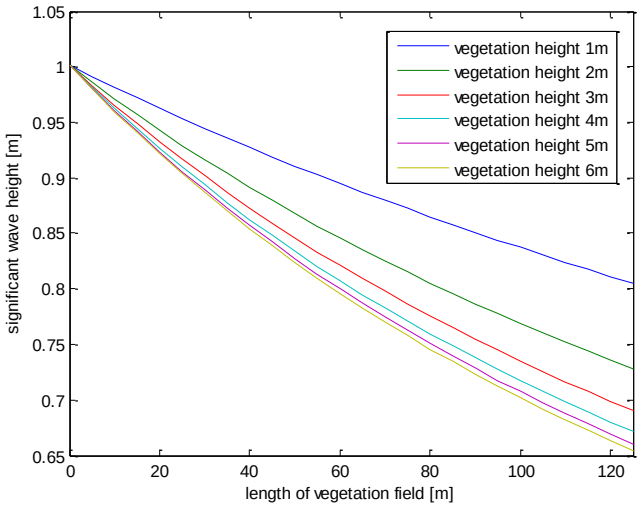

Figure 3-8: Effect of vegetation height on wave attenuation

It can be concluded that larger portion of the wave energy is damped at the upper water layer. The increase rate of damping effect becomes less and less significant with the increase of vegetation length. Compare the two results from vegetation height of 5 m and vegetation height of 6 m, the difference is minor. This can be explained by the difference of water particle velocity at different elevations of water column. The wave has a period of 5 s, which gives a deep water wave length of 39 m. Since water depth (20 m) is larger than half of the wave length, deep water condition can be regarded. The horizontal water particle velocity in deep water is formulated as:

$$u = wae^{kz}\sin(wt - kx)$$

Equation 3-8

Where w is angular frequency, a is wave amplitude, k is wave number, z is vertical coordinate positive upward, with z= -20 m at the location of bottom. Water particle velocity will be decreasing when it gets closer to the bottom. According to equation *(A- 4)* the damped energy will decrease correspondingly. As a result, same length of vegetation in the lower column would result in less wave energy damping than that in upper column. It can be inferred that at the bottom there is hardly damping since the horizontal velocity of water particles at that position is nearly zero, in the case of deep water.

3.5.2 Vegetation diameter

Three diameters are chosen for sensitivity analysis. Even though these values are chosen arbitrarily, they do present the influences of vegetation diameter on the effect of wave attenuation. These diameters values are listed in Table 3-6 and the result is indicated in Figure 3-9.

Table 3-6: Vegetation diameter

Vegetation diameter [m]
0.01
0.02
0.03

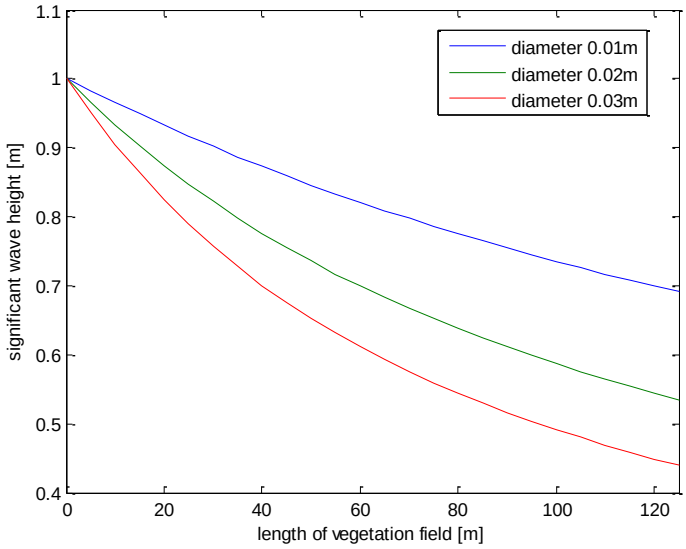

Figure 3-9: Effect of vegetation diameter on wave attenuation

This complies with the theory obtained in 3.1. According to Equation 2-2, the larger the vegetation diameter, the larger drag force will be exerted on the waves, which leads to larger damping.

3.5.3 Vegetation density

Vegetation density is the number of vegetation stems per square meter. Three sets of values are chosen.

Table 3-7: Vegetation density

Vegetation density [/m^2]
200
400
600

The larger the number of vegetation per unit area, the more damping will be exerted on waves. The result is illustrated in the figure below:

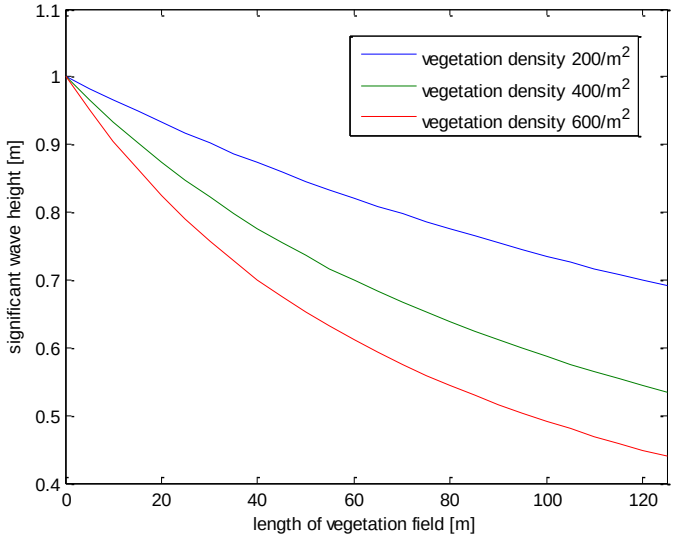

Figure 3-10: Effect of vegetation density on wave attenuation

The result in Figure 3-10 is exactly the same as that in Figure 3-9. This is because the products of C_D, b_v and N are the same for these two sections.

3.6 Wave spectrum

Irregular wave is considered as combinations of some regular waves components with various frequencies and energy. An analysis regarding energy damping along frequency domain is carried out to determine wave energy dissipation pattern along wave frequencies. Only spectrum for one period is presented here. More spectra are provided in Appendix C.

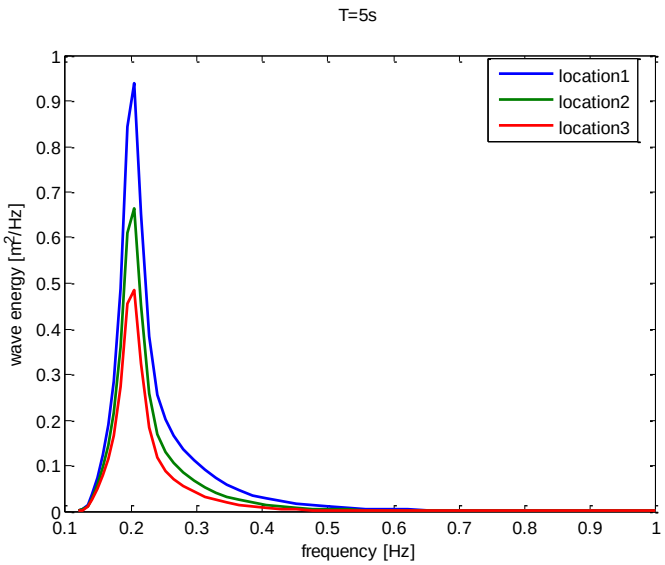

Figure 3-11: Wave spectrum for T=5 s

From all the figures related to the spectrum analysis, the following conclusions are drawn:

- The largest portion of energy dissipation occurs around the peak frequency in absolute sense. This feature verifies influence of wave height on wave damping. At peak frequency, the wave component contains the largest energy. As a result the largest dissipation of energy occurs around this frequency.
- As peak period increases, the wave spectrum tends to become narrower and narrower.
- At low frequency domain (somewhat lower then peak frequency), hardly any energy dissipation is seen. This is in accordance with finding about wave period: larger wave period results in less damping.
- At frequency domain somewhat higher than peak frequency, certain degree of energy damping is observed. The energy dissipation shows decreasing trend as the wave period increases. This is in accordance with the finding from the influence of wave period: shorter wave results in higher dissipation.
- With the increase of peak wave period, the energy loss is decreasing. We can easily observe this phenomenon from the closer and closer positions of the three curves as the peak wave period increases. This is in accordance with the theory regarding effect of wave period on wave attenuation: larger wave period gives rise to less dissipation.

3.7 Other aspects of sensitivity

In addition to the analysis above, other aspects like influences of smaller vegetation patch and directional spreading are also investigated.

The wave height variance in the whole computational area is presented as Figure 3-12. The wave height decreases gradually along the vegetation field.

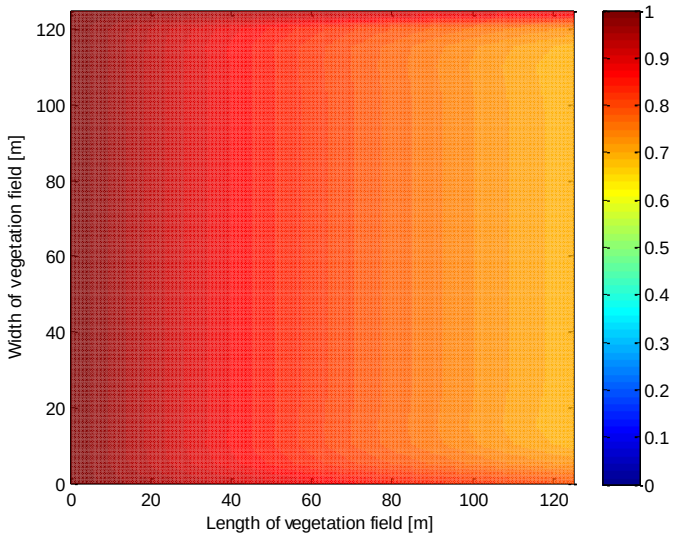

Figure 3-12: Wave height for the whole computational area

Also, a vegetation patch which is smaller than computational area is chosen to show the contrast with full vegetation area. It shows that smaller vegetation field leads to less wave dissipation.

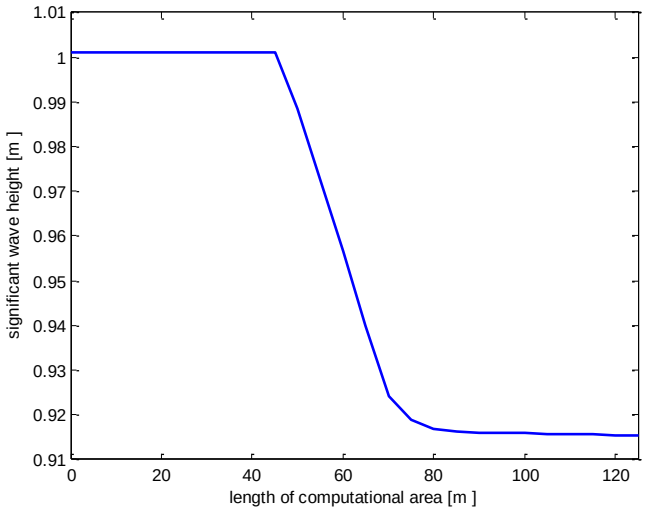

Figure 3-13: Wave height change for vegetation patch

Compared with simulation for full vegetation in which the wave height decreases along the whole domain, the wave height Figure 3-13 only reduces in the middle part of computational area where the vegetation exists. Besides, the wave attenuation is less significant than that of full vegetation. This is reasonable as the waves pass through less vegetation field, so less attenuation is obtained. The wave and vegetation patch (green area) are depicted in the Figure 3-14.

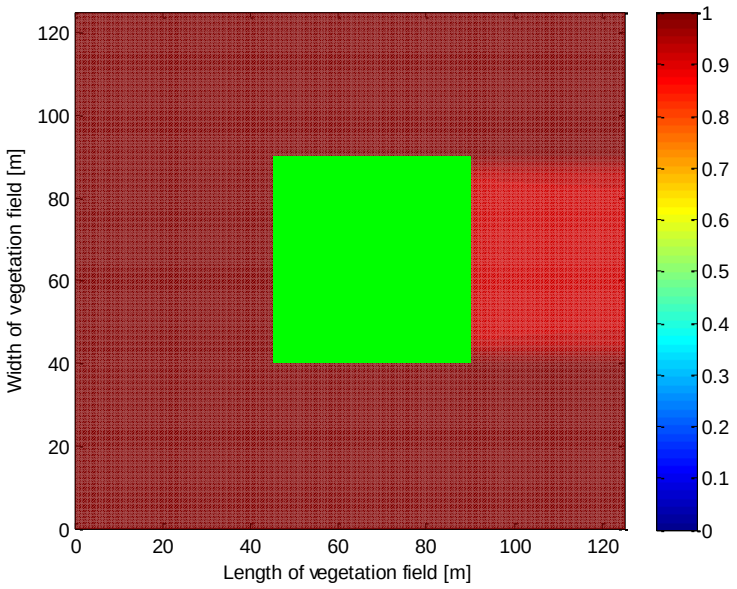

Figure 3-14: Wave height diagram for small vegetation patch

Last but not least, the influence of directional spreading is also investigated. Six values of coefficient of directional spreading are varied. The differences of wave height change for different sets are presented in the Figure 3-15. 5 are an indication number of real offshore region while 800 indicates the wave spreading is minimal and unidirectional approaching is conserved.

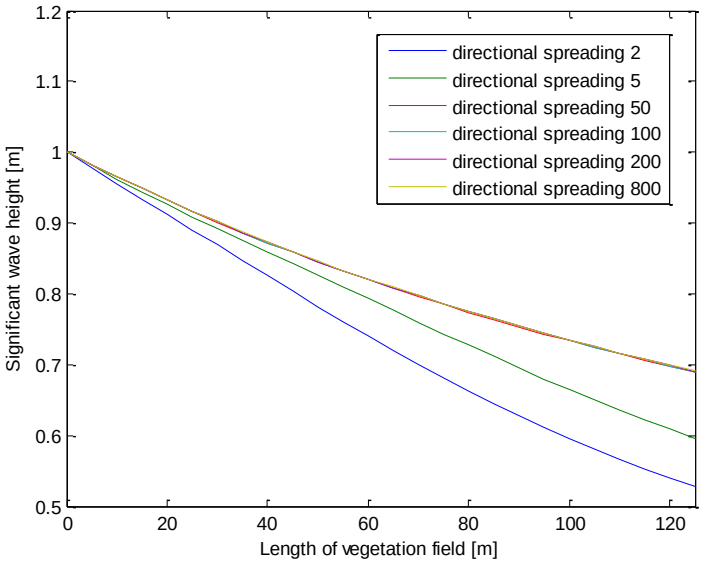

Figure 3-15: Influence of directional spreading on the wave height

Larger coefficient of directional spreading indicates less spreading, and as a consequence less energy is lost. As seen from the figure above, wave with directional spreading coefficient of 2 results in the least wave energy compared with other sets. A wave diagram for the whole computational area is drawn for coefficient of 2 in Figure 3-16. As can be seen, due to the spreading, there is transition from larger wave height to smaller wave height behind the vegetation patch instead of straightforward change as showed in Figure 3-14.

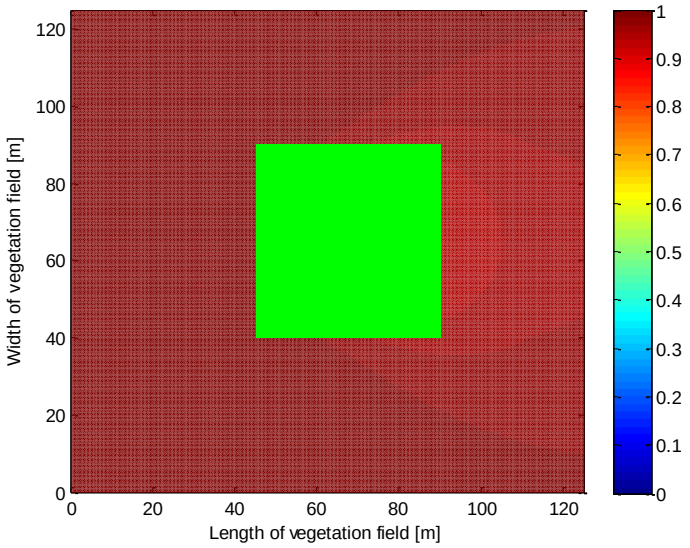

Figure 3-16: Wave height diagram for spreading coefficient of 2

3.8 Discussion

For the sensitivity analysis some simplifications are made. The objective of sensitivity analysis is to test the model with regard to sensitivity response and check whether it complies with the theory. Therefore it is not necessary to put much effort on them. However, it is good to observe them and improve these aspects in subsequent study.

- For all the simulations that have been performed above, the computational area is set identical to the vegetation field, which is super simplified. However, the sensitivity analysis is just performed to give a presentation with respect to the individual influence of each parameter involved in this model. As a result some details are omitted. Though, for the subsequent calibration a new grid is supposed to be created in order to comply with the physical experiment, and all the necessary details will be included.
- Parameters such as drag coefficient and vegetation diameter are chosen without much consideration. In the sensitivity analysis stage, the accuracy of these values is not emphasized. For the later calibration, much attention is required to use appropriate values which reflect the real circumstances.
- The analysis performed above is based on two dimensional computations. Besides, one dimensional simulation was run for all the cases above to compare them. By contrast with results in two dimensions, the difference is hardly noticeable.

3.9 Conclusion

To summarize all the results obtained in the analysis, some conclusions are listed as below.

- Larger wave height (wave period being constant) undergoes energy damping in greater extent.
- Wave with large peak period (wave height being constant) throughout vegetation field shows less wave damping.
- Largest portion of energy is dissipated around peak frequency for irregular waves in absolute sense.
- Larger vegetation height, vegetation diameter and vegetation density result in more energy dissipation.
- The wave attenuation effect in the upper water column is more significant than that in the lower column.

These conclusions are in accordance with theory presented in section 3.1. However, the applicability of this model to the real cases remains to be investigated as the drag coefficient has not been verified. Therefore it is required to calibrate this model. Making this model applicable in modeling the real situations will be explored in the next chapter, in which the calibration is carried out with the data obtained from physical experiments.

4 Calibration

This floating seaweed model modified in SWAN has not been verified regarding its effectiveness. Therefore calibrating this numerical model is required. As stated previously the method to calibrate this model is to determine a proper drag coefficient with the available experimental data.

This chapter describes the calibration of the numerical model with experimental data obtained from flume test. By means of fitting the model simulation with experimental results, it is expected to obtain a suitable drag coefficient which makes the numerical model capable of modeling the real condition. This procedure lays the basis for the application of this numerical model in real case.

4.1 Approach

In the expression of energy dissipation term *(A- 4)*, u represents the horizontal water particle velocity under the condition that stiff plant is assumed. In the case of flexible vegetation it is supposed to be the relative velocity between water particle and vegetation. In this study the relative velocity is not used since it is not monitored and also it is hard to be determined. Besides, vegetation is schematized as stiff cylinder in SWAN. Consequently the velocity of water particle is used instead of relative velocity to represent the dissipated energy, which leads to an overestimation of the energy dissipation caused by flexible vegetation. It requires necessary modification of drag coefficient in order to properly represent the energy dissipation by flexible vegetation. In this context, the drag coefficient serves as a bulk parameter which accommodates the uncertainty of other parameters related to the floating vegetation model. As a result the bulk drag coefficient is the factor left to be calibrated. Besides, different vegetation possesses different property of flexibility, which indicates different relative velocity to water particle. It leads to different rate of energy dissipation, which can be represented by different bulk drag coefficient. As a consequence the calibration is performed individually for different types of mimics which represent different types of seaweed.

The traditional method of calibration and validation of drag coefficient goes as follows:

1. The calibration is carried out by means of fitting the experimental data and numerical simulation. This fitting is done by adjusting drag coefficient to achieve a best fitted relation between numerical model result and physical data. Through this stage a tuned drag coefficient is acquired.
2. Applying the above-obtained drag coefficient to the simulation with another vegetation density which corresponds to a second set of experiments. Then check whether the

model is still equal to describe the experimental results properly, namely, checking if the tuned drag coefficient is still valid. If not, repeat these two steps until a most desirable drag coefficient is obtained.

Different from the conventional way in which experimental data for one vegetation density is used as calibration while experimental data for a second vegetation density is used for validation, in this study one best-fitted trend line is employed for all data for one type of vegetation mimic, due to the limitation of the number of available data. Also, the best-fitted drag coefficient for the two vegetation densities shows quite different values, which makes the conventional method least applicable.

It has been verified that the drag coefficient depends not only on wave characteristics but also vegetation properties. Various wave conditions as well as vegetation characteristics give rise to distinct drag coefficients. As a result the drag coefficient is determined as function of wave characteristic and vegetation property. Two parameters are generally used to represent the wave and vegetation characteristics. One is Keulegan-Carpenter number (KC-number) and the other is Reynolds number.

- KC-number is a dimensionless parameter which describes relative importance of the drag forces over inertia force for object in an oscillatory fluid flow. The equation reads:

$$KC = \frac{u_{max} T_p}{b_v}$$

Equation 4-1

u_{max} is the maximum horizontal velocity of the orbital motion of wave. T_p is the peak wave period. b_v is the characteristic length scale of the object. In this study it refers to the vegetation width or diameter. The maximum horizontal velocity of wave motion is determined at the surface and is calculated as:

$$u_{max} = \frac{\sigma a}{\tanh(kh)} = \frac{\left(\frac{\pi H}{T_p}\right)}{\tanh\left(\frac{2\pi h}{L}\right)}$$

Equation 4-2

σ is angular frequency of wave, a is wave amplitude which is half of wave height, k is wave number, h is water depth, H is wave height, L is wave length. Substituting this expression in Equation 4-1, finally KC-number reaches:

$$KC = \frac{\pi H}{b_v \tanh\left(\frac{2\pi h}{L}\right)}$$

Equation 4-3

- The Reynolds number is also a frequently used term to indicate the relative importance of momentum force and viscous force for given flow conditions. It is formulated as:

$$Re = \frac{u_{max} b_v}{v}$$

Equation 4-4

Substituting Equation 4-2 to Equation 4-4 leads to Reynolds number expression:

$$Re = \frac{\left(\frac{\pi H}{T_p}\right) b_v}{\tanh\left(\frac{2\pi h}{L}\right) v}$$

Equation 4-5

σ is angular frequency, a is wave amplitude, k is wave number, h is water depth, H is wave height, L is wave length. v is kinematic viscosity of water which is $10^{-6}\, m^2/s$.

In the experimental setup the deep water condition is not met. The wave length needs to be calculated with aid of dispersion equation, which is given as:

$$L = \frac{gT^2}{2\pi} \tanh\left(\frac{2\pi d}{L}\right)$$

Equation 4-6

L is wave length in arbitrary water depth d. T is wave period. This dispersion relationship is an implicit expression which required an iteration process to calculate the wave length. An explicit expression which approximates the solution closely is given by Eckart (1952):

$$kd \approx \alpha(\tanh \alpha)^{-1/2} \quad with\ \alpha = \omega^2 \mathrm{d}/\mathrm{g}$$

Equation 4-7

As a result the wave length is obtained as:

$$L = \frac{gT^2}{2\pi}\left(\tanh \frac{4\pi^2 d}{gT^2}\right)^{1/2}$$

Equation 4-8

After obtaining the calibrated drag coefficients for all wave conditions, a best-fitted trend line is achieved between drag coefficient and KC-number and Reynolds number.

4.2 Experiments setup

The experiment was carried out in a wave flume in Technology University of Braunschweig in Germany. The flume has a dimension of 90 m in length, 1 m in width and 1.25 m in depth. At the end of the flume, rocks with a length of few meters are placed to absorb waves so as to eliminate the reflection. The flume used is the right one in Figure 4-1.

Figure 4-1: Flume used for the experiment (the one at right hand)

In the flume test, there exist three dissipation sources: bottom and boundary friction, H profile (which represents the hosting structure) and vegetation mimics. The individual effect of each dissipation source needs to be determined. To achieve this goal three scenarios have been considered for the experiments setup. Each of the scenarios has a specific objective. For the first scenario, neither H profile nor vegetation mimics are implemented, which is intended to see the effect of inherent influencing factors which are present in the flume test, like bottom friction and boundary of the flume or other disturbing effect if applicable. In the second scenario only H profile is applied to test the damping effects of hosting structures. In addition to these two scenarios, both the H profiles and vegetation mimics are implemented in the third scenario, which is intended to present the overall dissipation of the scaled seaweed aquaculture.

In the experimental setup, a vegetation field with length of 4.2 m and width of 0.33 m is implemented in the experiment. Within this field the manufactured vegetation mimics are implemented. Two vegetation densities (five strings and ten strings) are varied for the vegetation, which represent 794 stems /m^2 and 397 stems /m^2 respectively. Along this vegetation field, five H profiles with height of 0.2 m are spaced with equal distance to each other to represent the hosting structure to which the seaweed is attached.

Figure 4-2: H profiles and mimics

For the water condition, the water depth is set as 0.67 m based on scaling from real conditions. As for wave conditions, a few sets of combinations are used. For each set, both regular waves and irregular waves are implemented. Mean wave period is used for regular wave and peak period is used for irregular wave. The wave conditions are listed below:

Table 4-1: Wave conditions implemented in experiment

Wave height [m]	0.1		0.2	
Wave period [s]	1.4	2.2	1.5	2.6

As for vegetation mimics used in the experiment, three sorts of material are utilized, namely plastics tubes, wooden rods and Christmas decoration, which represent Laminaria digitata, Saccharina latissima and Ulva lactura respectively. For plastic tubes and wooden rods, the length of each mimic is 7 cm and the diameter is 5 mm. The Christmas decoration shows different configuration. It is formed in a bunch instead of existing as individual objects. The diameter of the bunch is set as 7 cm, the same as the length of the other two vegetation mimics.

Figure 4-3: Vegetation mimics: tube (left), wooden rod (middle) and Christmas decoration (right)

Along the flume, in total 10 wave gauges are implemented along the flume. Each gauge measures the water surface elevation at its own location. The measured information is transported to computer and each measuring point represents one channel. Three of them are located 4 m before the vegetation field, noted as 1, 2 and 3. One gauge is implemented right before the vegetation field which is at location number 4, three in the middle of vegetation field which are 5, 6, 7, three at the lee side of vegetation field, namely 8, 9 and 10. In addition, two ADV are implemented on both sides of vegetation field at location 4 and 8 to measure the particle velocity. The side view is shown in Figure 4-4.

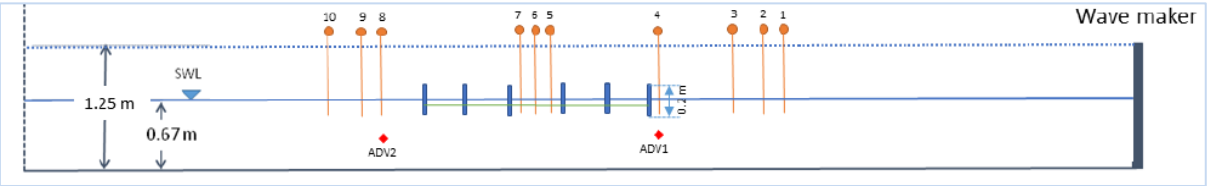

Figure 4-4: Experiment setup

4.3 Vegetation description

This study concerns seaweed aquaculture in North Sea. Therefore three sorts of native vegetation are investigated in terms of their characteristics in order to find representative vegetation mimics and relevant dimension. These three kinds of seaweed are laminaria digitata, saccharina latissima and ulva lactuca, shown in Figure 4-5.

Laminaria digitata is a sort of large brown alga mostly found in the sub littoral zone of North Atlantic Ocean. This kind of seaweed is tough in texture and in dark brown color which can grow to two to three meters. It possesses a conical holdfast with a number of spreading root-like protrusions which functions as anchorage of the plant to the rock. The stipe is flexible and oval in cross section. The blade is large and shaped like the palm of a hand with quite a few finger-like segments. Plastic tubes are used as mimics for this sort of vegetation.

Saccharina latissima is yellowish brown algae. The blade is relatively long but narrow. This seaweed is able to grow to 3 m long and 20 cm wide. The central part of frond is dimpled a little bit and rougher while the margins are smoother with a wavy edge. The frond is secured to the rock by a claw-like holdfast and a short, pliable and cylindrical stipe. Wooden rods are chosen to represent this type of plant in the experiment.

Ulva lactura is a thin flat green alga growing from a discoid holdfast. The margin is somewhat ruffled. This seaweed is relatively shorter compared with the other two types of seaweed. Normally the length can reach 40 cm. The membrane is two cells thick, with a soft and translucent texture. Considering its feature, Christmas decoration is opted to model this vegetation in the flume test.

Figure 4-5: Vegetation laminaria digitata (left), saccharina latissima (middle) and ulva lactuca (right)

4.4 Numerical model setup

4.4.1 Model setup for regular waves

The model is set up the same as the experimental setup with regards to dimension, without scaling. Since not the full length of flume is implemented with vegetation, this numerical model is set just to cover relevant information. The length of computational area starts from point 4 and extends to point 10 to cover the wave information and vegetation field. As a result, the computational area is set as 6 m times 1 m.

The frequency domain is set according to the guidelines in the user manual of SWAN. The lowest frequency is set as somewhat smaller than 0.7 times of peak frequency while the highest frequency is set as somewhat higher than three times of peak frequency. The spectral direction is set as half circle. The directional spreading coefficient is set as 500 in order to achieve unidirectional incidence of waves. In order to resolve the directional spreading angle which is approximately 3° with such a directional spreading coefficient, the directional space is divided to 90 sectors with each sector of 2°.

However, there is remarkable inconsistency between target wave height and the measured wave height. For accuracy reason the measured wave height is used. The input wave period is used as listed in Table 4-1 as this parameter shows consistency between target value and the measured value. The MEAN wave period is used for regular waves.

4.4.2 Model setup for irregular waves

The setup of simulation for irregular waves is basically the same as that for regular waves, except for that the wave boundary changes to JONSWAP shape spectrum, which is the wave spectrum implemented in the flume test. The wave period uses the value obtained in the data analysis. Besides, the PEAK period is used instead of MEAN period.

4.5 Determination damping effect caused by only vegetation

As presented previously, three scenarios of experimental conditions are tested. In order to determine the effect of vegetation, the effects of bottom friction, boundary effect and influence of hosting structures have to be deducted from the third test scenario. After deducting the effect of structures and other dissipation factors, we get the effect of wave attenuation generated only by seaweed. The approach is as follows:

The incident wave height is noted as H_{in}. The out-coming wave heights for the three scenarios are H_{out1}, H_{out2} and H_{out3} respectively. The energy dissipated by bottom and boundary effect can be presented as H_{in}^2-H_{out1}^2 (this is only symbolic rather than exact representation) as wave energy is proportional to square of wave height. For the second scenario the dissipated energy by H profiles and bottom friction is expressed as H_{in}^2-H_{out2}^2.

For the third scenario the dissipated energy is H_{in}^2-H_{out3}^2 which results from the total effect of bottom friction, boundary effect, H profiles and vegetation mimics. Then the energy dissipated merely by vegetation is obtained as [(H_{in}^2-H_{out3}^2)-(H_{in}^2-H_{out2}^2)] = H_{out2}^2-H_{out3}^2. The remaining energy is represented by [H_{in}^2 – (H_{out2}^2-H_{out3}^2)] = H_{in}^2-H_{out2}^2+H_{out3}^2. Then the remaining wave height is $\sqrt{H_{in}^2 - H_{out2}^2 + H_{out3}^2}$. Use H_{in} as boundary wave condition in the numerical model, adjusting the drag coefficient until the out-coming wave height reaches the same value as remaining wave height. This resulted drag coefficient is representative of damping effect of floating vegetation only.

However, the above-mentioned determination of influence of only vegetation may be superfluous. As the hosting structures are implemented in the experiment, it is only necessary to calibrate the drag coefficient with the data from the third scenario. The impact of hosting structure is included in the calibrated drag coefficient.

4.6 Data processing and acquisition

The data processing is conducted separately for regular wave and irregular wave, due to different characteristics of time series.

4.6.1 Regular waves

Around 10000 surface elevations have been recorded at each measuring point. The sampling duration is around 180 seconds with frequency of 60 Hz. After converting the water surface data to a graph, it shows that in some parts the measurements show wiggles. The preliminary method to determine the wave height is described as follows: a span of relatively stable duration with nearly 30 waves is taken, and the time series are smoothed with a Mat-lab script for the convenience of determining maximum and minimum values properly. Then some maximums and minimums are obtained, and the mean wave height is calculated. All the 10 measuring points are analyzed. However, the method used above is only suitable when the wave is harmonic. Checking the wave profile it is shown that there exists some sort of nonlinearity. It shows that wave crest is somewhat steeper than wave trough. Therefore, for the purpose of determining the mean wave height more accurately, a better method proposed by Prof.dr.ir Ad J.H.M Reniers was used, which is to calculate the variance of surface elevation η with Mat lab. The root mean square wave height is calculated as:

$$H_{rms} = \sqrt{8\eta}$$

Equation 4-9

Similar to the previous method, under each wave condition, all the time series are checked and a span is found where the time series are relatively stable in the beginning part of time series after the wave has developed fully. For example, for wave condition (H=0.2 m, T=1.5

s), the selected data starts from time point of 50 s and 20 waves are chosen. The same holds for wave (H=0.1 m, T=2.2 s). For wave condition (H=0.2 m, T=2.6 s), span is taken starting from time of 30 s and 15 waves are picked while for wave (H=0.1 m, T=1.4 s) the chosen waves start from time point of 60 s and 20 waves are targeted. All the chosen span are located in the early part of the time series, as the rear part shows some hints of irregularities and the beginning part displays wiggles related to wave developing.

After all wave height at each point is achieved, attention is paid to the usability of the data. After data analysis is completed, some results are unexpected. Basically, when incident waves pass through vegetation field and H profiles, the waves are supposed to show some height reduction. However, for some channels, for example, in the second scenario, channel 5 and 9 has higher wave height than incident wave height. The reason behind the unexpected data is explored, given in Appendix D. Despite this, the other data are still applicable to determine the incident wave height and the out-coming wave weight, and Channel 5 is not involved in the determination.

After obtaining the wave height at each point, the incident and out-coming wave height for each wave condition is determined. The method is described as follows:

Two groups of points are classified. Group 1 comprises of points 1 to 4 while group 2 consists of point 8 to 10. Disregarding those values which show inconsistency with other points or contradiction with theory in each group, the average of points 1 to 4 are taken as the incident wave height and the mean value of point 8 to 10 are considered as out-coming wave height. Points 5, 6 and 7 only provide some insights into how the wave height changes along the vegetation field. An example of determining incident wave height is given: For plastic tubes 10 strings (H=0.2 m, T=1.5 s) measured wave height for wave gauges 1 to 4 are: 0.175 m, 0.179 m, 0.181 m and 0.172 m. As can be seen that the wave height increases a bit from gauge 1 to gauge 3 and a remarkable decrease is observed at point 4. Also wave height at point 1 is close to that of point 4. It was decided to disregard a value which shows difference no less than 5 mm from point 1. Therefore point 3 is not considered as it is 6 mm higher than point 1. Then the mean of the rest three wave heights is taken as incident wave height.

4.6.2 Irregular waves

For irregular wave, the data is processed by a Mat-lab program provided by Ivo Wenneker from Deltares. Significant wave height and peak period are obtained through this program. The determination of KC-number or Reynolds number employs the root mean square wave height, which is obtained by dividing the significant wave height by a factor $\sqrt{2}$. The same as regular wave, incident wave condition is used for determining KC-number or Reynolds number.

4.7 Results of data analysis

4.7.1 Regular waves

The data processing is performed based on individual scenario. The results are presented individually.

For the first scenario, for the all wave conditions formulated in Table 4-1, the wave height does not show noticeable reduction, as can be observed in Figure 4-6. What is noteworthy is that at channel 5 the wave height is much larger than the other channels, which is due to disturbance during the experiment. However, this does not influence the result of determination of incident and out-coming wave height as channel 5 is not considered. Based on the data it can be concluded that the flume bottom does not cause effective wave energy dissipation within the interested distance.

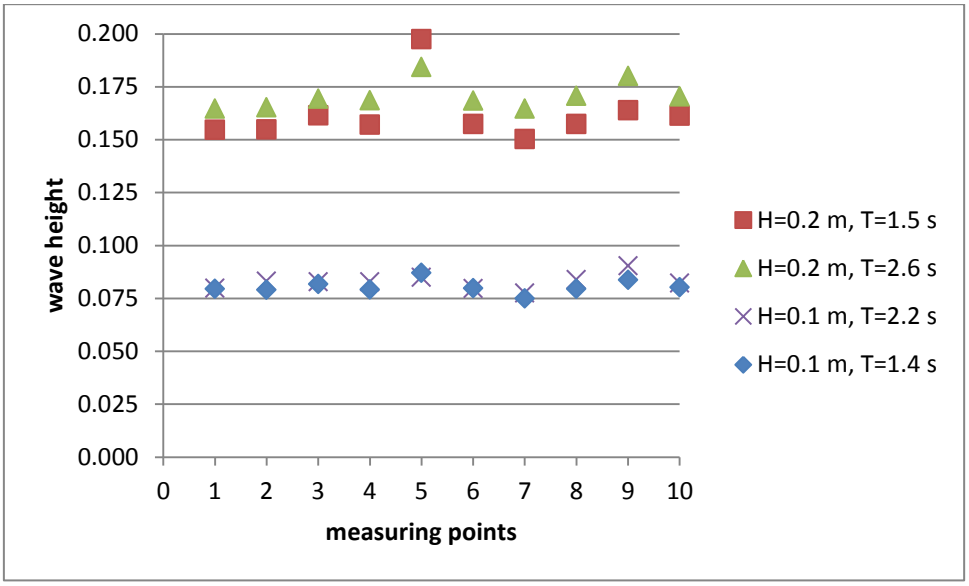

Figure 4-6: Measured wave height in first scenario

For the second scenario, as shown in Figure 4-7, the similar phenomenon is observed at channel 5. The rest of the data shows that the impact of H profile on wave energy dissipation is minimal.

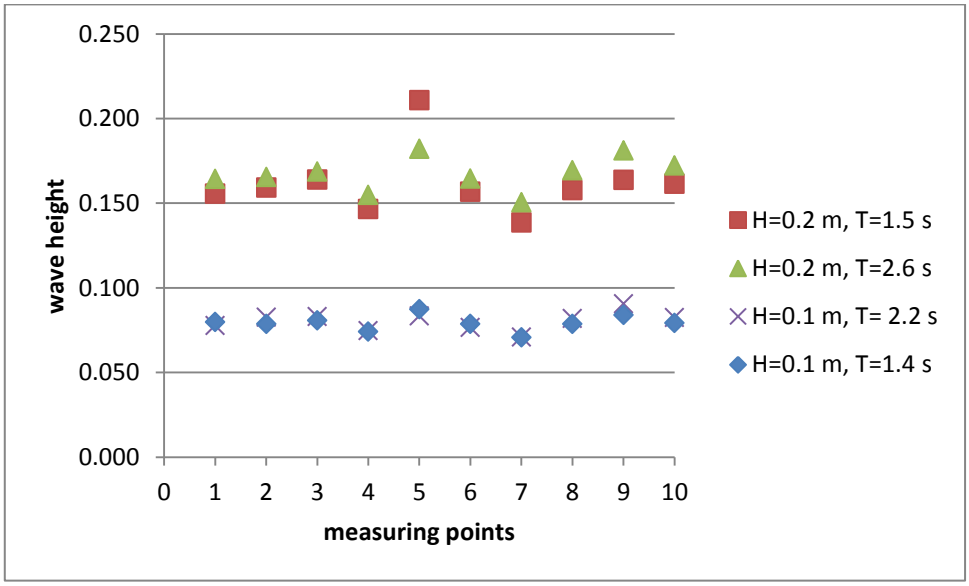

Figure 4-7: Measured wave height in second scenario

For the third scenario, the incident wave height is determined to serve as the initial wave height for the simulation and the out-coming wave acts as a remaining wave height in the simulation when adjusting the drag coefficient. The results are presented in calibration sections for individual vegetation.

4.7.2 Irregular waves

From the results of first scenario and second scenario, the same as regular wave, it is seen that the influences of bottom friction and H profiles are not considerable. Calibration is performed individually for three kinds of vegetation. The results are presented in calibration section.

4.8 Calibration for regular waves

4.8.1 Calibration of Laminaria digitata

This section presents the calibration for vegetation Laminaria digitata. The plastic tubes are used as mimics. The incident wave height and out-coming wave height are obtained by the method described in section 4.6. The wave heights are obtained as followed:

Table 4-2: Incident wave and out-coming wave heights for tubes

	Tubes 10 strings		Tubes 5 strings	
	Incident	Out-coming	Incident	Out-coming
H=0.2 m, T=1.5 s	0.175	0.157	0.175	0.162
H=0.2 m, T=2.6 s	0.185	0.180	0.185	0.180
H=0.1 m, T=2.2 s	0.09	0.086	0.087	0.087
H=0.1 m, T=1.4 s	0.089	0.08	0.089	0.083

In the numerical model, the input wave height is set as incident height in Table 4-2. The calibration is performed through adjusting continuously the drag coefficient until the modeling output is the same as the out-coming wave height. The drag coefficients for these sets are determined as:

Table 4-3: Drag coefficient for tubes

	Cd (Tubes 10 strings)	Cd (Tubes 5 strings)
H=0.2 m, T=1.5 s	1.14	1.45
H=0.2 m, T=2.6 s	0.52	1
H=0.1 m, T=2.2 s	1.44	0
H=0.1 m, T=1.4 s	1.8	2.2

Obviously, the data for the case of (H=0.1 m, T=2.2 s) in tubes 5 strings is not usable since it does not show any dissipation. Therefore this data is disregarded, and then the relation between the drag coefficient versus KC-number and Reynolds number are presented in Figure 4-8.

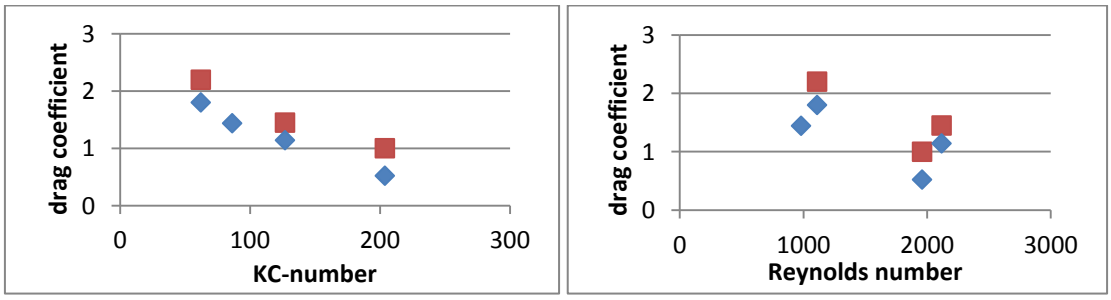

Figure 4-8: Relation between Cd and KC-number (left) or Reynolds number (right)

Blue dots indicate data for 10 strings while red dots refer to 5 strings. The same holds for all the figures following. From the figure it can be seen that the drag coefficient for smaller vegetation density is larger than that for higher vegetation density. It is also observed that drag coefficient decreases with the increase of KC-number. For Reynolds number the trend is not clear. Larger Reynolds number can lead to higher drag coefficient.

Then a best-fitted line is generated with curve fitting tool in Mat lab. Two types of trend are generally used, one is exponential function and the other is power function. A comparison between these two relations is made before opting for the suitable one.

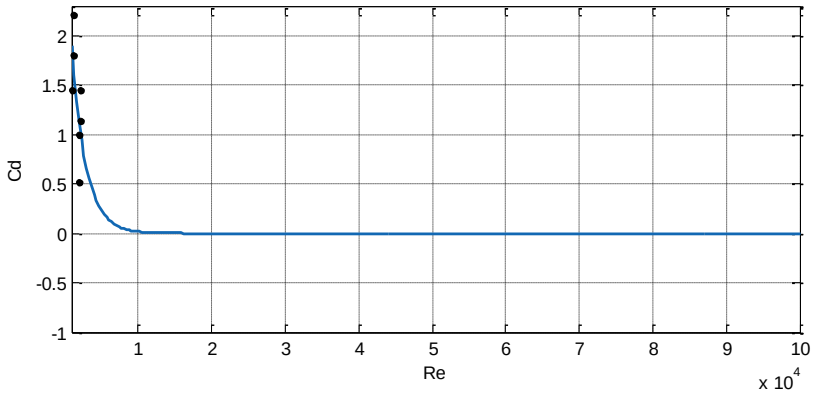

Figure 4-9: Fitting with exponential function

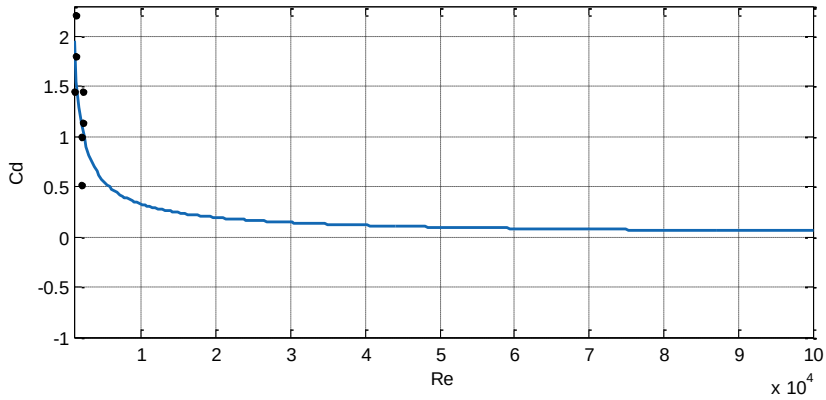

Figure 4-10: Fitting with power function

Figure 4-9 presents the fitting with exponential function. The fitting function is obtained as:

$$C_d = 3.063 * e^{-0.0005181 R_e}$$

Equation 4-10

It is observed from the figure that when Reynolds number is larger than 10000 the drag coefficient reaches nearly zero.

Figure 4-10 shows the fitting with power function. The fitting function is reached as:

$$C_d = 332.4 * {R_e}^{-0.7526} + 3.772 * 10^{-10}$$

Equation 4-11

This fitting curve says the drag coefficient approaches 0.06 within the given domain of Reynolds number.

In real situation, the Reynolds number is much larger than that in the experimental setup. For example, a wave with height of 0.68 m, period of 5.76 s, in water depth of 30 m, with

vegetation diameter 30 cm, the Reynolds number arrives at 78784. Substituting in the exponential function the drag coefficient is obtained as 5.74E-18, which is practically nothing. In the power function a drag coefficient of 0.07 is obtained. According to empirical value, the latter is more reasonable. Checking for other vegetation mimics, the same conclusion is drawn. Therefore, the power function is used in this study.

Besides, due to the much larger vegetation width in real situation than that of mimics used in the test, the KC-number in real situation will be quite smaller than the range obtained in experiment, which leads to a very large drag coefficient. An example is given below. Fitting drag coefficient with KC-number gives the following figure:

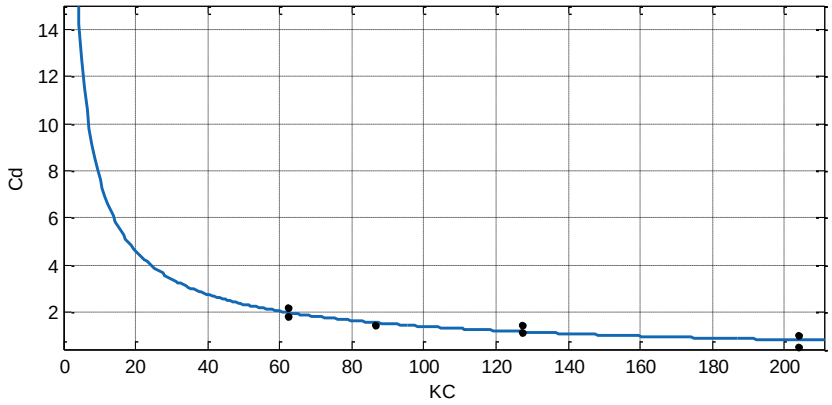

Figure 4-11: Fitting with KC-number

The fitting function is:

$$C_d = 42.1 * KC^{-0.7385} + 1.311 * 10^{-13}$$

Equation 4-12

The same example as above is given for the real situation. A wave with height of 0.68 m, period of 5.76 s, in water depth of 30 m, with vegetation diameter 30 cm, the KC -number arrives at 5.04. It leads to a drag coefficient of 12.75 when applying Equation 4-12. This value is extraordinarily high for drag coefficient of vegetation. The similar findings are gained for the other two types of vegetation. The applicability of KC-number is rendered poor. Therefore only the Reynolds number is used and presented in this section.

As conclusion, the relation between drag coefficient and Reynolds number is Equation 4-11 and the fitting curve is Figure 4-10.

4.8.2 Calibration of Saccharina latissima

This section describes the calibration of vegetation Saccharina latissima. For this kind of vegetation the wooden rods are used in the experiment as mimic. This sort of mimic shares the dimension as that of plastic tubes. The wave height data are gained as follows.

Table 4-4: Incident and out-coming wave heights for wooden rods

	Wooden rods 10 strings		Wooden rods 5 strings	
	Incident	Out-coming	Incident	Out-coming
H=0.2 m, T=1.5 s	0.175	0.158	0.175	0.163
H=0.2 m, T=2.6 s	0.185	0.180	0.185	0.180
H=0.1 m, T=2.2 s	0.087	0.087	0.089	0.088
H=0.1 m, T=1.4 s	0.089	0.08	0.089	0.081

For wave conditions (H=0.1 m, T=2.2 s), vegetation density of 10 strings do not show any energy dissipation and vegetation density of 5 strings shows hardly any wave height reduction. This set would give a drag coefficient of zero or nearly zero, which deviates a lot from the rest of data set, making this set data unusable. Therefore this set of data is not considered in the calibration. The drag coefficients for these sets are determined as:

Table 4-5: Drag coefficient for wooden rods

	Cd (Wooden rods 10 lines)	Cd (Wooden rods 5 lines)
H=0.2 m, T=1.5 s	1	1.3
H=0.2 m, T=2.6 s	0.48	1
H=0.1 m, T=1.4 s	1.7	3

Plotting drag coefficient along Reynolds, the below figures are obtained:

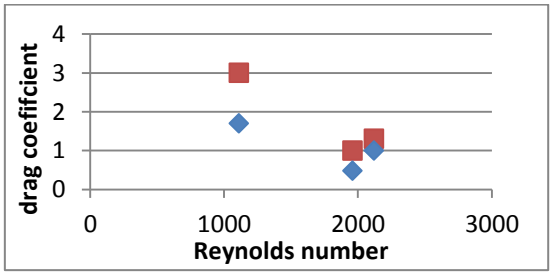

Figure 4-12: Relation between Cd and Reynolds number

The fitting curve is obtained as:

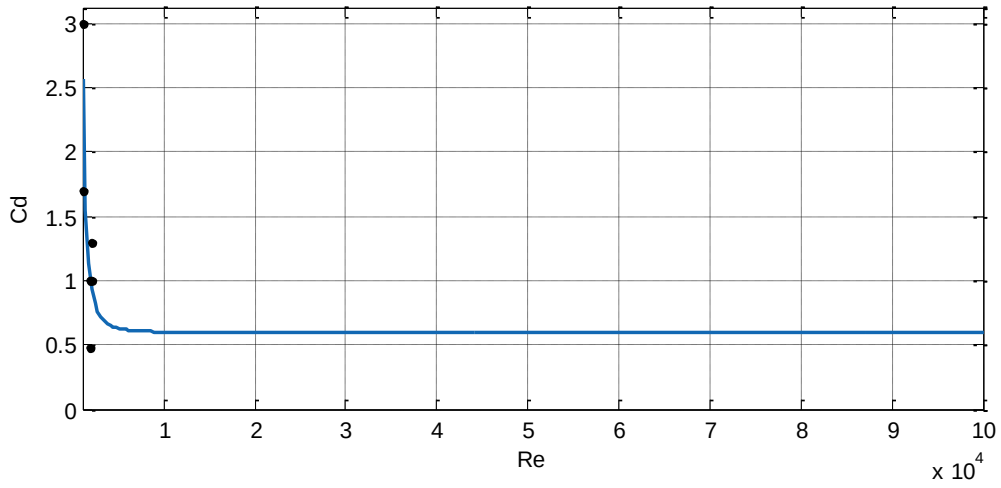

Figure 4-13: Fitting curve for Saccharina latissima

As the reynolds number reaches beyond 10000, the drag coefficient approaches infinitely to 0.6. The function is achieved as:

$$C_d = 1.729 * 10^8 * {R_e}^{-2.626} + 0.5959$$

4.8.3 Calibration of Ulva lactura

This part describes the calibration of Ulva lactura. Christmas decoration is used to model this sort of plant. The Christmas decoration differs from the other two types of mimics in the respect of configuration. They are not like the other two vegetation mimics for which each piece is placed individually. It is hard to determine the number of Christmas decoration since they exist as a bunch. To cope with this problem, vegetation density is set the same as that of the other two types of vegetation, and the degree of dissipation is signified by the drag coefficient. The wave input and output values are obtained as in the table below.

Table 4-6: Incident and out-coming wave heights for Christmas decoration

	Christmas 10 strings		**Christmas 5 strings**	
	Incident	Out-coming	Incident	Out-coming
H=0.2 m, T=1.5 s	0.175	0.142	0.175	0.155
H=0.2 m, T=2.6 s	0.185	0.171	0.185	0.178
H=0.1 m, T=2.2 s	0.089	0.081	0.090	0.087
H=0.1 m, T=1.4 s	0.088	0.068	0.088	0.078

The drag coefficients for these sets in are determined as:

Table 4-7: Drag coefficient for Christmas decoration

	Cd (Christmas 10 lines)	Cd (Christmas 5 lines)
H=0.2 m, T=1.5 s	2.2	2.4
H=0.2 m, T=2.6 s	1.45	1.4
H=0.1 m, T=2.2 s	3.6	2
H=0.1 m, T=1.4 s	4.9	4.1

The plotting is presented as follows:

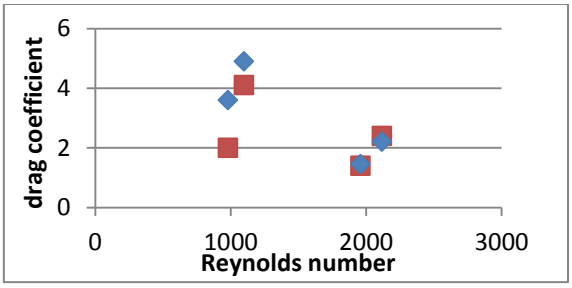

Figure 4-14: Relation between Cd and Reynolds number

The fitting curve is:

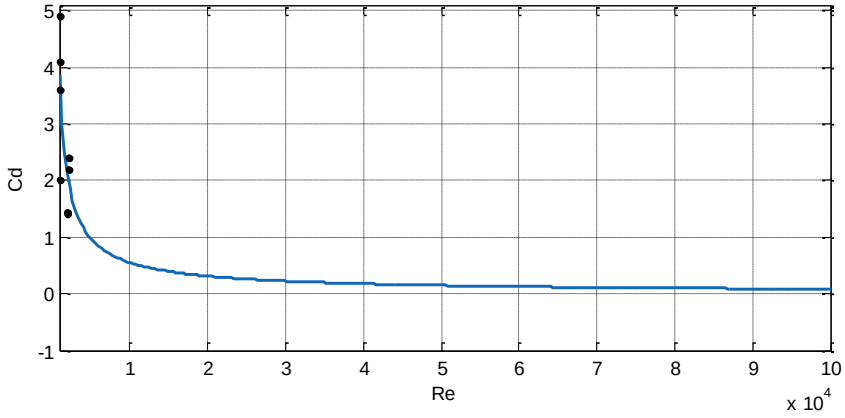

Figure 4-15: Fitting curve for Ulva lactura

The function is obtained as:

$$C_d = 1008 * {R_e}^{-0.8153} + 2.481 * 10^{-9}$$

Due to the large drag coefficient obtained in the experiment, the fitting curve shows a large steepness at the early part as the Reynolds number increases. This leads to a quite small drag coefficient when Reynolds number arrives at larger than 50000.

It can be observed that the drag coefficient for Christmas decoration ranges from 1.4 to 4.9, and that for the other two types of vegetation range from 0.5 to around 2.5. It can be seen that Christmas decoration gives rise to the most significant dissipation.

4.9 Calibration for irregular waves

4.9.1 Calibration of Laminaria digitata

The incident and out-coming waves are determined as follows:

Table 4-8: Incident and out-coming wave heights for tubes

	Tubes 10 strings		Tubes 5 strings	
	Incident	Out-coming	Incident	Out-coming
H=0.2 m, T=1.5 s	0.147	0.129	0.145	0.131
H=0.2 m, T=2.6 s	0.172	0.161	0.170	0.162
H=0.1 m, T=2.2 s	0.087	0.081	0.085	0.082
H=0.1 m, T=1.4 s	0.078	0.069	0.078	0.071

The drag coefficients for these sets are determined as:

Table 4-9: Drag coefficient for tubes

	Cd (Tubes 10 strings)	Cd (Tubes 5 strings)
H=0.2 m, T=1.5 s	1.5	2.3
H=0.2 m, T=2.6 s	1.4	2.1
H=0.1 m, T=2.2 s	2.3	2.4
H=0.1 m, T=1.4 s	1.8	2.8

The plotting of drag coefficient as function of Reynolds number and is presented below.

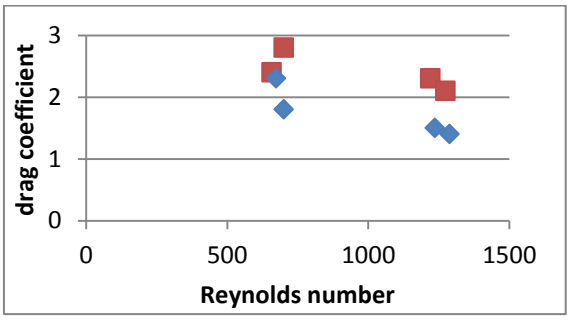

Figure 4-16: Relation between Cd and Reynolds number

The fitting trend line is given as below.

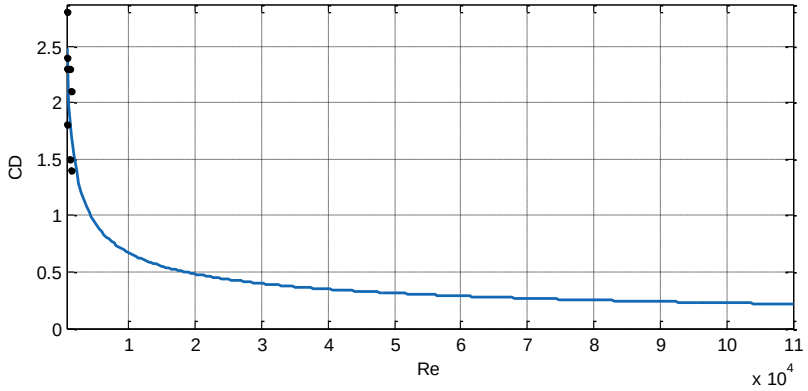

Figure 4-17: Fitting curve for Laminaria digitata

The fitting function is:

$$C_d = 51.34 * {R_e}^{-0.4716} + 0.0002885$$

4.9.2 Calibration of Saccharina latissima

The measured wave height is given as below.

Table 4-10: Incident and out-coming wave heights for wooden rods

	Wooden rods 10 lines		Wooden rods 5 lines	
	Incident	Out-coming	Incident	Out-coming
H=0.2 m, T=1.5 s	0.145	0.126	0.145	0.130
H=0.2 m, T=2.6 s	0.171	0.161	0.170	0.162
H=0.1 m, T=2.2 s	0.085	0.080	0.085	0.081
H=0.1 m, T=1.4 s	0.078	0.067	0.078	0.070

The calibrated drag coefficients for these sets in are determined as:

Table 4-11: Drag coefficient for wooden rods

	Cd (Wooden rods 10 strings)	Cd (Wooden rods 5 strings)
H=0.2 m, T=1.5 s	1.65	2.5
H=0.2 m, T=2.6 s	1.3	2.1
H=0.1 m, T=2.2 s	2	3.3
H=0.1 m, T=1.4 s	2.35	3.2

Plotting drag coefficient along Reynolds number the following are obtained:

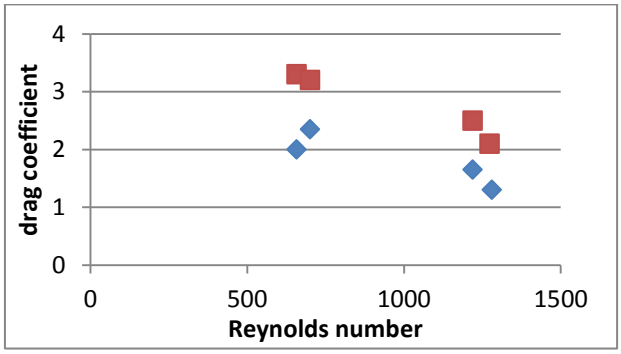

Figure 4-18: Relation between Cd and Reynolds number

The fitting curve is:

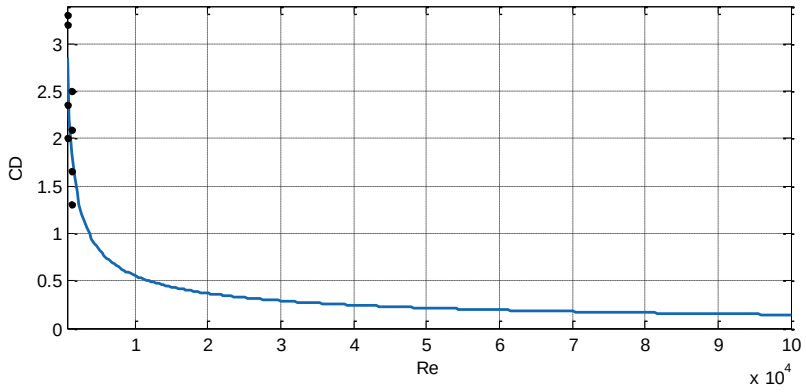

Figure 4-19: Fitting curve for Saccharina latissima

The fitting function is:

$$C_d = 127.3 * {R_e}^{-0.5904} + 9.04 * 10^{-9}$$

4.9.3 Calibration of Ulva lactura

After proccessing data, the following incident and out-coming wave heights are obtained:

Table 4-12: Incident and out-coming wave heights for Christmas decoration

	Christmas 10 lines		**Christmas 5 lines**	
	Incident	Out-coming	Incident	Out-coming
H=0.2 m, T=1.5 s	0.148	0.113	0.144	0.122
H=0.2 m, T=2.6 s	0.172	0.154	0.169	0.157
H=0.1 m, T=2.2 s	0.085	0.074	0.085	0.077
H=0.1 m, T=1.4 s	0.078	0.057	0.078	0.063

The drag coefficients for these sets are determined as:

Table 4-13: Drag coefficient for Christmas decoration

	Cd (Christmas 10 lines)	Cd (Christmas 5 lines)
H=0.2 m, T=1.5 s	3.5	4
H=0.2 m, T=2.6 s	2.4	3.2
H=0.1 m, T=2.2 s	4.9	6.8
H=0.1 m, T=1.4 s	5.65	7

The relation regarding drag coefficient versus Reynolds number is as below.

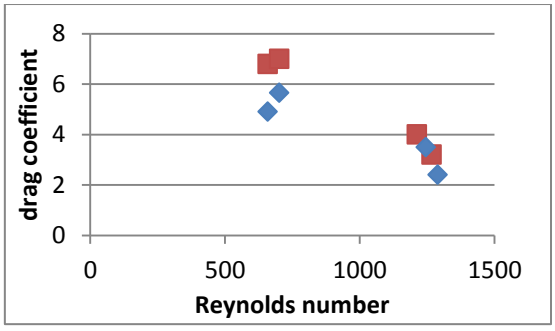

Figure 4-20: Relation between Cd and Reynolds number

Fitting all the data in one trend line, the following is achieved:

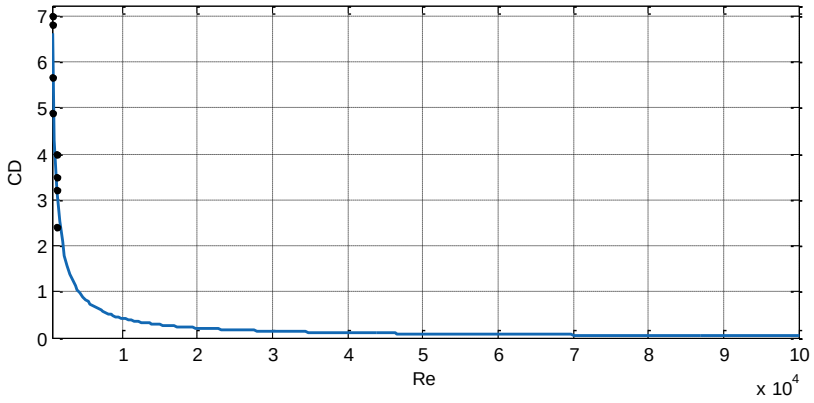

Figure 4-21: Fitting curve for Ulva lactura

The fitting function is:

$$C_d = 3831 * {R_e}^{-0.989} + 2.75 * 10^{-8}$$

4.10 Horizontal particle velocity

For the determination and Reynolds number, the measured incident wave height and corresponding wave period are used for the calculation of maximum horizontal velocity of the orbital motion of wave. Another option is to use the measured particle velocity. The measured particle velocity is also analysed. However, the measured data shows significant

inconsistency between each other. The usability of this data is rendered quite questionable. The analysis is presented in Appendix E.

4.11 Discussion

- The drag coefficient obtained in the calibration is rather high compared with the findings from Suzuki (2011), especially for Christmas decoration. This is because the Christmas decoration results in much larger dissipation, but its dimension are set the same as the other two sorts of vegetation mimics as it is impossible to quantify its dimension characteristics. This leads to the question whether the vegetation mimics used are truly representative the vegetation or the vegetation density setting is not appropriate.
- Also, it was observed that the vegetation mimics move up and down along with the motion of waves, therefore the vertical damping would play a role. This damping mechanism is not interpreted in the numerical model, and its influence is transferred to the bulk drag coefficient, which may also contribute to a large drag coefficient.
- From the perspective of the data itself, quite some questionable data are observed. Either the two vegetation densities show the same amount of dissipation, or specific vegetation for a specific wave condition does not show appropriate amount of dissipation. This leads to some unusable data.
- From the analysis of first scenario and second scenario, it has been noted that there is hardly any damping caused by bottom friction, boundary effect and H profiles. The trustworthiness of this finding remains to be discussed. Alternatively, it can be understood that the bottom friction and attenuation effect of H profiles do not manifest themselves due to its insignificant influence or measurement error when the vegetation mimics are not implemented, but when combined with vegetation mimics, they do contribute to wave energy dissipation. This may also explain why such a large drag coefficient is obtained.
- For each type of vegetation with specific vegetation density, only four data are available. In order to obtain a relatively good statistical trend, sufficient number of data is required. The limited number of experimental data for this study makes the result less convincing since the conclusion is drawn based on such limited number of data.
- The Reynolds number is determined based on incident waves. Since the wave height changes along the vegetation field, the dissipation effect along the vegetation field will vary. However, it is not possible to define the changing drag coefficient along the vegetation field for the present, as it contradicts with input rule in SWAN. As a result

the incident wave characteristics are used to determine the relation between drag coefficient and wave characteristics instead of using an ever-changing wave characteristic along vegetation field. It is also recommended to use the velocity of measured particle velocity if the data is usable.

4.12 Conclusion

The calibration is intended to give a proper representation the field condition in the flume scale. The results for two vegetation densities give quite distinct drag coefficient, which makes the validation ineffective. Besides, the number of available data is limited, which leads to questionable trustworthiness of the result. What is more, the bandwidth of Reynolds number is quite limited. Whether the relation obtained is still applicable to higher range of Reynolds number remains to be investigated.

Despite all the concerns, the drag coefficient decreases with the Reynolds number generally. A case study is conducted with the obtained drag coefficient relation to present how the model reflects the field condition.

5 Case study

As stated in the research goal, the objective of this research is to investigate the impact of floating seaweed aquaculture on wind waves. In chapter 4 the relation between calibrated drag coefficient and Reynolds number is obtained. With this relation, a drag coefficient will be determined and it will be applied in this case study. The case study is carried out to present the attenuation effect of seaweed aquaculture in the North Sea.

5.1 Background

The concerned location is located in North Sea where a few wind farms are going to be built for the goal of sustainable use of energy. Our specifically concerned location is Borssele wind farm zone, which is in the southern part of Dutch North Sea, close to the Dutch-Belgian border. These wind farms are developed for electricity productivity. To make full advantage of marine space, seaweed aquacultures are also operated among this region. Through this case study it aims to find out the influences of these seaweed aquaculture with regards to wave attenuation, which will lead to the hydrodynamic changes which may further influences sediment transport in the coastline. More direct effect is related to the wave load on the wind turbine supporting structure.. The location of Borssele wind farm zone is shown as below:

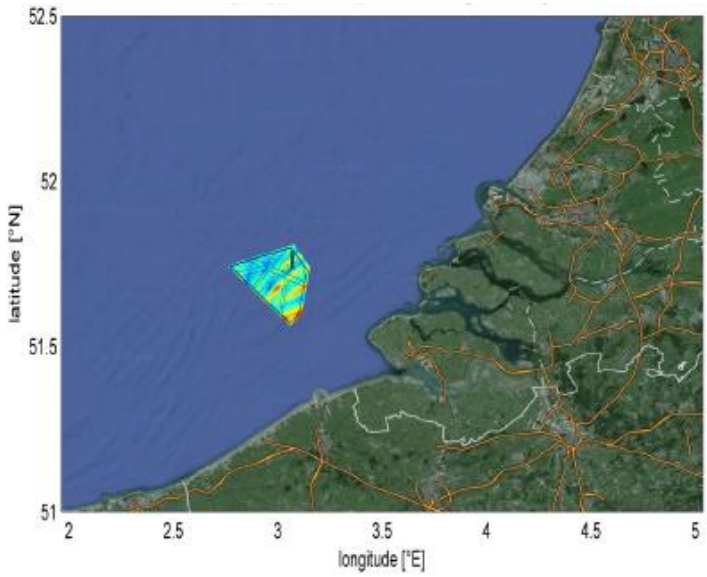

Figure 5-1: Location of case study

This wind farm zone is divided into four wind farm sites. For the present, the region “I” is considered to be operated with seaweed aquaculture. It is indicated as the upper right part of Borssele zone in Figure 5-1 with letter “I”.

5.2 Scenario definition

In the offshore region where wind farm are present, wind entwines with vegetation to have an influence on the local wave condition. Also bottom friction may contribute to wave dissipation. In order to see individual effect of related elements on the wave attenuation, a few scenarios are differentiated to compare the results between them and provide a clearer presentation of impact of vegetation.

Table 5-1: Scenario setup

Scenario number	Conditions considered
Scenario 1	without vegetation, without wind, with wave
Scenario 2	with vegetation, without wind, with wave
Scenario 3	without vegetation, with wind, with wave
Scenario 4	with vegetation, with wind, with wave

Each specified scenario serves for a specific purpose. Scenario 1 is intended to show the dissipation caused by physical processes which comprises bottom friction, white-capping and depth-induced breaking. With scenario 2 it is expected to present the magnitude of energy dissipation due to the presence of vegetation. In scenario 2 the wind is not implemented. This corresponds to the experimental setup where the wind is not an input. In scenario 3, only the wind is implemented to see how the wave changes under the influence of wind. Through simulation of scenario 4 the real circumstances are presented, where all the involved parameters are implemented. This scenario is performed to see how local wave climate changes owing to introduction of seaweed aquaculture to the wind farm, which is the research goal of this study.

5.3 Boundary condition determination

In this section the determination of boundary condition is presented. They are differentiated between wave condition and wind condition.

5.3.1 Boundary wave condition

The boundary wave information is provided in the period 1992-2011 (20 years). The information includes significant wave height, peak wave period and wave direction. In order to determine the dominant wave condition, the wave height and wave direction have been used to produce a wave rose. Different colors represent different wave height bands, and the length of color bar indicates the probability of occurrence. This rose illustrates how waves with different significant heights are distributed over different directions with certain probability of occurrence, as shown in Figure 5-2.

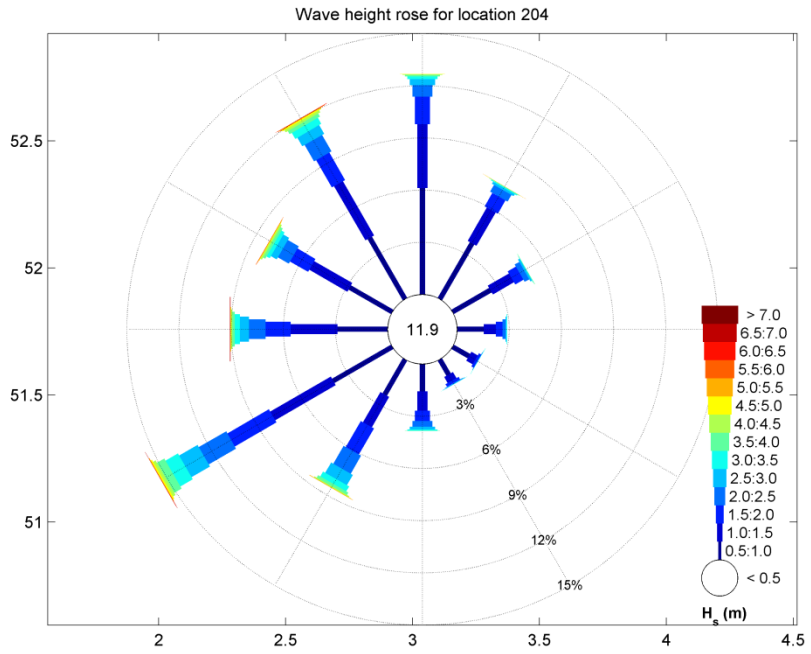

Figure 5-2: Wave height rose

The wave rose shows that the dominant wave directions are N, NNW and SWW. Besides, the majority of waves fall in the band of 0.5-1 m and a considerable part is within the band of 1-1.5 m.

Twelve direction sectors are differentiated for simulations. In order to determine the operational wave properly, a bar graph regarding the probability over various wave height bands is generated. The wave heights are divided into a few bands, the percentage of the number of wave heights falling within each band over the total number of waves in each direction is determined. Only the information from the North direction is presented here, the results of the rest of direction sectors are presented in Appendix H. A bar graph for North direction is obtained in Figure 5-3. It shows that wave height band 0.5-1 m and 1-1.5 m accounts for the highest percentage. These two bands are used for determination of dominant wave characteristics.

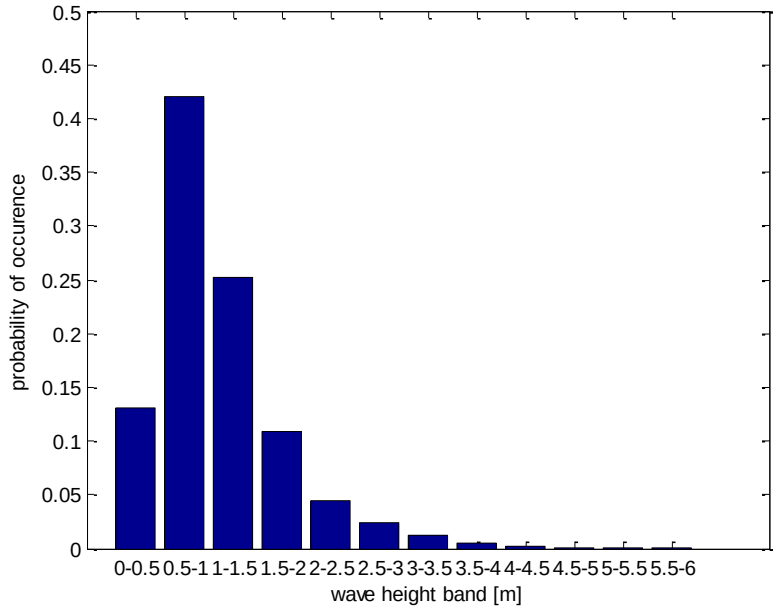

Figure 5-3: Wave height bar graph

Within this range, each wave height is considered to obtain the representative wave height for all the waves in this band. These waves are noted as H_1, H_2 … H_n. A root mean square wave height is determined for these waves. The formula for determining this characteristic wave height is:

$$H_{rms} = \sqrt{\sum_{1}^{n} {H_n}^2}$$

Equation 5-1

Finally H_{rms} arrives at 0.9596 m. This is representative of significant wave height for the wave bands chosen. This value is used as significant wave height directly in SWAN input instead of converting to significant wave height by applying a factor of $\sqrt{2}$. This is due to the fact that the data information itself is given in name of significant wave height. Even though the principle of root mean square wave height is applied here, it serves as only a method to reach the representative value for all these considered waves, as root mean square wave height represents the wave energy most closely. The similar idea holds for wave period determination in the next section. Peak wave period is used even though the mean value of wave period of chosen waves is determined.

The corresponding wave period for each wave falling in band 0.5-1.5 m is showed in Figure 5-4. The wave period is plotted versus the corresponding wave height.

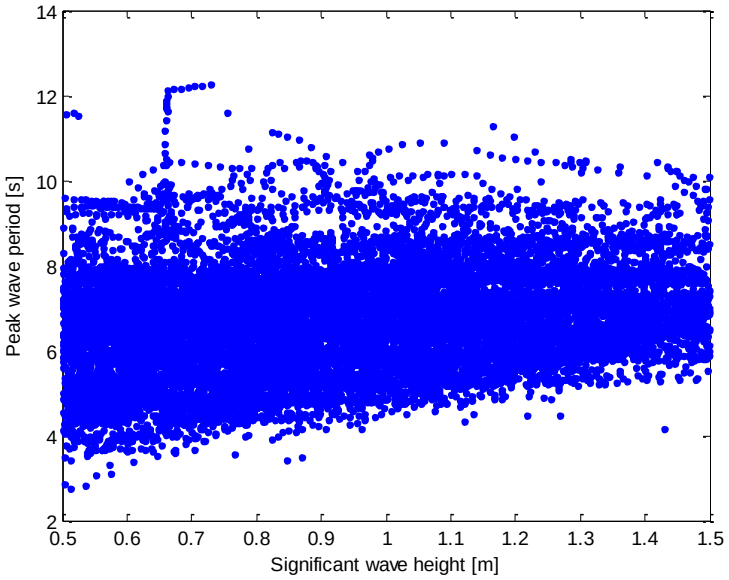

Figure 5-4: Wave period distribution for wave height band 0.5-1.5 m

As can be seen clearly, the wave period ranges from around 3 s to approximately 12 s, with concentration at around 7 s. More accurate method is used to find the representative wave period. These wave periods are named as T_1, T_2 …T_n. The mean wave period is obtained by:

$$T_{mean} = \frac{T_1 + T_2 + \cdots + T_n}{n}$$

Equation 5-2

The mean wave period reaches 6.7119 s. This value is implemented as peak wave period in the numerical setup.

5.3.2 Boundary wind condition

The wind information is given for the same period as wave condition. For each wind data it is given in the form of two vectors in Cartesian convention. These two vectors are denoted as u and v. u is the horizontal vector and v indicates the vertical vector. The wind speed is calculated by:

$$Wind = \sqrt{u^2 + v^2}$$

Equation 5-3

For the direction, this is determined in nautical convention, i.e. wind from North is considered as zero and the degree is counted clockwise. The transformation to nautical direction is carried out in Mat lab, with “mod (270-atan2d (v, u), 360)” command.

After determining both the wind speed and wind direction for each wind element, the wind characteristic corresponding to the chosen dominant waves in the each direction sector is obtained. The same principle of energy method is applied. Wind energy power per unit area is formulated as:

$$P = \frac{1}{2}\rho v^3$$

Equation 5-4

P is wind energy power per unit area, ρ is air density and v is wind speed.

The formula indicates that wind energy is proportional to the third power of wind speed. Based on energy averaging, the representative wind speed is obtained by the following method:

Scale the each wind speed to power 3, take the mean value of them, and then scale it back with power 1/3. The mathematical expression to determine the mean wind speed is formulated in Equation 5-5. The wind components are noted as W_1, W_2…W_n. In this context "mean" signifies energy representing rather than in conventional sense.

$$W_{mean} = \sqrt[3]{\frac{{W_1}^3 + {W_2}^3 + \cdots + {W_n}^3}{n}}$$

Equation 5-5

Mean wind speed is obtained as 5.5137m/s.

The wind direction is determined as the mean value of wind directions of these concerned wind elements. It reaches at 125.9°. The wind information is implemented in the SWAN model in the form of two vectors: horizontal one (u) and vertical one (v). The mean wind speed value is decomposed in the wind direction. Consequently the following is obtained:

Table 5-2: Wind vector implemented in simulation for North direction

Direction	u (m/s)	v (m/s)
North	-4.467	3.232

Conventionally, the wave direction is supposed to be close to wind direction since wind is the energy source to generate waves when speaking of wind waves. When we compare the wave direction and wind direction obtained here, it displays that there is weak accordance between wave direction and wind direction. This is because the wave is generated in the region some distance away and propagates to this concerned domain, while the wind is locally representative. Besides, the North direction actually covers the waves approach from 345° to 15°, the corresponding wind directions are more scattered if waves within a range of direction are considered. Therefore it is not strange that wave direction shows remarkable deviation from wind direction.

5.4 Model setup

The computational gird is defined in spherical dimension, based on the actual latitude and longitude of the concerned area. The resolution is around 50 m × 50 m and the extent is approximately 45 km × 45 km. the directional space is in full circle and is divided into 36 sectors. The frequency domain is from 0.04 to 1 Hz. The upper frequency should be set higher if small wave period is present. This is necessary since wind can locally generates small waves. Nonetheless, the wave period for our operational condition is determined as 6.7119 s. The upper limit of 1Hz is quite enough to meet the setting requirements of SWAN.

The input is determined after obtaining the wave and wind information. Both wave and wind information is characterized with the dominant value during this period of 20 years. The wave height, wave period and the wind speed are implemented with above-obtained values. The wave direction is set as coming from North. Wind direction is set as 125.9°. The input parameters for wind are the two vectors obtained in Table 5-2.

5.4.1 Bathymetry

The bathymetry data is given in great detail with an area of approximately 45 km × 45 km, the same as the computational area. The water depth ranges from approximately 10 m to nearly 40 m. the resolution is around 200 m × 200 m. The Southeast part of this area is closer to the Dutch coast line. Therefore it shows a decreasing water depth when approaching to the right-lower corner of the domain.

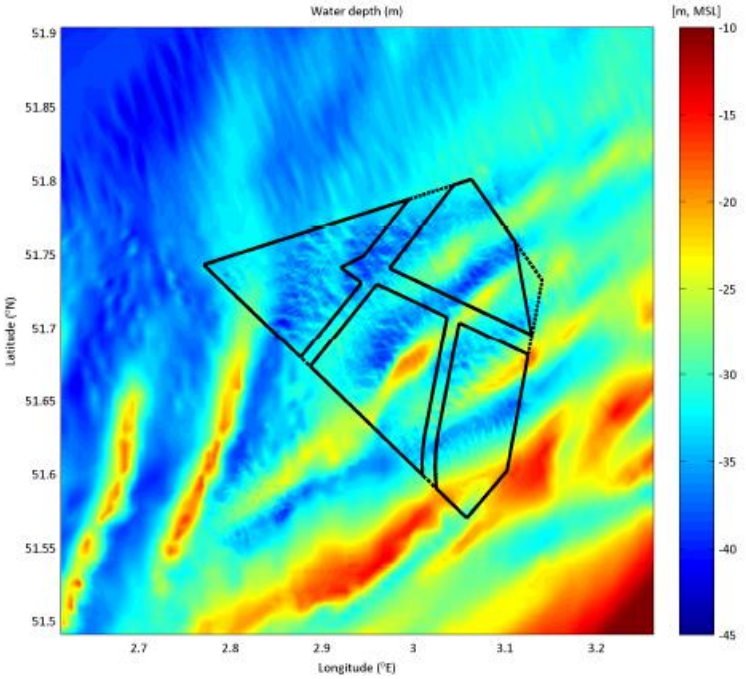

Figure 5-5: Bathymetry

5.4.2 Vegetation parameters determination

The concerned three sorts of seaweed are investigated in terms of their physical properties which are required for the model setup. The involved parameters are number of seaweed per square meter (N), length of seaweed (L) and width of seaweed (W). The information concerning these three parameters is kindly provided by Brandenburg Willem. These data are listed in Table 5-3.

Table 5-3: Vegetation indication parameters

Seaweed type	N	L(m)	W(cm)
Laminaria digitata	4	1.5-2	15-50
Saccharina latissima	4	1.5-2.5	15-25
Ulva lactuca	4	0.3-0.5	10-30

The information is suggested to be considered only as indication as it is hard to provide exact number for these parameters. In the numerical setup, 4 are given to vegetation density (N), and the mean value of range for length and width are employed for vegetation length and vegetation width respectively. The values of parameters implemented in the model are as follows.

Table 5-4: Vegetation parameters implemented in the modelling

	N	L(m)	W(m)
Laminaria digitata	4	1.75	0.3
Saccharina latissima	4	2	0.2
Ulva lactuca	4	0.4	0.2

5.4.3 Drag coefficient determination

The drag coefficient depends on the Reynolds number, which is further dependent on the water depth. The water depth varies for different points as the bathymetry is not constant. Consequently the drag coefficient for each grid point in the simulation is not equal. However, for the present it is impossible to apply different drag coefficient for each grid point due to the limitation of SWAN input. For simplification, a general water depth of 30 m is used when determining the drag coefficient. The difference is negligible, as the comparison below tells.

Take vegetation Laminaria digitata as an example. Apply parameters (H= $0.96/\sqrt{2}$,$T_p = 6.7$, $b_v = 0.3$, $L = gT^2/2\pi$ =70.9, $v = 10^{-6}$) into the Reynolds number Equation 4-5.

From the bathymetry of the vegetated region it can be observed that the water depth in the vegetated area ranges from 25 m to 40 m.

The drag coefficient formula for Laminaria digitata is:

$$C_D = 51.34 * Re^{-0.4716} + 0.0002885$$

Equation 5-6

Then the water depth is varied to see how sensitive the drag coefficient reacts to the change of water depth. These three water depths give to almost the same drag coefficient.

Table 5-5: Sensitivity response of drag coefficient over water depth

Water depth (h)	C_D
30	0.229386
25	0.227944
40	0.230219

Compared with water depth of 30 m, the drag coefficient difference is 0.36% for water depth of 40 m and 0.63% for water depth 25 m. Obviously the difference is negligible. The similar results are obtained for the other two types of vegetation. Therefore water depth of 30 m is accurate enough in determining the drag coefficient.

After obtaining the vegetation parameters, the drag coefficient for each type of vegetation is to be determined. This calls the preceding result of formula of drag coefficient over Reynolds number since the relation over KC-number has been proved to be ineffective.

For these three sorts of vegetation, the obtained drag coefficient differs from each other. The drag coefficient for North direction is obtained as follows. For other direction sectors, the drag coefficients are given in Appendix H.

Table 5-6: Drag coefficient determination

Type of seaweed	Drag coefficient formula	Drag coefficient
Laminaria digitata	$51.34 * Re^{-0.4716}$	0.23
Saccharina latissima	$78.964 * Re^{-0.511}$	0.185
Ulva lactuca	$1798.9 * Re^{-0.858}$	0.067

From the data it says that the drag coefficient obtained in the case study shows different pattern from that obtained in the experiment. In the calibration stage larger drag coefficient is obtained for vegetation mimics for Ulva lactuca. This phenomenon results from the steepness difference between these trend line functions. The trend line of drag coefficient relation for Ulva lactuca is steeper than the rest of two, which implies a sharper decrease of drag coefficient when a large Reynolds number is obtained.

5.4.4 Vegetation field

As for the vegetation, the real situation with regard to the project is considered. Our interest area is located in the zone 1 (upper right corner zone in Figure 5-1) as shown in Figure 5-6.

This zone is implemented with vegetation. Outside this region no floating seaweed is planted. This vegetation input is realized through creating a matrix in mat lab. The size and resolution of vegetation grid is created the same as the computational grid. First a value of zero is applied to each grid point, and then a value of 4 representing the vegetation density is applied for grid points within the vegetation field.

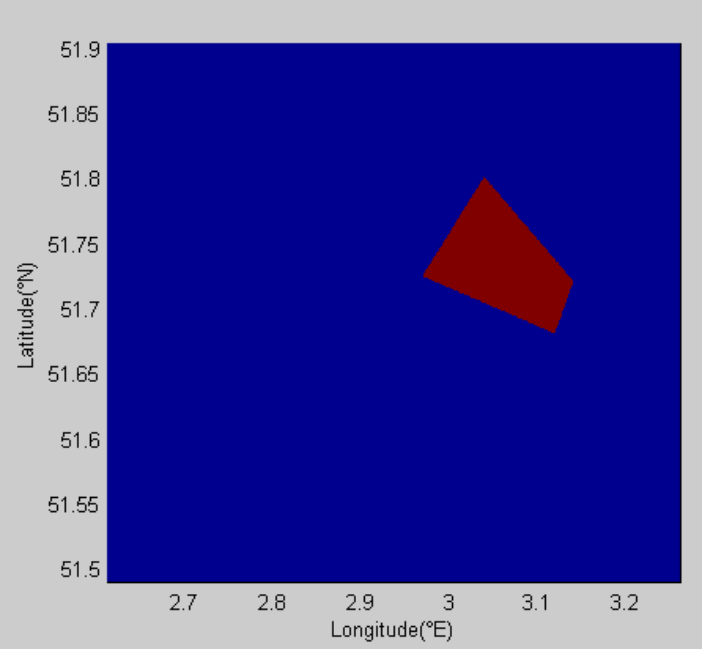

Figure 5-6: Vegetated area in the model domain

Remarks about the setup:

- Current is not considered in this study. The current will intertwine with waves which will complicate the situation. Then it is not obvious to see only the attenuation effect of vegetation.
- Sea level rise is not taken into consideration. It will have a minimal influence at the offshore region with such relatively deep water.
- Diffraction is switched off as SWAN does not handle diffraction properly. Actually diffraction does not influence the result at all. According to the SWAN user manual, the spatial resolution around the tip of diffraction obstacle should be 1/5 to 1/10 of dominant wave length. In this model setup the wave length reaches 70.3 m, which is much larger than 5 to 10 times of the width dimension of seaweed. A simulation with diffraction gives exactly the same result as that without diffraction.

5.5 Case study results

5.5.1 Laminaria digitata

This section presents the simulation results for those scenarios listed in Table 5-1 for seaweed Laminaria digitata. Each scenario represents the impact of specific input parameters on the wave.

5.5.1.1 Scenario 1

Scenario 1 is set up to check the influence of bottom friction, white-capping and breaking. The wave height for the whole computational domain is presented as below.

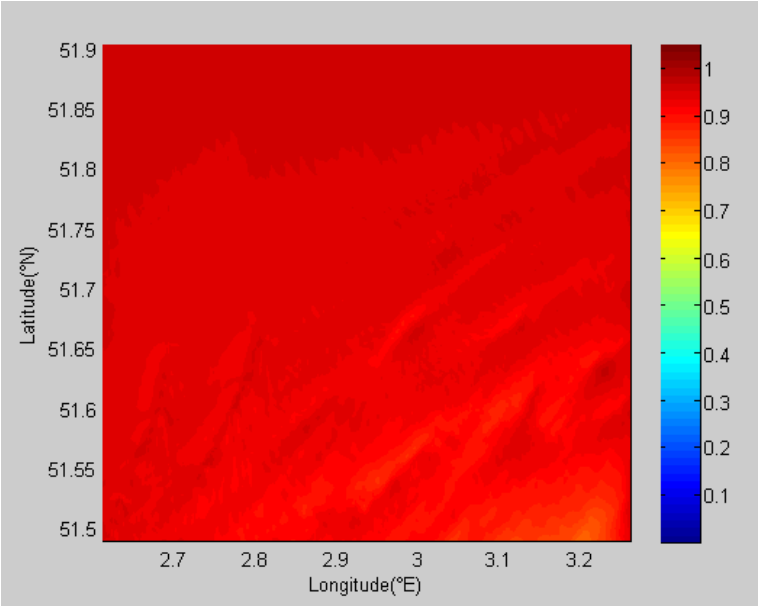

Figure 5-7: Wave height diagram for scenario 1 for Laminaria digitata

In this model setup, only physical processes like bottom friction, depth-induced breaking and white-capping are implemented. The waves approach from the North. A decreasing trend has been seen for the wave height due to friction when waves travel to south. Nonetheless, the reduction is minimal. At the left corner of South boundary the wave height reaches approximately 0.94 m with a reduction of nearly 2 cm, except for a patch at the right-lower corner where the wave height decreases to 0.85 m. However, this is due to some reason other than friction. At some locations the wave height is smaller than the rest of area as it is shown by the lighter red region from Figure 5-7. In the beginning it was thought that this phenomenon occurs due to the bottom friction, which is reasonable since greater bottom friction is exerted on the waves at location with smaller water depth. The area with smaller wave height corresponds to area with smaller water depth, with the smallest wave height observed at the area with smallest water depth (the right lower corner of the domain).

However, when the bottom friction and other physical processes are switched off in the simulation, this wave pattern still exists, as the new diagram in Figure 5-8 shows.

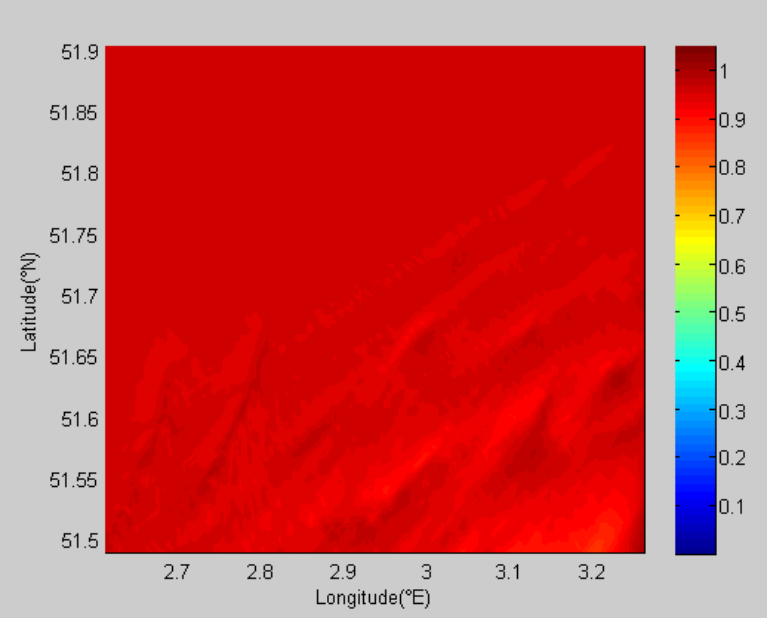

Figure 5-8: Wave height diagram without physical processes for Laminaria digitata

Obviously there is no wave height reduction caused by bottom friction, judging from the smooth upper part of the diagram. But in the area with small water depth the wave height shows similar pattern as when bottom friction is on. The reason lies in the so-called “shoaling effect”. When the wave approaches from large water depth (deep water) to relatively less deep water, the group velocity increases slightly first and then decreases. In this bathymetry the water depth is still considerable and the group velocity increases slightly. As a result the wave energy decreases based on balance of energy transport. This leads to a slight decrease of wave height.

5.5.1.2 Scenario 2

This scenario describes the wave energy dissipation caused by vegetation only. The following figure is obtained based on the simulation result.

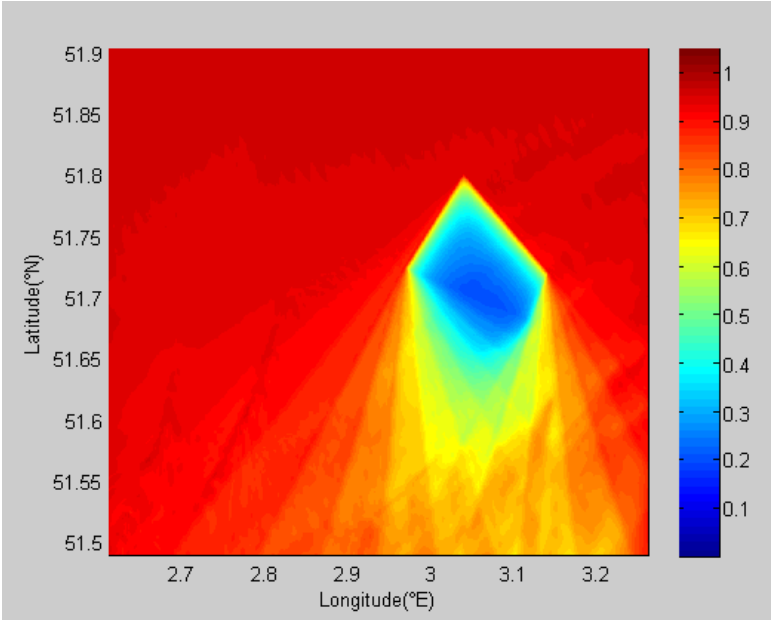

Figure 5-9: Wave height diagram for scenario 2 for Laminaria digitata

In this figure the wave height ranges from 0.96 m (incident wave height) to around 0.26 m, with the smallest wave height existing in the center of vegetation area. When the waves pass through the vegetation field, the wave height experiences a significant decrease. Significant amount of wave energy is dissipated away. What is remarkable is that in the later part of vegetation field the waves start to grow. At the ending of the vegetation field the wave height reaches nearly 0.47 m. This phenomenon occurs due to the directional spreading. The wave energy is higher in the adjacent area where less or no seaweed is vegetated. Therefore the higher wave energy transports to the region with smaller wave height. Behind the vegetation field, the wave height continues to grow. At the South boundary the wave height reaches approximately 0.75 m, with an increasing trend from left to right where the wave height is nearly 0.92 m. this is because the right part of the domain is more influenced by the vegetation field, so more wave energy is consumed to offset the low wave energy behind the vegetation field. The left part is located farther so the influence of vegetation is less effective.

5.5.1.3 Scenario 3

In this scenario the effect of wind is investigated.

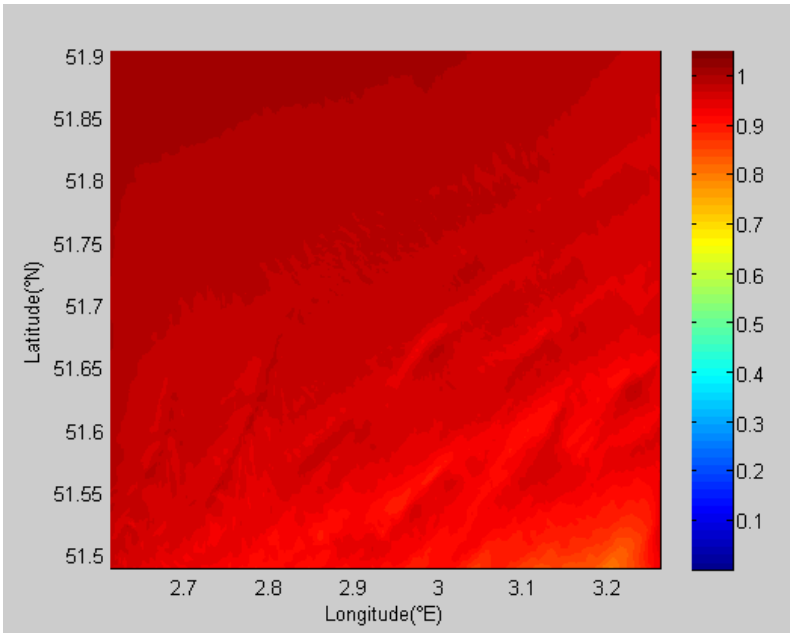

Figure 5-10: Wave height diagram for scenario 3 for Laminaria digitata

This scenario shows that the wind contributes to the wave growth. The wind approaches from direction of 125.9° in nautical convention. Therefore it has been observed a wave height developing from right-lower corner to the left-upper corner of this domain. The wave height amounts to around 1.0 m at the left-upper corner. It is observed that the wind makes contribution to wave growth in the direction of wind approaching, with an increase of 4% in this case.

5.5.1.4 Scenario 4

In this scenario, all the relevant conditions in the real situation are taken into consideration in the simulation. This reflects the site condition with the intervention of seaweed.

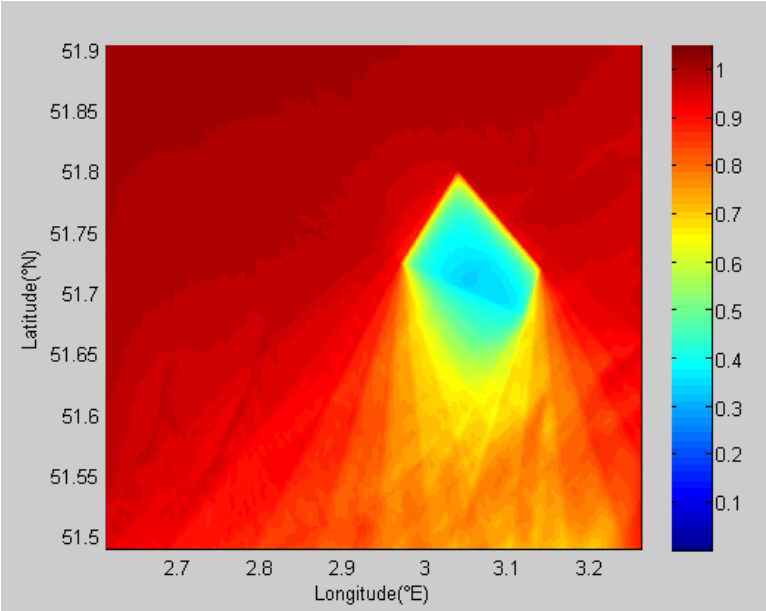

Figure 5-11: Wave height diagram for scenario 4 for Laminaria digitata

Compared with scenario 2, the wave energy dissipation by seaweed in this scenario is less as the wind offset the energy loss in some degree. The smallest wave height within vegetation field is observes as 0.37 m while it is 0.26 m for scenario 2. At the South boundary, the wave height at the right part behind the vegetation field is around 0.75 m.

5.5.2 Saccharina latissima

Vegetation Saccharina latissima shows a little bit difference from Laminaria digitata for the vegetation properties. This vegetation has somewhat longer length than Laminaria digitata and the vegetation width is two thirds of that of Laminaria digitata. The drag coefficient is somewhat smaller than that of Laminaria digitata with a different drag coefficient relation. Only scenario 2 and 4 are presented here as scenario 1 and 3 are the same for all the three types of seaweed.

5.5.2.1 Scenario 2

The wave height for the whole domain is presented as:

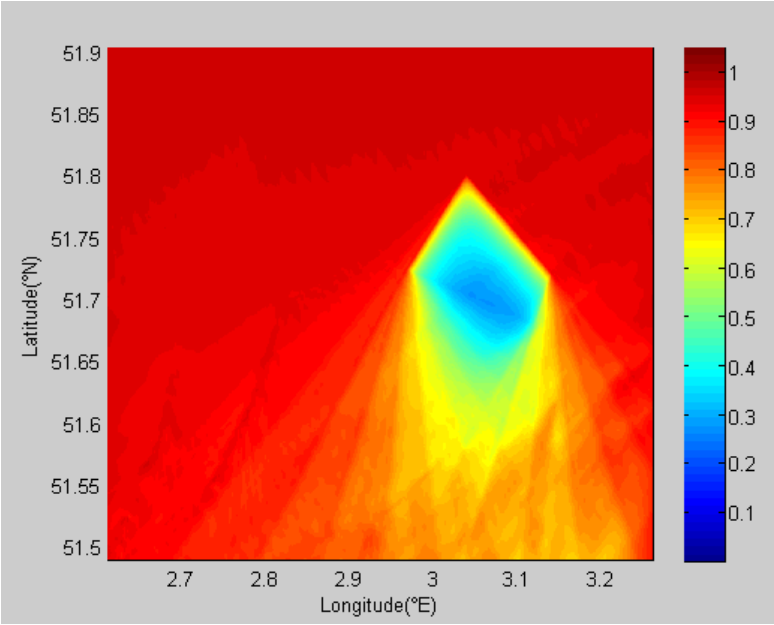

Figure 5-12: wave height diagram for scenario 2 for Saccharina latissima

This figure shows quite similar result as Laminaria digitata. The distinction is that this type of seaweed gives rise to less dissipation. The smallest wave height reads 0.34 m within the vegetation field in contrast with that of 0.26 m for Laminaria digitata. At the South boundary the difference between these two types of seaweed is not noticeable.

5.5.2.2 Scenario 4

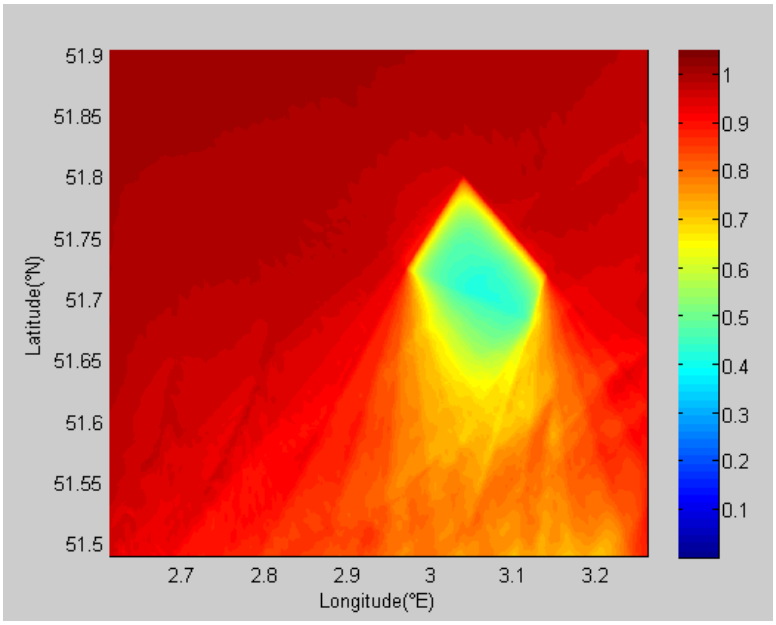

Figure 5-13: Wave height diagram for scenario 4 for Saccharina latissima

In a similar way, this scenario gives less energy dissipation compared with scenario 2. It shares the same features as Laminaria digitata except for less energy dissipation within the vegetated area.

5.5.3 Ulva lactuca

Vegetation Ulva lactuca shows much difference from Laminaria digitata regarding the vegetation properties. The vegetation length is only one fifth of that of Saccharina latissima and the width is the same as that of Saccharina latissima. Also, this type of vegetation possesses a much smaller drag coefficient than the other two types of vegetation. Scenario 2 and scenario 4 are described in this section as they show distinct results from the other vegetation.

5.5.3.1 Scenario 2

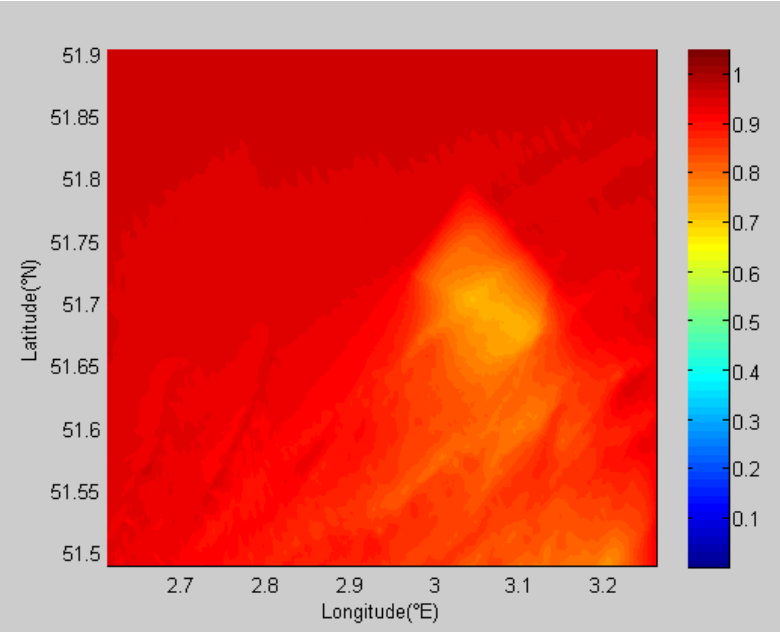

Figure 5-14: Wave height diagram for scenario 2 for Ulva lactura

Compared with the seaweed Laminaria digitata, this vegetation shows much less energy dissipation inside the vegetation field. This is not surprising as such a small drag coefficient is obtained for this type of vegetation. The smallest wave height in the center of vegetation field is 0.75 m, compared with 0.26 m for Laminaria digitata. It indicates that this vegetation attenuates wave in the least significant magnitude. This is foreseeable based on the smaller drag coefficient, shorter length and smaller vegetation width.

5.5.3.2 *Scenario 4*

Similarly, this scenario shows even less energy dissipation by seaweed compared with scenario 2 because of wind energy inputting. The smallest wave height is nearly 0.81 m within vegetation field. This seaweed presents hardly any influence on the waves.

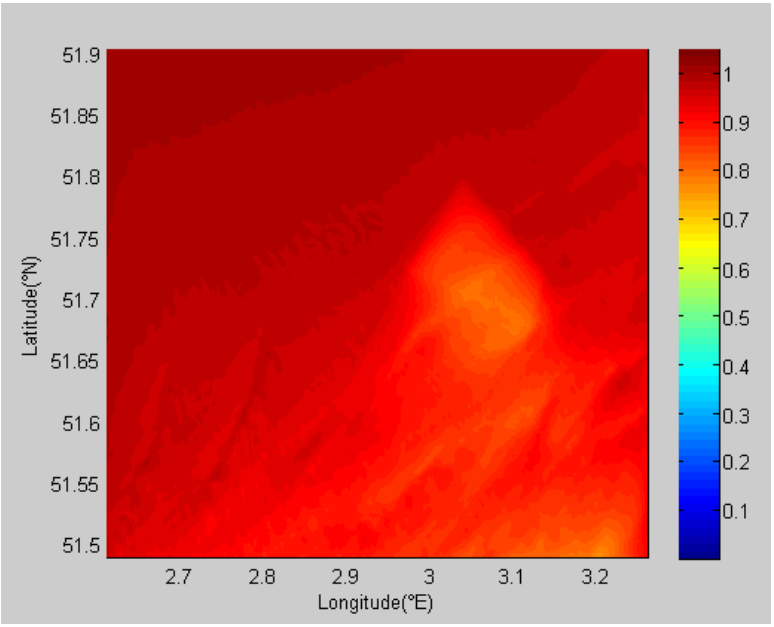

Figure 5-15: Wave height diagram for scenario 4 for Ulva lactuca

Apart from the wave height decrease, the change of the wave period is also noticed. From the output it is observed the wave period increases a bit. This is because wave component with small wave period is dissipated more effectively. So the wave period increases somewhat generally. This is in accordance with the conclusion in the sensitivity analysis that smaller wave period leads to higher dissipation.

In this section only the result for North direction is presented. Results for other direction sectors can be found in Appendix J. Besides, since Laminaria digitata results in the most significant wave attenuation, its impact is critical. As a result only results for this type of vegetation are presented in Appendix J.

5.5.4 Quantification of wave dissipation

Due to the irregular shape of this vegetation field, the directional spreading plays a significant role in the wave height developing behind and even within the vegetation field. This makes it hard to quantify the wave attenuation effect of seaweed. To achieve this goal, a square shape of vegetation field is implemented so as to eliminate the influence of directional spreading within the vegetation field. Besides, the size of the square is varied to see how the size of vegetation field affects the energy dissipation. The side length is varies as 4 km × 4 km, 8 km × 8 km and 12 km × 12 km. the vegetation patch of 4 km × 4 km is presented in Figure 5-16 and the rest are shown in Appendix I.

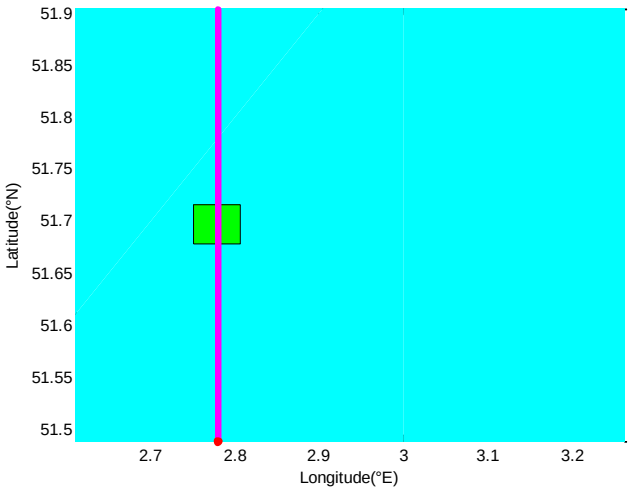

Figure 5-16: Vegetation field with size of 4 km × 4 km

The wave height in the whole computational domain is presented in the figure below.

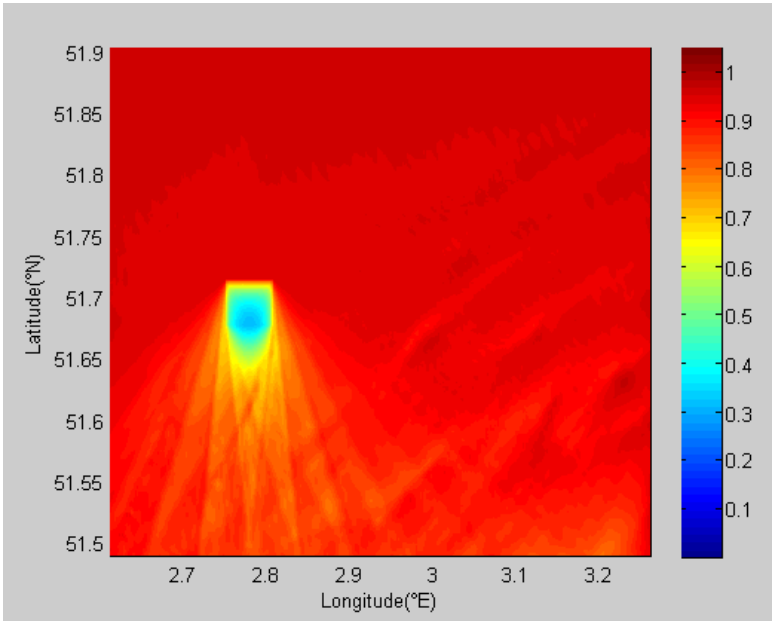

Figure 5-17: Wave height diagram for vegetation size of 4 km × 4 km

The wave heights at the starting point of vegetation field and at the ending of the field are used to determine the ratio of remaining wave height. In this section the bottom friction is neglected as it accounts for minor impact. Also the wind is not implemented. On the one hand it complicates the determination as it offsets the wave energy within the vegetation field. On the other hand only effect of seaweed is interested. The ratios of remaining wave height are determined in table below.

Table 5-7: Ratio of remaining wave height for different vegetation size

Vegetation side length	4 km × 4 km	8 km × 8 km	12 km × 12 km
Ratio of remaining wave height	33.1%	22.3%	17.9%

As can be observed that wave energy is dissipated tremendously and the dissipation is more significant with the increase of vegetation size. Also it is clear that the remaining wave height does not reduce double fold when the length of vegetation doubles. This is because most of the wave energy is dissipated at the early part of the vegetation field. The dissipation effect is more considerable when wave height is larger.

Behind the vegetated area an increase of the wave height is noticed. At the crossing point between South boundary of computational area and central line of vegetation field (the red dot in Figure 5-16), the wave height with presence of vegetation and wave height without the presence of vegetation field are obtained to determine the difference due to the introduction of seaweed aquaculture to the wind farm. The wave height at the crossing point in the presence of vegetation is named as H_1, and the wave height without vegetation at the same point is named as H_2. The ratio of H_1 over H_2 is obtained as follows.

Table 5-8: Ratio H_1/ H_2 for different vegetation size

Vegetation side length	4 km × 4 km	8 km × 8 km	12 km × 12 km
Ratio H_1/ H_2	92.9%	86%	70.5%

Table 5-8 says that 92.9% of the original wave height remains with the presence of seaweed for vegetation size of 4 km × 4 km. This percentage decreases correspondingly when the vegetation field size increases. This crossing point is under the maximum degree of influence of the vegetation since it is closest to vegetation field. For other region, this wave height ratio is supposed to be higher, which means less influence of vegetation is exerted. Considering the results both from Table 5-7 and Table 5-8, it is observed that even though the wave energy is dissipated in a great extent within the vegetation field, the wave develops behind the vegetation field. The seaweed aquaculture imposes a local impact in the wave height reduction.

Now the case of real vegetation area is considered. The vegetation patch is around 6 km in its longest diagonal dimension. Now the seaweed Laminaria digitata is considered as it shows the most significance of wave dissipation. Comparing scenario 3 and scenario 4, the ratio of remaining wave height at the South boundary at longitude 3.05° is obtained as 0.75/0.87=86.2%. If the computational area is set larger, the wave developing is supposed to continue, which results in less impact of vegetation field. The distance between South boundary of computational area and coastline is around 20 km. Within this 20 km there

should be more wave developing due to directional spreading and larger wind zone. Then the wave loss near the coastline due to presence of seaweed aquaculture is even smaller.

5.6 Discussion

Some comments are made for the uncertainty in the model. They uncertainties complicate the impact of seaweed aquaculture on wind waves.

- In the real situation the vegetation field is not completely covered with seaweed. Instead, they are implemented in many patches. There are gaps between different patches. For simplification this aspect is not considered as it is complicated to create such a vegetation grid. In the numerical setup the whole vegetation area is occupied with seaweed. Therefore, the simulation result gives an overestimation of the real situation in terms of amount of energy dissipation.
- Hosting structure is not investigated with respect to its effect on the wave attenuation. The reason is that SWAN cannot handle the simulation of small floating structure. However, the obtained calibrated drag coefficient in chapter 4 already incorporated the impact of floating structure, with the schematized H profiles being implemented in the flume test.
- In the parameterizing the diameter of vegetation in the model setup, the width of given vegetation is used. The accuracy of this setting is not verified. However, no scientifically accurate method is available for the present.
- In the determination of drag coefficient, the drag coefficient is obtained with the calibrated drag coefficient function from chapter 4. Due to the large difference of Reynolds number, the drag coefficient shows quite different value than that in the experiment, especially for vegetation Ulva lactuca. This poses much uncertainty to the applicability of drag coefficient function.

5.7 Conclusion

From the analysis of this chapter, it is observed that the seaweed contributes to significant wave attenuation within the vegetation field. The seaweed Laminaria digitata shows the most significance of wave attenuation while seaweed Ulva lactuca displays the least dissipation. However, due to directional spreading the waves start to grow even within the vegetation field where less seaweed is present. Within a computational domain of approximately 45 km $\times$ 45 km nearly 85% of wave height remains at the out-going boundary. It can be inferred that if the domain is set larger, the influence of seaweed would be even slighter. From the results it demonstrates that the seaweed aquaculture only imposes a local effect. It may make a big difference to the wind turbine as there are fewer loads exerted on wind turbine supporting structure. As for the impact on the sediment transport, since the wave height does not

encounter a remarkable change, the influence on sediment transport would not be remarkable.

6 Conclusions and recommendations

In the previous chapters, it has been presented the research background and its meaning, the model description, sensitivity analysis of this model, calibration of the model and its application in the real case. In this chapter, the conclusion will be drawn based on the findings. The research questions will also be answered. Considering the uncertainty in this study, a reflection is made on the results. Apart from that, recommendations will be provided for future studies considering the uncertainty, the drawbacks and neglected parts in this study.

6.1 Conclusion

First the research questions will be answered. The conclusion is given in the answer to the last research question.

Research question 1: How to model floating vegetation with the available vegetation module in SWAN?

This study is carried out with wave modeling program SWAN. In SWAN there already exists a vegetation module where the damping effect of bed-mounted vegetation is addressed. The aquatic plants are modeled as stiff cylinders. The energy dissipation is calculated as work carried out by plant-induced force expressed in a Morison-type equation. This model cannot meet the need of the current research as floating vegetation is concerned in this study. It leads to necessary modification on the original model. Two approaches are proposed to meet the requirement of modeling floating seaweed. The first model is developed by dividing the water column into two layers. The lower layer is occupied with only water while the upper layer is implemented with vegetation. With such modification implemented in SWAN it is able to run simulation when floating seaweed is in. However, this model can only be applied in flat-bed case as the vertical layer stratification is homogenous which means that the height of each layer is constant. The non-flat seabed is made unachievable in the model. To cope with this, the second approach is come up with. The principle is to modify the interval of integration of dissipation term. The original dissipation term is obtained by performing integration from the bottom of bed (where the vegetation starts) to the top of vegetation. The new term is retained through integrating from the bottom of vegetation to the water surface, which accommodates the feature of floating vegetation. This method fundamentally resolves the problem of inability to cope with non-flat seabed of the first model. These two models are essentially the same in terms of calculating the energy dissipation caused by floating seaweed.

Research question 2: How to make the floating seaweed model applicable to real situation?
Since this floating seaweed model is newly developed, its applicability to real situation remains to be verified by calibration. To calibrate this model relevant data is required. As it is quite costly and time-consuming to conduct a field test in the field condition, a scaling test in the flume is considered. The experiment comprises of three scenarios with their own specific objective. Scenario 1 is set up to see the effect of bottom friction and boundary influence. Scenario 2 is intended to obtain the difference regarding wave height after the intervention of H profiles (representing hosting structures). Lastly scenario 3 copes with the situation where vegetation mimics are implemented in the flume. It gives the picture of wave attenuation of floating seaweed aquaculture schematized in the flume.
With the data obtained in the flume test, the calibration is carried out. The numerical model is set up to resolve the relevant dimension of experiment setup. The incident wave height obtained in the experiment is set as boundary condition in the simulation. Through adjusting the drag coefficient, the calibrated drag coefficient is obtained when the out-going wave height in the simulation is the same as that from the experiment. With all the data obtained, a few drag coefficients are gained as function of Reynolds number. Then a relation between drag coefficient and Reynolds number is achieved.
Research question 3: What is the impact of the large-scale seaweed aquaculture in the offshore wind farm on wave climate in the North Sea?
Based on the calibrated model, a real case is set up to study the impact of large-scale seaweed aquaculture on wind waves. Three seaweed species are differentiated for the case study as they show different vegetation properties. The vegetation density, vegetation width and vegetation height are set according to characteristic of local cultivation. The wave and wind condition use the dominant value from year 1991-2010. The results show that within the vegetation field much wave energy is dissipated. Also the amount of attenuation is species specific due to different vegetation characteristics. However, waves start to grow even from the rear part of vegetation field, which results from directional spreading. Waves gain more growth with the increase of distance from vegetation field. From the simulation results it is seen that the large-scale seaweed aquaculture only imposes local influence on waves. It may be of importance to wind turbines as smaller waves generate fewer loads on wind turbine supporting structure.

6.2 Reflection on the results

The results above are obtained based on available experimental data and proper method which can be achieved to the best. Nonetheless, some aspects may have an impact on the effectiveness of the result.

First, there exists uncertainty in the experiment data. It shows quite some noise in the data. Also the incident wave height does not show consistency among different sets. This may impose serious problem on the usability of the data. Second, the calibration for Christmas decoration results in much higher drag coefficient than expected. This is because the dimensions parameters are set the same as the other two types of vegetation mimics while this sort of mimics give rise to significant dissipation. It is impossible to quantify the dimension of Christmas decoration. This brings big doubts on how accurate the parameter setting is and how reliable the vegetation mimics represent the prototype vegetation. Lastly, the parameterizing of vegetation diameter in the case study brings uncertainty as well. The true dimension of seaweed (width) is not comparable to the schematized dimension (diameter of cylinder) in the SWAN model. It is hard to determine a diameter which truly indicates the drag force.

Considering all the uncertainty above, it is questionable whether the seaweed aquaculture has a significant influence on the wind waves or not. Further studies with more effort on the accuracy are required to draw a sound conclusion. To improve this study, some recommendations are proposed to future studies.

6.3 Recommendations

Quite some aspects remain to be discussed in terms of its influence on the research results. Some aspects are ignored due to technical problem, like implementing small floating structure in SWAN. A few other points need to be improved since they are not treated in a proper way, such as the experimental setup. In this section the discussion are made in three categories to provide recommendations for further study.

6.3.1 Recommendations for the modified SWAN-model

- The same as in original vegetation module in SWAN, this floating vegetation model does not take into consideration of vertical damping. The ignorance of vertical velocity may make sense for bottom-mounted vegetation, as the vertical motion is restricted. However, it can be questionable in the case of floating seaweed as floating plant can move up and down in the presence of waves. This is far more complicated aspect. Therefore it is not included in this research. The damping in vertical direction is transferred to the bulk drag coefficient. It is recommended to use a CFD model which is able to model the vertical motion of object.
- The mooring line or hosting structure is not incorporated in this model. As known SWAN does not handle computation of floating structure as it is a phase-averaging program. The damping effect of mooring line or hosting structure is also represented

in the drag coefficient. It is suggested to use a phase-resolving program like Open Foam to model seaweed aquaculture more accurately.

- One drag coefficient is applied for all the computational grid points. However, the drag coefficient is supposed to change along the vegetation field as the wave condition alters after dissipation. It is suggested to develop a more advanced version of SWAN in which the drag coefficient can be determined at each grid point with the local wave information.

6.3.2 Recommendations for the experiments

The experiment shows unpleasant performance. Quite a few improper settings are observed. These points lead to some inapplicable data for the calibration. It undermines the accuracy of the research result. These aspects are listed below:

- The wave maker was not calibrated before commencing the experiment. This is seen from the remarkable difference between target wave height and measured wave height. Proper calibration needs to be carried out beforehand.
- The vegetation mimics used in the flume test are plastic tubes, wooden rods and Christmas decoration. The first two sorts of mimics do not show any flexibility at all. To what extent these vegetation mimics represent their prototype is an issue. Especially for Christmas decoration, it gives a very high drag coefficient in the flume test. It is suggested to choose the proper mimics which represent the characteristics of seaweed prototype.
- During the visit to the flume test, it has been observed that some mimics fall down after one wave running, and the water level drops down after a few tests. They add more uncertainty to the result.
- Some wave gauges show unexpected data. Wave gauge 5 gives higher wave height than other gauges. Also, ADV shows quite different result for different scenarios, which makes the data unusable. It should be due to some measurement error. It is suggested to arrange the measuring properly.
- The data results show unsatisfactory results. For some wave conditions two vegetation densities give the same amount of dissipation. It also leads to the infeasibility of validation. Accuracy of measuring needs to be emphasized.
- The number of data is quite limited. Only data for four wave conditions are provided. This makes the calibrated drag coefficient relationship less general and its applicability to real cases remains rather questionable. It is advised to carry out more experiments to give a relatively sufficient number of data for calibration.

6.3.3 Recommendations for case study

Some notes are also made for case study. It is advisable to improve these aspects in order to give a better representation of impact of large scale of seaweed aquaculture on waves.

- The vegetation parameters (vegetation density, vegetation width and vegetation length) use the indication numbers. A range is given for the vegetation length and width. Then the mean value is employed. There is certain degree of uncertainty in these parameters. If more accurate method of parameterizing is available, it may give more accurate results.
- The vegetation field is considered to be occupied by vegetation in the whole vegetated area. In reality the seaweed is operated in some patches and there are gaps between patches. For simplification as well as due to information unavailability this is not considered in the model setup. It is recommended to give a more accurate vegetation grid, taking into consideration of the gaps between patches.
- Mooring lines or hosting structures are not considered. It is recommended to use the phase-resolved modeling program which accounts for the impact of these structures.

Appendix A – Background of wave physics and SWAN

In this appendix relevant wave background knowledge is presented so as to provide a full picture of waves and wave energy dissipation. Besides, SWAN is explained concerning its principle.

A.1 Waves

Waves are interpreted as “vertical motions of water surface” in the field of hydraulic engineering. Wave is characterized as wave height, wave period and wave length. An example for harmonic wave is given in the figure below:

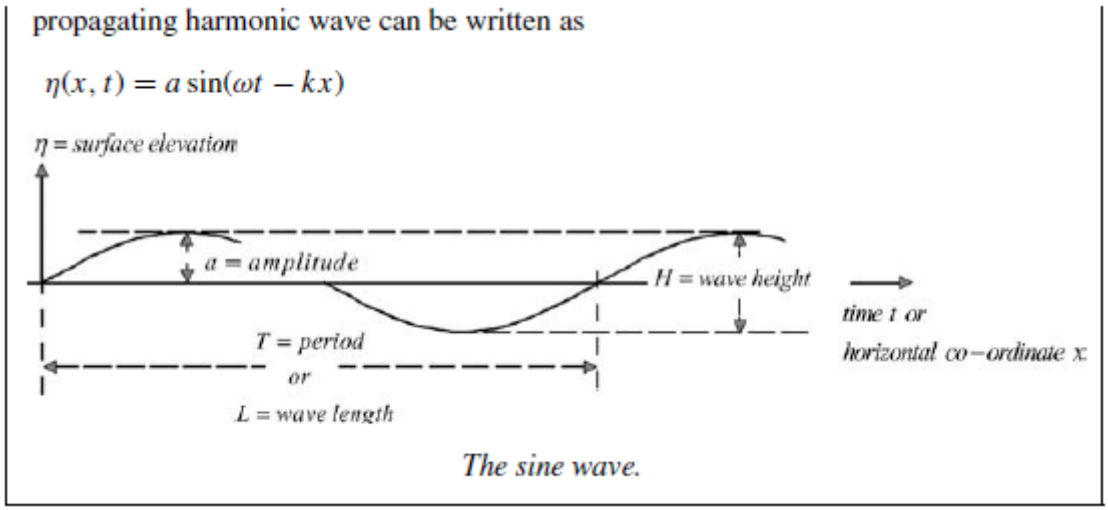

Figure A- 1: Definition of wave

A.2 SWAN

SWAN is a third-generation wave model developed by Delft University of Technology. This wave model copes with random waves in coastal area and inland water. In SWAN, various physical processes are accounted for: wave generation by wind, wave propagation in time and space, shoaling, refraction because of depth and current, triad and quadruplet interactions, white capping due to limit of wave steepness, depth-induced breaking, wave-induced set-up, transmission and reflection against obstacles, dissipation due to aquatic vegetation, turbulent flow, viscous fluid mud and diffraction. In this study, the most relevant module is vegetation module. This module deals with energy dissipation caused by bottom-mounted seaweed.

In SWAN the governing equation is action balance equation. It indicates that the energy density is distributed over frequencies and propagation direction. The action density is

defined as $N = E/\sigma$. N is action density, E is energy density and σ is wave frequency. Action density is conserved during propagation.

$$\frac{\partial N}{\partial t} + \frac{\partial c_x N}{\partial x} + \frac{\partial c_y N}{\partial y} + \frac{\partial c_\sigma N}{\partial \sigma} + \frac{\partial c_\theta N}{\partial \theta} = \frac{S_{tot}}{\sigma}$$

(A- 1)

A.3 Dissipation by vegetation

SWAN performs calculations based on change of wave energy flux. When waves propagate through vegetation fields, they lose energy due to the work carried out on vegetation. Based on linear wave theory and with waves normally incident to coastline and parallel contours, the energy dissipation can be presented as:

$$\frac{\partial E c_g}{\partial x} = -\varepsilon_v$$

(A- 2)

Where E=$(1/8)\rho g H^2$ which indicates wave energy density, and ρ is water density, g is acceleration of gravity, H is wave height, c_g indicates group velocity. c_g=nc, $c = \sqrt{(g/k)\tanh kh}$ is wave celerity, k is wave number, n=$(1/2)[1 + (2kh/\sinh 2kh)]$, x is the onshore coordinate and ε_v is time-averaged rate of energy dissipation per unit horizontal area induced by vegetation.

In vegetation module of SWAN, the vegetation is schematized as stiff cylinders. Regarding energy dissipation by vegetation, the energy loss is calculated as actual work carried out by the vegetation due to the drag force induced by plant. This force is represented by a Morison-type equation:

$$dF = C_I \rho \frac{\pi D^2}{4} \frac{du}{dt} + C_D \frac{1}{2} \rho D u |u|$$

(A- 3)

C_I is inertia coefficient, ρ is water density, D is diameter of vegetation, C_D is drag coefficient, u is water particle velocity. The first term on the right hand represents inertial force which is caused by the acceleration of water particles, and the second one represents drag force which is caused by water particle velocity. For relatively stiff plants the drag force is dominant and the inertial force is neglected. So only the drag force is considered to contribute to the energy loss. Therefore, the dissipation term can be presented more specifically:

$$\varepsilon_v = \overline{\int_{-h}^{-h+\alpha h} F_x u dz}$$

(A- 4)

Where $F_x = C_D \frac{1}{2} \rho D N u|u|$, which takes into account the number of stems N. h is water depth, ah is vegetation height, u is water particle velocity and z is the vertical coordinate. The over-bar indicates time-averaging.

Dalrymple et al. (1984) expressed the energy dissipation term as:

$$\varepsilon_v = \frac{2}{3\pi} \rho C_D b_v N \left(\frac{kg}{2\sigma}\right)^3 \frac{\sinh k\alpha h^3 + 3 \sinh k\alpha h}{3k \cosh kh^3} H^3 \quad \text{(A- 5)}$$

b_v is the width of vegetation. This formula was modified by Mendez & Losada (2004) who extended the application to irregular waves with wave height characterized in Rayleigh distribution. The following formula is given by them:

$$\varepsilon_v = \frac{1}{2\sqrt{\pi}} \rho C_D b_v N \left(\frac{kg}{2\sigma}\right)^3 \frac{\sinh k\alpha h^3 + 3 \sinh k\alpha h}{3k \cosh kh^3} {H_{rms}}^3 \quad \text{(A- 6)}$$

Appendix B – Exploration on the width of simulation domain and grid cell

In the setup for sensitivity analysis, attention has been paid to the choice of width of computational area.

The width of computational area should not be chosen too small. Otherwise the output values would be influenced by lateral absorbing boundary, if the lateral boundary condition is not imposed. Several widths of computational area are chosen to present the distinction. For these runs no vegetation is implemented. The result is showed in Figure B- 1:

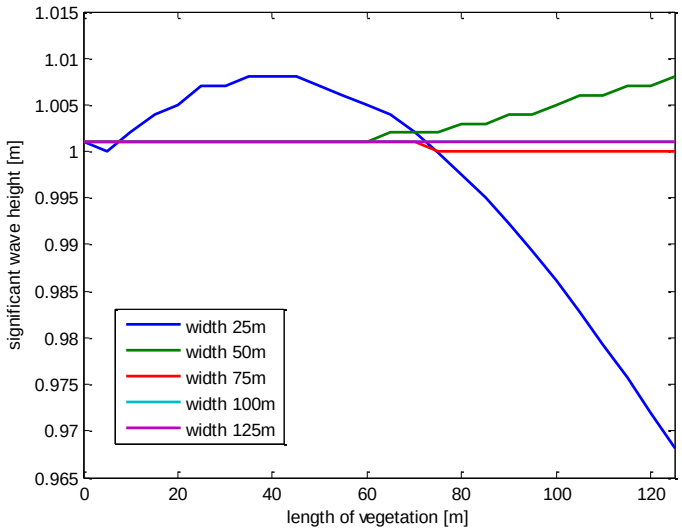

Figure B- 1: Impact of computational width on modelling results

As can be seen from the figure, small width of computational area may lead to unrealistic values. When the width is more than 75 m the difference disappears. Preferably the computational width is set more than 100 m in order to eliminate the influences of lateral boundary. As a result the width of computational area is chosen as 125 m.

Besides, a few grid sizes have been tried to determine whether the grid size plays a role on the accuracy of simulations. The result shows that the difference between these four sets is hardly noticeable, as presented in Figure B- 2. Consequently grid size of 5 m is chosen.

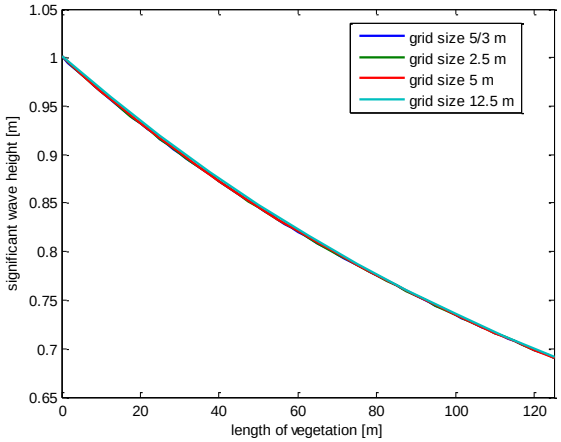

Figure B- 2: Impact of grid size on modelling results

Appendix C – Wave spectrum analysis in sensitivity analysis

The wave spectrum in sensitivity analysis is given in this appendix. A few peak wave periods are chosen and different characteristics are manifested.

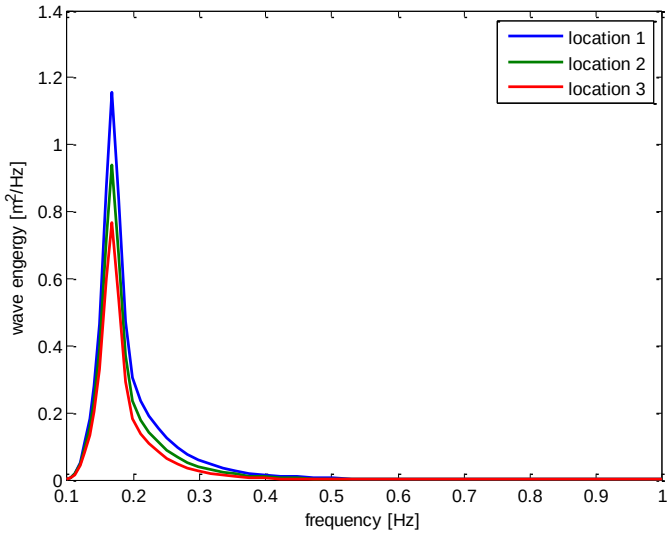

Figure C- 1: Wave spectrum for Tp=6 s

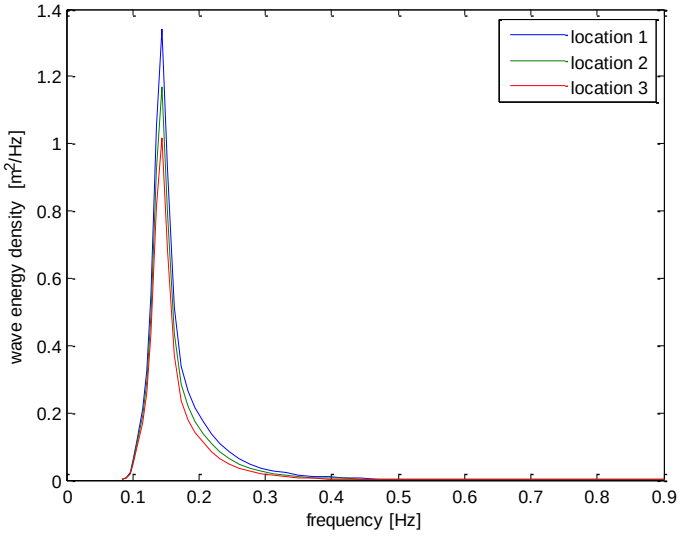

Figure C- 2: Wave spectrum for Tp=7 s

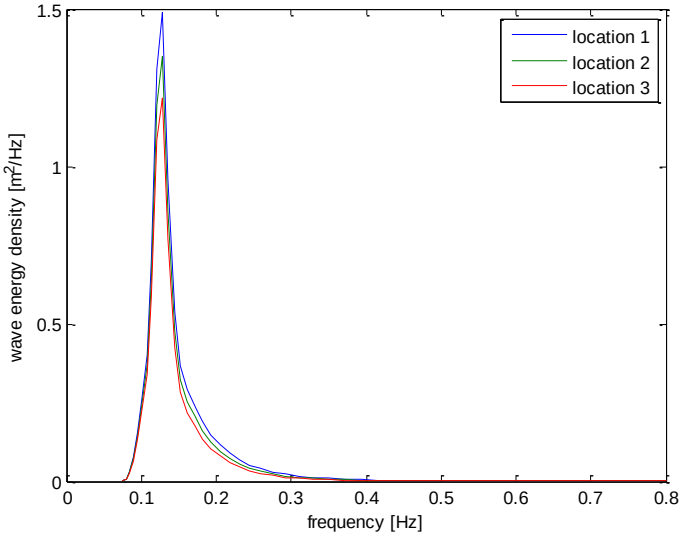

Figure C- 3: Wave spectrum for Tp=8 s

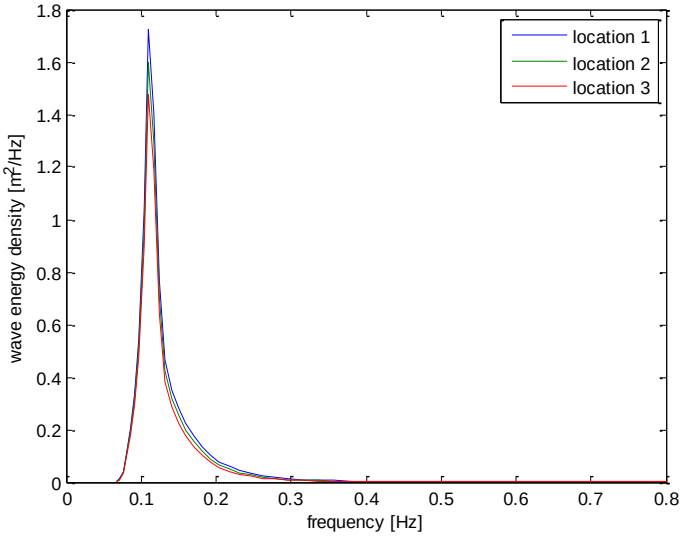

Figure C- 4: Wave spectrum for Tp=9 s

Appendix D – Exploration the reason behind unexpected data

This appendix illustrates the investigation on the untrustworthiness of certain data from the experiment. From the result of first and second scenario it is shown channel 5 gives significantly larger wave height than the other channels even though it should shows dissipation compared with channel 4. Besides, wave height from channel 9 give inconsistent value with channel 8 and channel 10. Channel 9 shows higher wave height than channel 8 and channel 10, which is beyond explanation. In the beginning, supposedly the unexpected data was attributed to reflection. The time series for channel 5 for (H=0.2 m, T=1.5 s) in first scenario is shown in Figure D- 1:

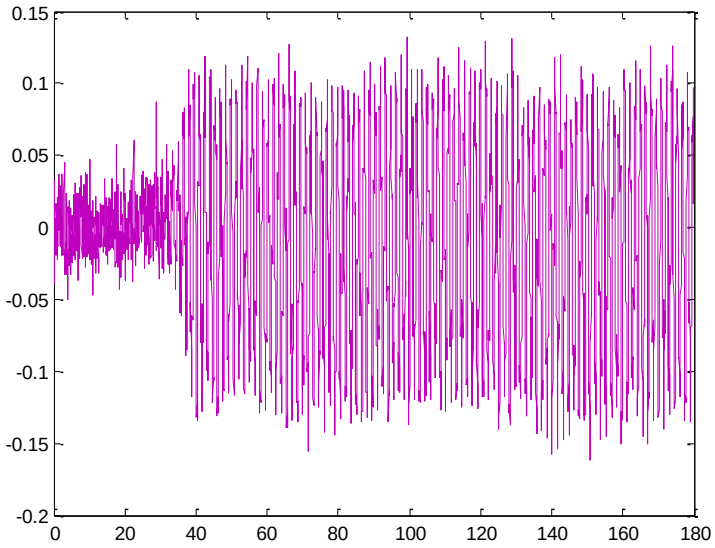

Figure D- 1: Example time series for channel 5

The time series shows large degree of disturbance. Water surface elevation is observed from the start of recording time, which contradicts with common sense, as the waves has not reached wave gauge 5 for the first 35 seconds. Also, this time series does not agree with the smoothness of time series of other channels. If the reflection inside the flume occurs, the time series should show reinforcing and cancelling of incident and reflective components at different time. The reflection pattern is not indicated in this time series. The only reason is left to the disturbance to wave gauge 5 by external force.

Then the cause for channel 9 is to be investigated. A closer look at the difference between channel 8 and channel 9 in first scenario (T=2.6s H=0.2m) shows that the wave height at channel 9 is higher than channel 8 from the beginning, which contradicts with reflection theory: when incident waves reach the end of flume, the reflective waves are generated.

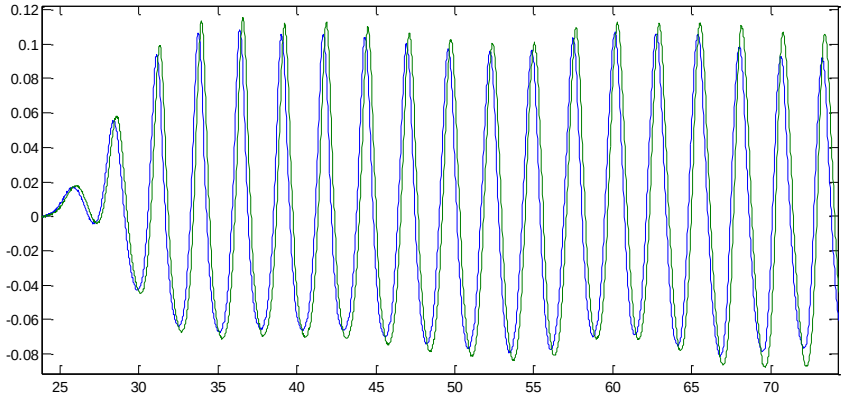

Figure D- 2: Time series of channel 8 (blue) and channel 9 (green) in first scenario

A similar phenomenon is observed in the second scenario for (H=0.2m T=2.6s) which is illustrated in the figure below:

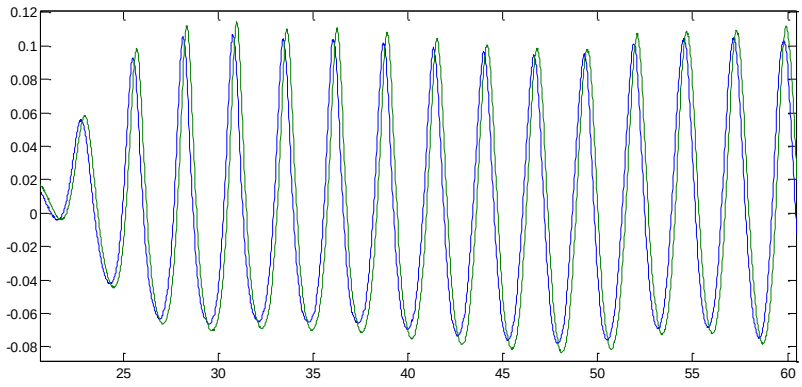

Figure D- 3: Time series of channel 8 (blue) and channel 9 (green) in second scenario

Based on the findings above, the reason of reflection is excluded. The higher wave height of channel 9 may result from the directional spreading. Since the vegetation mimics are only implemented one third of the flume width, the wave in the region between flume wall and vegetation boundary would be larger. Behind the vegetation field, the higher waves will offset the lower wave height. However, this cause is refuted by the wave height at channel 10. Channel 10 gives almost the same wave height as channel 8. If the wave height increase at channel 9 is due to directional spreading, there should also be wave height increase at channel 10. The cause remains unknown. As a result, the usability of data from channel 9 remains skeptical when determining the out-coming wave height.

Appendix E – Horizontal particle velocity analysis

As displayed in the experimental set up, two ADV are implemented both before and behind the vegetation field. They are noted as Ch015 and Ch016. Two methods are used to determine the particle velocity. One is the same as wave height determination which is to calculate the variance while the other is only to determine the magnitude of positive value. The first method has drawback because there is certain degree of asymmetry between maximum positive value and minimum negative value. This is owing to wave shoaling. The absolute value of maximum velocity is not close to that of minimum velocity. This is shown in the figure below. It shows that the maximum positive value reaches 0.3 m/s while the absolute value of minimum negative velocity is somewhat smaller than 0.2m/s.

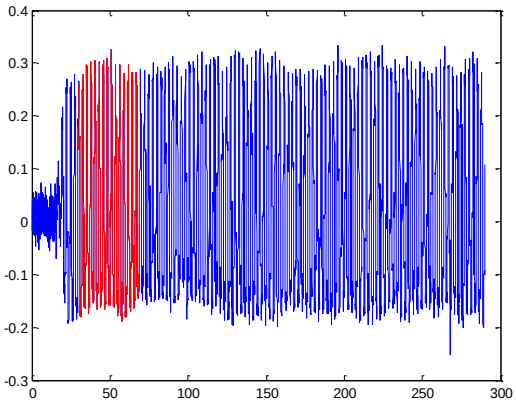

Figure E- 1: Asymmetry between positive maximum and absolute of negative minimum

Therefore, a mat lab script is made to determine the mean maximum velocity for the same span as where the wave height is determined. With this script some maximum values are obtained. The mean of these maximums is taken as the particle velocity. The following tables are obtained. The asteroid indicates inapplicable since lots of wiggles are shown in the time series.

From the data obtained, it can be seen that generally the velocity at Ch016 is somewhat smaller than that at Ch015. This complies with theory. After dissipation by vegetation, the wave height deceases in some degree. As a result the particle velocity decreases correspondingly. What is also worth observing is that the particle velocities for tubes are only half of that for wooden rods and Christmas decoration. This does not make any sense at all. The particle velocity depends on the wave height and wave period and vertical location measured. If the measured point remains the same during experiment, the particle velocity

should be more or less the same for the same wave conditions. The applicability of the measured velocity data is rendered poor due to inconsistency.

Table E- 1: Measured horizontal velocity for vegetation mimics tubes

	tubes 10 strings (m/s)		tubes 5 strings (m/s)	
	Ch015	**Ch016**	**Ch015**	**Ch016**
H=0.2 m, T=1.5 s	0.0959	0.0739	0.0984	0.0834
H=0.2 m, T=2.6 s	0.1612	0.1332	0.1661	0.1381
H=0.1 m, T=2.2 s	0.0746	0.0816	0.0791	*
H=0.1 m, T=1.4 s	0.0514	0.0579	0.0484	0.0481

Table E- 2: Measured horizontal velocity for vegetation mimics wooden rods

	Wooden rods strings (m/s)		Wooden rods 5 strings(m/s)	
	Ch015	**Ch016**	**Ch015**	**Ch016**
H=0.2 m, T=1.5 s	0.2188	0.1644	0.195	0.1677
H=0.2 m, T=2.6 s	0.2897	0.267	0.2778	0.2612
H=0.1 m, T=2.2 s	0.1546	0.1519	0.1504	0.139
H=0.1 m, T=1.4 s	0.1236	0.0981	0.1345	0.1073

Table E- 3: Measured horizontal velocity for vegetation mimics Christmas decoration

	Christmas decoration 10 strings (m/s)		Christmas decoration 5 strings (m/s)	
	Ch015	**Ch016**	**Ch015**	**Ch016**
H=0.2 m, T=1.5 s	0.197	0.1488	0.1974	0.162
H=0.2 m, T=2.6 s	0.2695	0.2482	0.2747	0.2522
H=0.1 m, T=2.2 s	0.1637	0.1366	0.1661	0.1321
H=0.1 m, T=1.4 s	0.1328	0.0791	0.1167	0.0934

Appendix F – Formulation of new expression of dissipation term by vegetation

For the case study, my first model is not able to carry out the simulation since the sea bed is not flat. In SWAN model, the height of each vegetation layer is constant. In order to make my model work, the first virtual layer should be inhomogeneous since the seabed is not flat. It contradicts the input rule of SWAN. Therefore, a new approach was come up with to meet the requirement. The principle of the new approach is to let SWAN read the vegetation information starting from the water surface while in original SWAN vegetation module the vegetation is read starting from the bed. This approach is to modify the interval of energy dissipation formula which is used in SWAN. The formula to calculate the amount of energy attenuation by vegetation is given as below:

$$\varepsilon_v = \overline{\int_{-h}^{-h+ah} F_x u dz}$$

F- 1

Where Fx is horizontal force on the vegetation which is given by $F_x = C_D \frac{1}{2} \rho D N u|u|$, u is water particle velocity, h indicates water depth and ah represents vegetation height. The over-bar means time-averaging. This gives rise to dissipation term according to Dalrymple et al (1984):

$$\varepsilon_v = \frac{2}{3\pi} \rho C_D b_v N \left(\frac{kg}{2\sigma}\right)^3 \frac{\sinh k\alpha h^3 + 3\sinh k\alpha h}{3k\cosh kh^3} H^3$$

F- 2

As modification, the interval of integral is changed and this results in a formula below:

$$\varepsilon_v = \overline{\int_{-ah}^{0} F_x u dz}$$

F- 3

Substituting the related expression:

$$\varepsilon_v = \int_{-\pi/\omega}^{\pi/\omega} \frac{\omega}{2\pi} |\sin \omega t| (\sin \omega t)^2 \, dt \int_{-ah}^{0} C_D \frac{1}{2} \rho b_v a^3 \omega^3 \frac{\cosh k(h+z)^3}{\sinh kh^3} dz$$

F- 4

The left part integration is independent on the second part. Therefore the integration is performed separately.

For the left part, due to symmetry, it can be changed to following form:

$$\int_{-\pi/\omega}^{\pi/\omega} \frac{\omega}{2\pi} |\sin \omega t| (\sin \omega t)^2 \, dt = \int_{0}^{\pi/\omega} \frac{\omega}{\pi} (\sin \omega t)^3 \, dt$$

$$= \int_{0}^{\pi/\omega} \frac{\omega}{\pi} (\sin \omega t)^2 (\sin \omega t) \, dt = \int_{0}^{\pi/\omega} \frac{\omega}{\pi} \frac{1 - \cos 2\omega t}{2} (\sin \omega t) \, dt$$

$$= \int_{0}^{\pi/\omega} \frac{\omega}{\pi} \left[\frac{1}{2} (\sin \omega t) - \frac{\cos 2\omega t}{2} (\sin \omega t) \right] dt = \int_{0}^{\pi/\omega} \frac{1}{\pi} \left[\frac{1}{2} (\sin \omega t) d\omega t - \frac{2\cos \omega t^2 - 1}{2} d \cos \omega t \right]$$

$$= -\frac{1}{2\pi} \cos \omega t_0^{\pi/\omega} + \frac{1}{3\pi} \cos \omega t^3{}_0^{\pi/\omega} - \frac{\cos \omega t^{\pi/\omega}}{2\pi}{}_0$$

$$= \frac{1}{\pi} - \frac{2}{3\pi} + \frac{1}{\pi} = \frac{4}{3\pi}$$

For the second part, all other parameters serve as coefficients since they are independent of the integration interval except $\cosh k(h+z)^3$.

Integration this part:

$$\int_{-ah}^{0} \cosh k(h+z)^3 \, dz = \int_{-ah}^{0} \cosh k(h+z)^2 \cosh k(h+z) \, dz$$

$$= \int_{-ah}^{0} (1 + \sinh k(h+z)^2) \cosh k(h+z) \, dz$$

$$= \frac{1}{k} \sinh k(h+z)_{-ah}^{0} + \frac{1}{3k} \sinh k(h+z)^3{}_{-ah}^{0}$$

$$= \frac{\sinh kh^3 - \sinh(kh - k\alpha h)^3 + 3 \sinh kh - 3 \sinh(kh - k\alpha h)}{3k}$$

This results in a new formula as below:

$$\varepsilon_v = \frac{2}{3\pi} \rho C_D b_v N \left(\frac{kg}{2\sigma} \right)^3 \frac{\sinh kh^3 - \sinh(kh - k\alpha h)^3 + 3 \sinh kh - 3 \sinh(kh - k\alpha h)}{3k \cosh kh^3} H^3$$

F- 5

The integration is based on the dissipation term obtained by Dalrymple et al (1984). In SWAN the dissipation term results from Mendez & Losada (2004) which made a modification on the formula above. They express the wave height variation as Rayleigh distribution, which leads to a factor of $\frac{3\sqrt{\pi}}{4}$ being multiplied to the term above. Also the root mean square wave height is employed instead of significant wave height. As a result the dissipation term reads as:

$$\varepsilon_v = \frac{1}{2\sqrt{\pi}} \rho C_D b_v N \left(\frac{kg}{2\sigma} \right)^3 \frac{\sinh kh^3 - \sinh(kh - k\alpha h)^3 + 3 \sinh kh - 3 \sinh(kh - k\alpha h)}{3k \cosh kh^3} {H_{rms}}^3$$

F- 6

After obtaining the new formula to calculate the energy dissipation caused by vegetation, it is implemented in the source code. The change is mainly on the iterative process for adding the different vegetation layers together. The original source code and the new one are both presented in the Appendix G.

This model is tested to see whether it works properly. In the original model the layers of vegetation is implemented with the first layer (the lower layer) as virtual layer plus a second vegetation layer. In the new model only one layer (the upper layer) is implemented as the new SWAN model reads the vegetation starting from the upper part. A test shows that these two models show exactly the same results.

Appendix G – Source code change

Original code:

```
      SAVE IENT
       DATA IENT/0/
       IF (LTRACE) CALL STRACE (IENT,'SVEG')

!      --- compute layer-independent vegetation dissipation factor

       KD    = KMESPC * DEP2(KCGRD(1))
       IF ( KD.GT.10. ) RETURN
       C     = 3.*KMESPC*(COSH(KD))**3
       SVEG1 = SQRT(2./PI) * GRAV**2 * (KMESPC/SMEBRK)**3 * SQRT(ETOT)
      &                    * NPLA2(KCGRD(1)) / C

!      --- compute dissipation factor for each layer and summed up

       SLAYH = 0.
       DO IL = 1, ILMAX
          SLAYH = SLAYH + LAYH(IL)
       ENDDO

       KVEGH = 0.
       C     = 0.
       D     = 0.
       SVEG2 = 0.

       IF ( DEP2(KCGRD(1)).GT.SLAYH ) THEN

          DO IL = 1, ILMAX
             KVEGH = KVEGH + KMESPC * LAYH(IL)
             SINHK = SINH(KVEGH)
             A     = C
             B     = D
             C     = SINHK**3
             D     = 3.*SINHK
             A     = C - A
             B     = D - B
```

```
      SVEG2 = SVEG2 + VEGDRL(IL)*VEGDIL(IL)*VEGNSL(IL)*(A + B)
   END DO

ELSE IF ( DEP2(KCGRD(1)).LT.LAYH(1) ) THEN

   SINHK = SINH(KD)
   A     = SINHK**3
   B     = 3.*SINHK
   SVEG2 = VEGDRL(1)*VEGDIL(1)*VEGNSL(1)*(A + B)

ELSE

   SLAYH1 = 0.
   SLAYH2 = 0.
   LAYPRT = 0.
   VGLOOP : DO IL = 1, ILMAX
      SLAYH1 = SLAYH1 + LAYH(IL)
      IF (DEP2(KCGRD(1)).LE.SLAYH1) THEN
         DO IK = 1, IL-1
            SLAYH2 = SLAYH2 + LAYH(IK)
         END DO
         LAYPRT = DEP2(KCGRD(1)) - SLAYH2
         DO IK = 1, IL-1
            KVEGH = KVEGH + KMESPC * LAYH(IK)
            SINHK = SINH(KVEGH)
            A     = C
            B     = D
            C     = SINHK**3
            D     = 3.*SINHK
            A     = C - A
            B     = D - B
            SVEG2 = SVEG2+VEGDRL(IK)*VEGDIL(IK)*VEGNSL(IK)*(A + B)
         END DO
         KVEGH = KVEGH + KMESPC * LAYPRT
         SINHK = SINH(KVEGH)
         A     = C
         B     = D
         C     = SINHK**3
         D     = 3.*SINHK
```

```
               A     = C - A
               B     = D - B
               SVEG2 = SVEG2 + VEGDRL(IL)*VEGDIL(IL)*VEGNSL(IL)*(A + B)
               EXIT VGLOOP
            END IF
         END DO VGLOOP

      END IF

!     --- compute total dissipation

      SVEGET = SVEG1 * SVEG2
```

New code:

```
     SAVE IENT
      DATA IENT/0/
      IF (LTRACE) CALL STRACE (IENT,'SVEG')

!     --- compute layer-independent vegetation dissipation factor

      KD    = KMESPC * DEP2(KCGRD(1))
      IF ( KD.GT.10. ) RETURN
      C     = 3.*KMESPC*(COSH(KD))**3
      SVEG1 = SQRT(2./PI) * GRAV**2 * (KMESPC/SMEBRK)**3 * SQRT(ETOT)/ C
      IF ( VARNPL ) SVEG1 = SVEG1 * NPLA2(KCGRD(1))

!     --- compute dissipation factor for each layer and summed up

      SLAYH = 0.
      DO IL = 1, ILMAX
         SLAYH = SLAYH + LAYH(IL)
      ENDDO

      KVEGH = 0.
      C     = 0.
      D     = 0.
      SVEG2 = 0.
```

```
IF ( DEP2(KCGRD(1)).GT.SLAYH ) THEN

   DO IL = 1, ILMAX
      KVEGH = KVEGH - KMESPC * LAYH(IL)
     KVEGH1 = KD + KVEGH
      SINHK = SINH(KVEGH1)
      A     = C
      B     = D
      C     = -SINHK**3 + SINH(KD)**3
      D     = -3.*SINHK + 3.*SINH(KD)
      A     = C - A
      B     = D - B
      SVEG2 = SVEG2 + VEGDRL(IL)*VEGDIL(IL)*VEGNSL(IL)*(A + B)
   END DO

ELSE IF ( DEP2(KCGRD(1)).LT.LAYH(1) ) THEN

   SINHK = SINH(KD)
   A     = SINHK**3
   B     = 3.*SINHK
   SVEG2 = VEGDRL(1)*VEGDIL(1)*VEGNSL(1)*(A + B)

ELSE

   SLAYH1 = 0.
   SLAYH2 = 0.
   LAYPRT = 0.
   VGLOOP : DO IL = 1, ILMAX
      SLAYH1 = SLAYH1 + LAYH(IL)
      IF (DEP2(KCGRD(1)).LE.SLAYH1) THEN
         DO IK = 1, IL-1
            SLAYH2 = SLAYH2 + LAYH(IK)
         END DO
         LAYPRT = DEP2(KCGRD(1)) - SLAYH2
         DO IK = 1, IL-1
            KVEGH = KVEGH - KMESPC * LAYH(IK)
           KVEGH1 = KD + KVEGH
            SINHK = SINH(KVEGH1)
            A     = C
```

```
                  B      = D
                  C      = -SINHK**3 + SINH(KD)**3
                  D      = -3.*SINHK + 3.*SINH(KD)
                  A      = C - A
                  B      = D - B
                  SVEG2 = SVEG2+VEGDRL(IK)*VEGDIL(IK)*VEGNSL(IK)*(A + B)
               END DO
               KVEGH = KVEGH - KMESPC * LAYPRT
               KVEGH1 = KD + KVEGH
               SINHK = SINH(KVEGH1)
               A      = C
               B      = D
               C      = -SINHK**3 + SINH(KD)**3
               D      = -3.*SINHK + 3.*SINH(KD)
               A      = C - A
               B      = D - B
               SVEG2 = SVEG2 + VEGDRL(IL)*VEGDIL(IL)*VEGNSL(IL)*(A + B)
               EXIT VGLOOP
            END IF
         END DO VGLOOP

      END IF

!     --- compute total dissipation

      SVEGET = SVEG1 * SVEG2
```

The parts which are to be modified have been marked in red in original code. The changed code is marked in light blue in the new code.

Appendix H – Boundary condition and drag coefficient for all direction sectors

Table H- 1: Boundary condition for all the direction sectors

Direction Sectors	H_{rms} [m]	T_{peak} [s]	Wind Direction [°]	Wind Speed [m/s]	U [m/s]	V [m/s]
0°	0.96	6.72	125.88	5.51	-4.47	3.23
30°	0.96	5.78	75.17	6.65	-6.43	-1.7
60°	0.95	5.3	83.18	6.82	-6.77	-0.81
90°	0.74	4.67	109.68	6.23	-5.86	2.1
120°	0.74	4.58	135.31	6.37	-4.48	4.53
150°	0.73	4.54	154.07	6.39	-2.79	5.74
180°	0.98	4.84	175.48	7.79	-0.61	7.77
210°	1.27	5.41	202.24	8.66	3.28	8.01
240°	1.04	5.21	227.39	7.55	5.56	5.11
270°	1.02	6	242.37	6.96	6.17	3.2
300°	1.02	6.13	252.09	6.15	5.86	1.89
330°	1.01	6.8	236.3	5.33	4.43	2.95

Table H- 2: Drag coefficient for each vegetation for all direction sectors

Direction sectors	Cd for Lamina	Cd for Saccharina	Cd for Ulva
0°	0.23	0.185	0.067
30°	0.215	0.17	0.059
60°	0.207	0.163	0.054
90°	0.22	0.175	0.062
120°	0.218	0.173	0.061
150°	0.218	0.173	0.06
180°	0.196	0.151	0.048
210°	0.183	0.139	0.042
240°	0.197	0.152	0.049
270°	0.205	0.161	0.053
300°	0.215	0.17	0.059
330°	0.225	0.18	0.065

Appendix I – Varied square vegetation field

This appendix presents the various vegetation fields in quantifying the effect of wave dissipation.

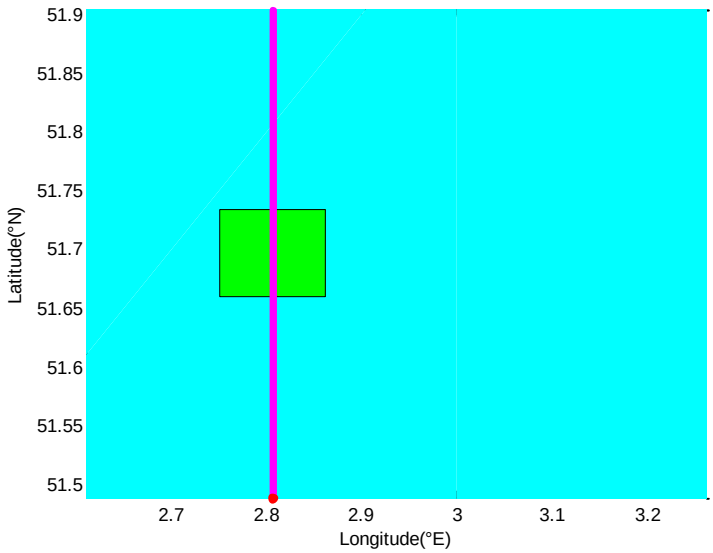

Figure I- 1: Vegetation field with size of 8 km × 8 km

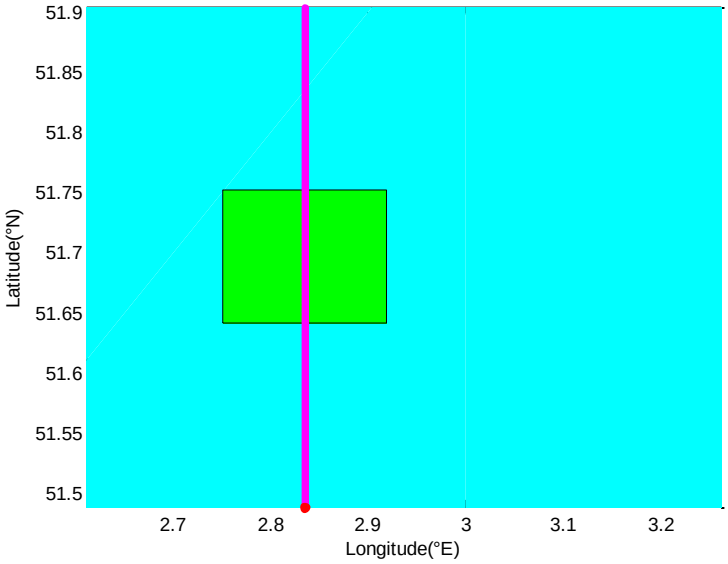

Figure I- 2: Vegetation field with size of 12 km × 12 km

Appendix J – Wave diagrams for Laminaria digitata for other direction sectors

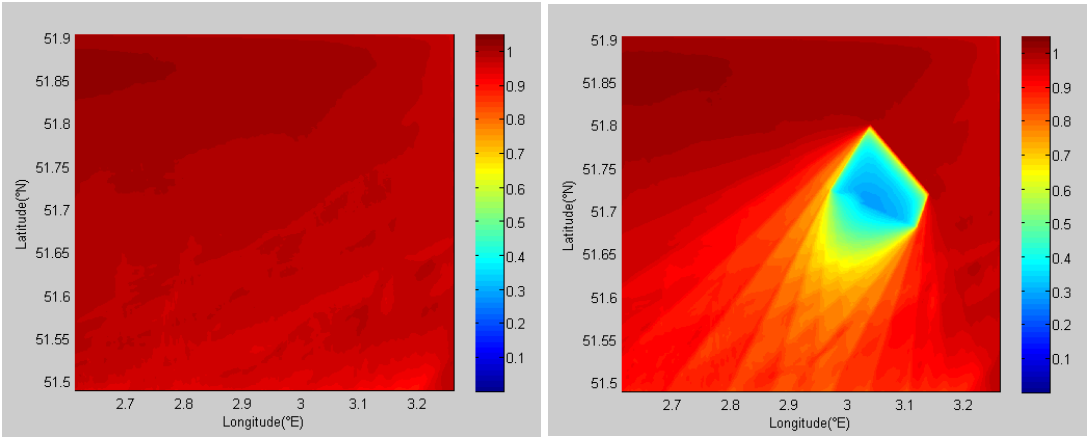

Figure J- 1: Wave diagram for scenario 3 (left) and scenario 4 (right) for wave direction 30°

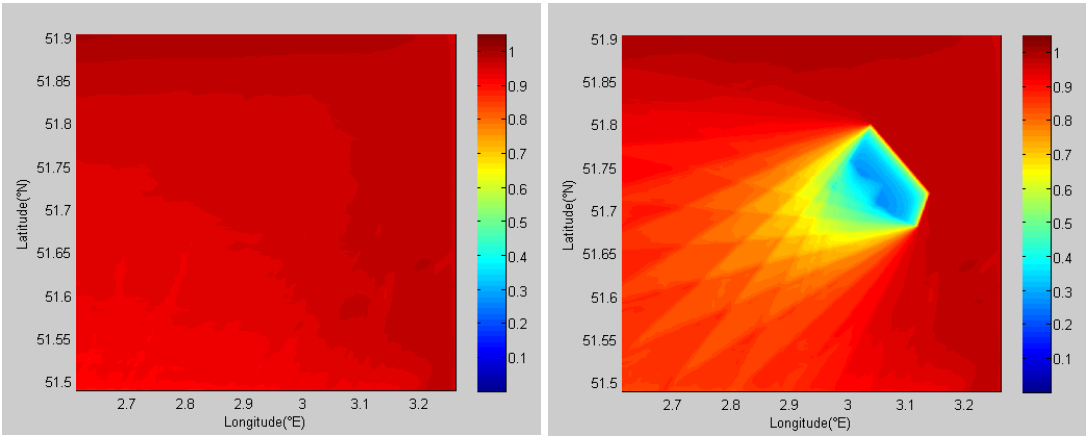

Figure J- 2: Wave diagram for scenario 3 (left) and scenario 4 (right) for wave direction 60°

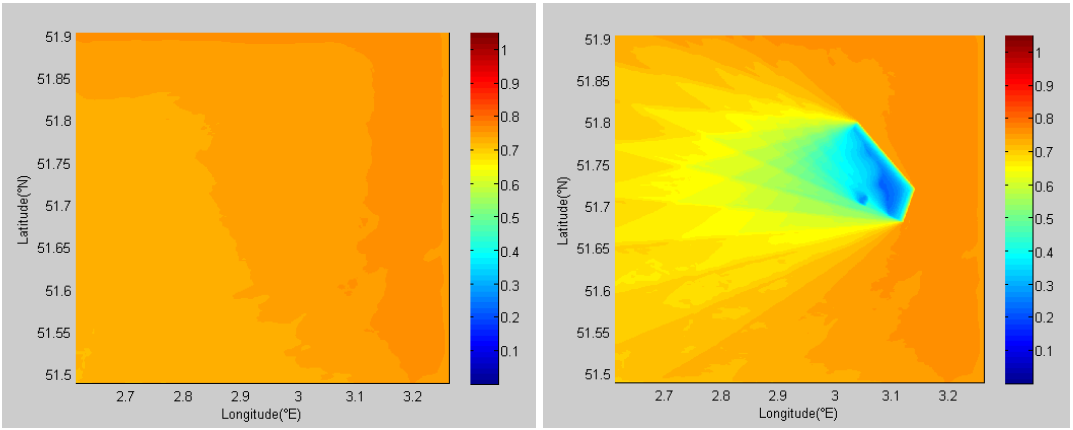

Figure J- 3: Wave diagram for scenario 3 (left) and scenario 4 (right) for wave direction 90°

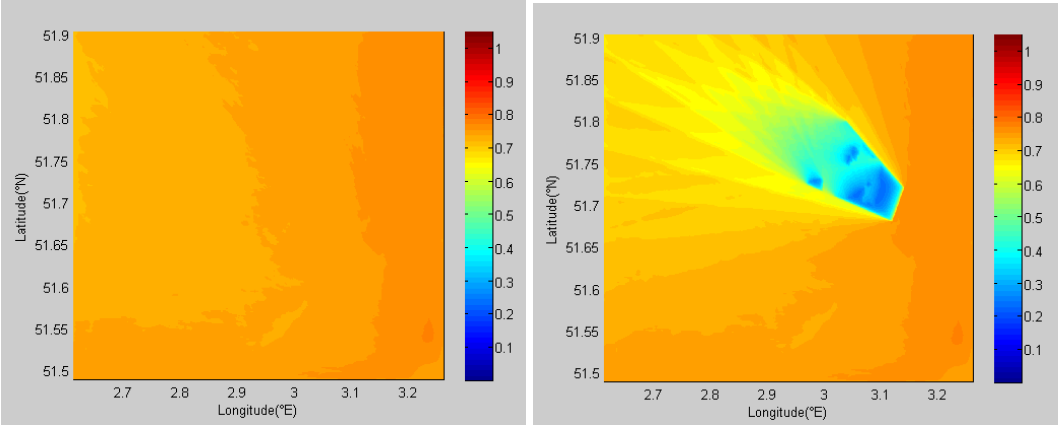

Figure J- 4: Wave diagram for scenario 3 (left) and scenario 4 (right) for wave direction 120°

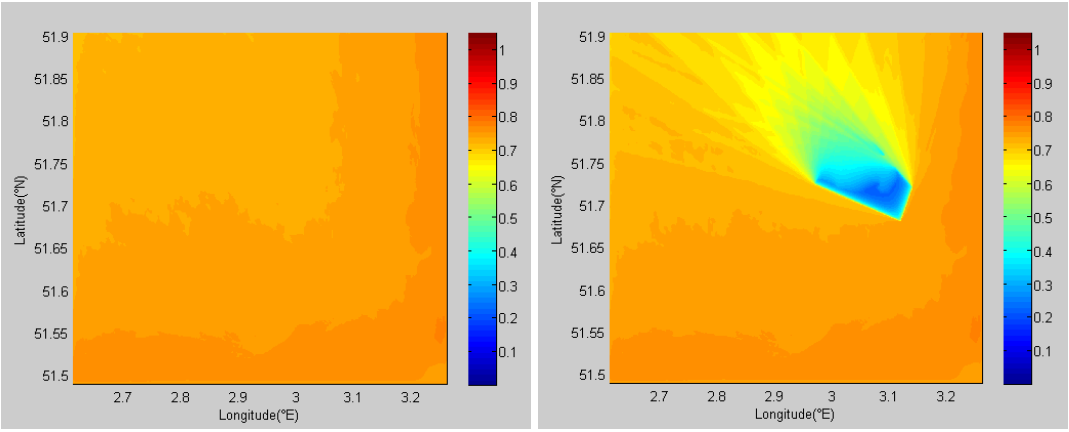

Figure J- 5: Wave diagram for scenario 3 (left) and scenario 4 (right) for wave direction 150°

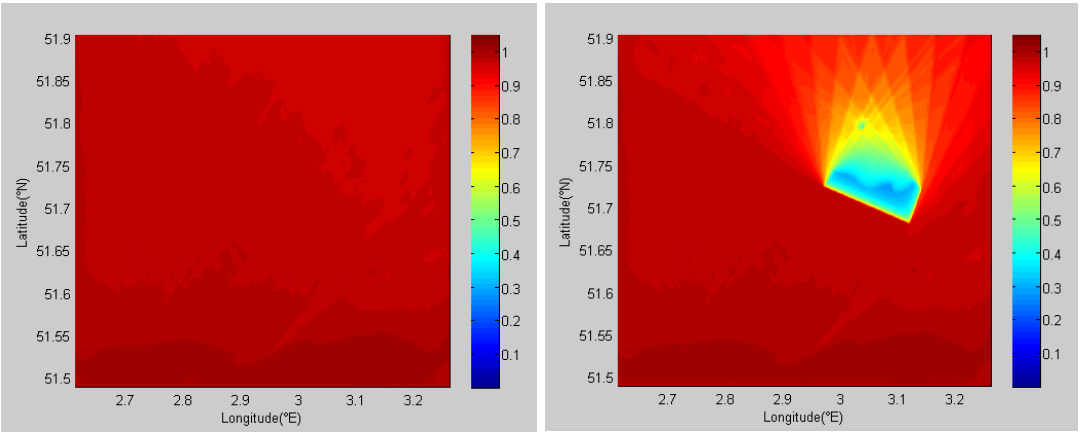

Figure J- 6: Wave diagram for scenario 3 (left) and scenario 4 (right) for wave direction 180°

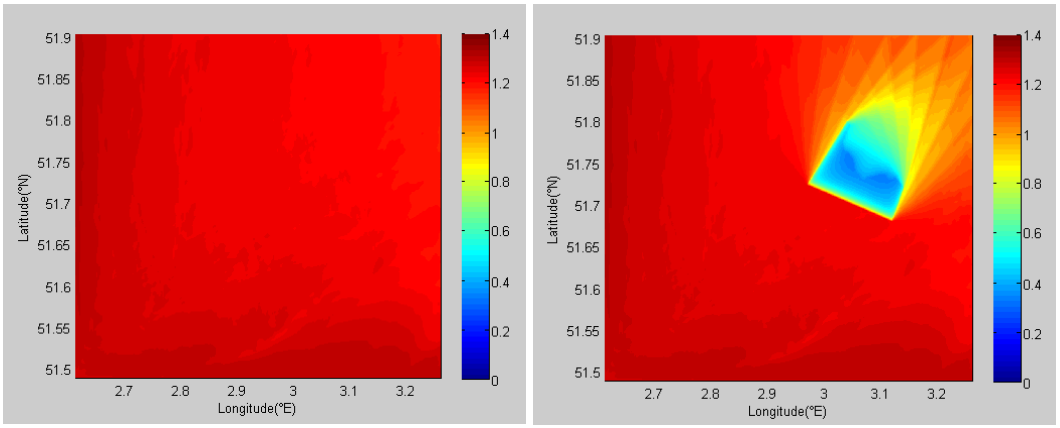

Figure J- 7: Wave diagram for scenario 3 (left) and scenario 4 (right) for wave direction 210°

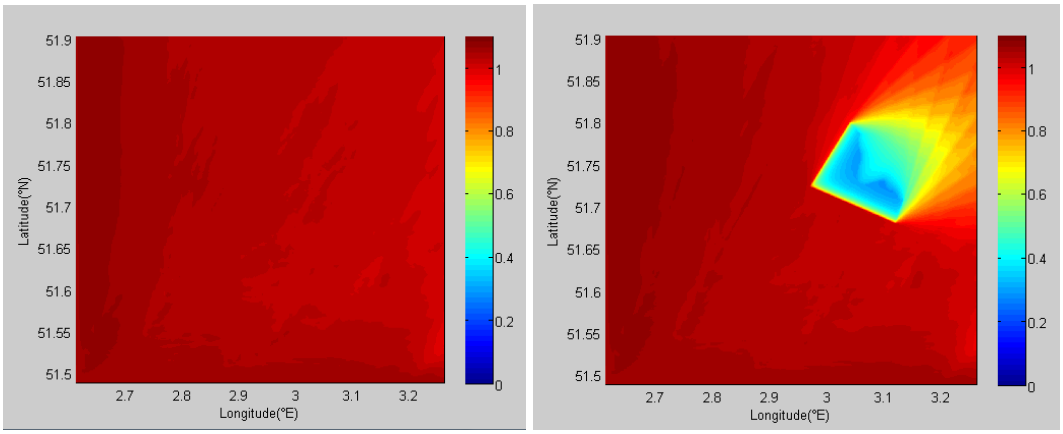

Figure J- 8: Wave diagram for scenario 3 (left) and scenario 4 (right) for wave direction 240°

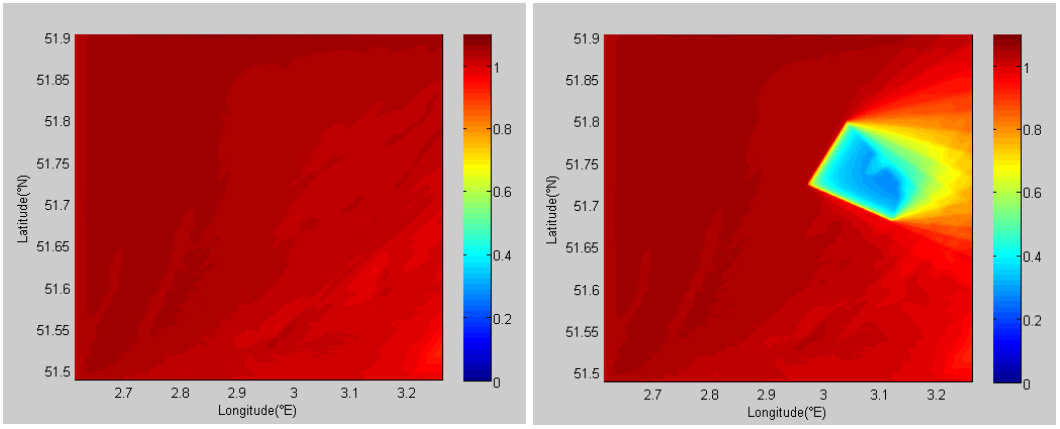

Figure J- 9: Wave diagram for scenario 3 (left) and scenario 4 (right) for wave direction 270°

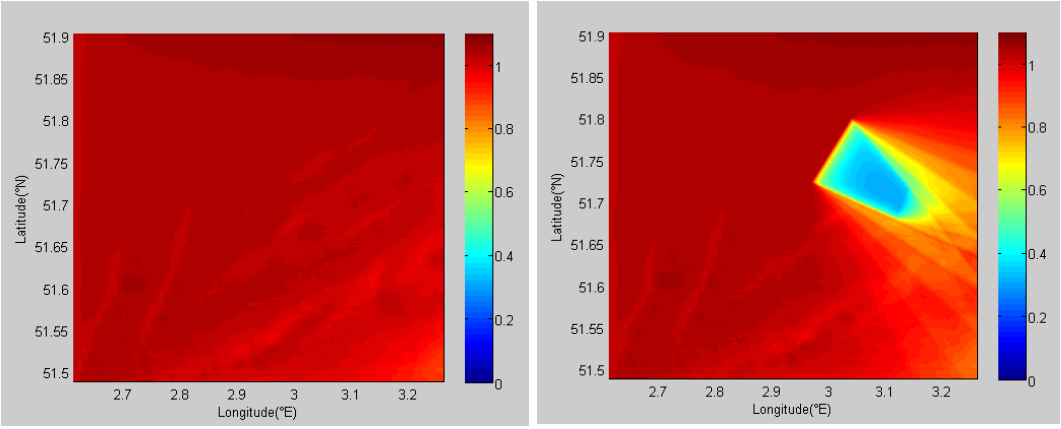

Figure J- 10: Wave diagram for scenario 3 (left) and scenario 4 (right) for wave direction 300°

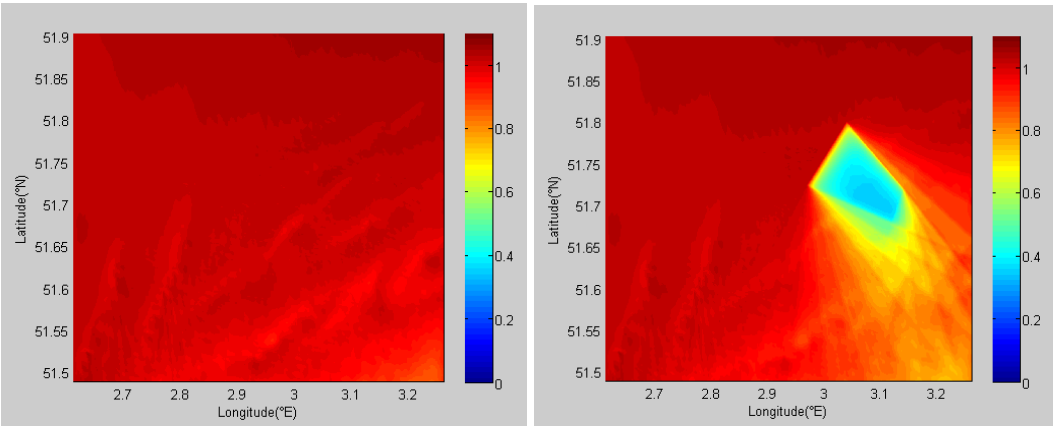

Figure J- 11: Wave diagram for scenario 3 (left) and scenario 4 (right) for wave direction 330°

Similar with the result for direction of 0°, the energy is dissipated significantly within vegetation field, but due to directional spreading the waves grow behind the vegetated area. In terms of impact on the sediment transport on the coastline, some direction sectors are not interested, such as direction sectors 120°, 150°,180°, 210° and 240° where the waves propagate off the coast.

References

Anderson, M. E., & Smith, J. M. (2014). Wave attenuation by flexible, idealized salt marsh vegetation. *Coastal Engineering*, *83*, 82–92. http://doi.org/10.1016/j.coastaleng.2013.10.004

Buck, B. H., & Buchholz, C. M. (2005). Response of offshore cultivated Laminaria saccharina to hydrodynamic forcing in the North Sea. *Aquaculture*, *250*(3-4), 674–691. http://doi.org/10.1016/j.aquaculture.2005.04.062

Dalrymple, R.A., Kirby, J.T., Hwang, P.A., 1984. Wave diffraction due to areas of energy dissipation. J. Waterw. Port Coast. Ocean Eng. 110 (1), 67-79.

Dijkstra, J. T., & Uittenbogaard, R. E. (2010). Modeling the interaction between flow and highly flexible aquatic vegetation. *Water Resources Research*, *46*(12), 1–14. http://doi.org/10.1029/2010WR009246

Folke, C., & Kautsky, N. (1992). Aquaculture with its environment: Prospects for sustainability. *Ocean & Coastal Management*, *17*(1), 5–24. http://doi.org/10.1016/0964-5691(92)90059-T

Hu, Z., Suzuki, T., Zitman, T., Uittewaal, W., & Stive, M. (2014). Laboratory study on wave dissipation by vegetation in combined current-wave flow. *Coastal Engineering*, *88*, 131–142. http://doi.org/10.1016/j.coastaleng.2014.02.009

Jadhav, R. S., Chen, Q., & Smith, J. M. (2013). Spectral distribution of wave energy dissipation by salt marsh vegetation. *Coastal Engineering*, *77*, 99–107. http://doi.org/10.1016/j.coastaleng.2013.02.013

L.H. Holthuijsen (2007). Waves in oceanic and coastal waters. Delft University of Technology and UNESCO-IHE

Mendez, F. J., & Losada, I. J. (2004). An empirical model to estimate the propagation of random breaking and nonbreaking waves over vegetation fields. *Coastal Engineering*, *51*(2), 103–118. http://doi.org/10.1016/j.coastaleng.2003.11.003

Newkirk, G. (1996). Sustainable coastal production systems: A model for integrating aquaculture and fisheries under community management. *Ocean and Coastal Management*, *32*(2), 69–83. http://doi.org/10.1016/S0964-5691(96)00066-X

Suzuki, T.(2011). Wave dissipation over vegetation fields. Ph.D. thesis, Delft University of Technology.

SWAN- User manuel. Delft University of Technology, Environmental Fluid Mechanics Section. http://www.swan.tudelft.nl (Version 41.01, April 2014).

Van Steeg, P., & Van Wesenbeeck, B. (2011). Large-scale physical modelling of wave damping of brushwood mattresses.